IEA INTERNATIONAL ENERGY AGENCY

Assessment of Photovoltaic Module Failures in the Field

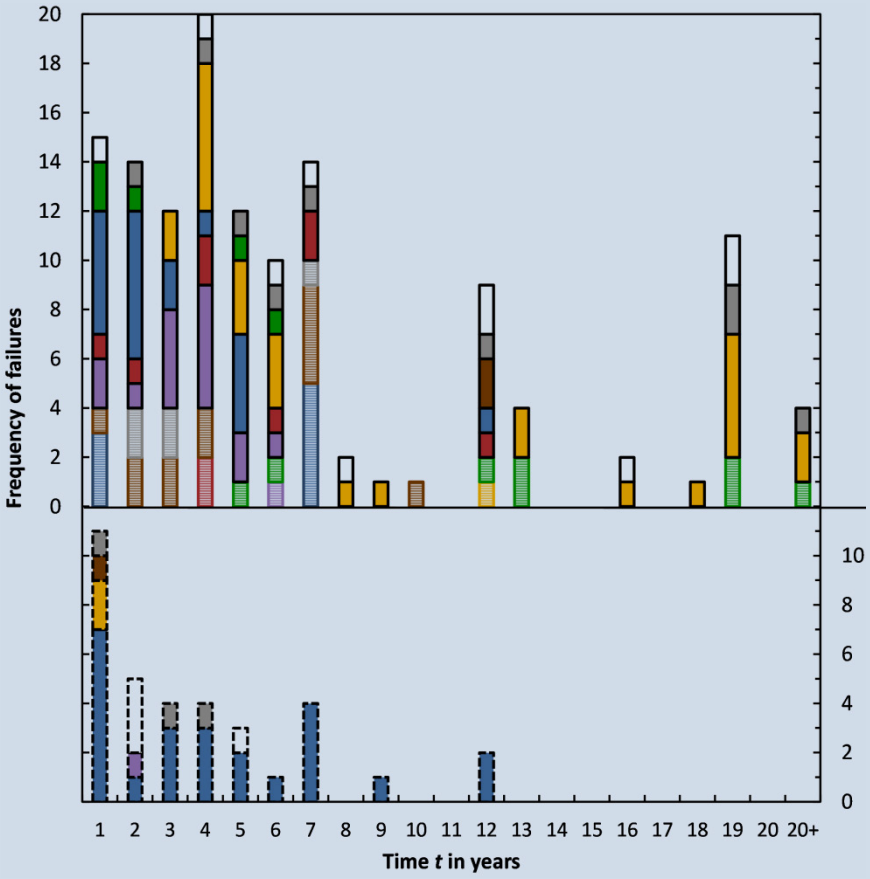

PVPS

PHOTOVOLTAIC POWER SYSTEMS PROGRAMME

Report IEA-PVPS T13-09:2017

Cover figure is from chapter 3.3.3, Fig. 49, where more detail is provided.

INTERNATIONAL ENERGY AGENCY
PHOTOVOLTAIC POWER SYSTEMS PROGRAMME

Assessment of Photovoltaic Module Failures in the Field

IEA PVPS Task 13, Subtask 3
Report IEA-PVPS T13-09:2017
May 2017

ISBN 978-3-906042-54-1

Authors:

Marc Köntges

Institute for Solar Energy Research Hamelin, Emmerthal, Germany

Gernot Oreski

Polymer Competence Center Leoben GmbH, Leoben, Austria

Ulrike Jahn, Magnus Herz

TÜV Rheinland Energy GmbH, Cologne, Germany

Peter Hacke

NREL, Golden, Colorado, USA

Karl-Anders Weiss

Fraunhofer Institute for Solar Energy Systems ISE, Freiburg, Germany

Authors:

Guillaume Razongles

CEA - INES, Le Bourget du Lac, France

Marco Paggi

IMT School for Advanced Studies Lucca, Italy

David Parlevliet

Murdoch University, Australia

Tadanori Tanahashi

National Institute of Advanced Industrial Science and Technology, Japan

Roger H. French

Case Western Reserve University, Cleveland, Ohio, USA

Contributing authors:

Mauricio Richter, Caroline Tjengdrawira

3E, BEL, Belgium

Arnaud Morlier

Institute for Solar Energy Research Hamelin, Emmerthal, Germany

Hengyu LI, Laure-Emmanuelle Perret-Aebi

Centre Suisse d'Electronique et Microtechnique SA

Karl A. Berger,

Austrian Institute of Technology GmbH, Center for Energy, Vienna, Austria

George Makrides

The University of Cyprus, PV Technology Laboratory, Cyprus

Werner Herrmann

TÜV Rheinland Energy GmbH, Cologne, Germany

Table of Contents

Foreword

The International Energy Agency (IEA), founded in November 1974, is an autonomous body within the framework of the Organization for Economic Co-operation and Development (OECD) which carries out a comprehensive programme of energy co-operation among its member countries. The European Union also participates in the work of the IEA. Collaboration in research, development, and demonstration of new technologies has been an important part of the Agency's Programme.

The IEA Photovoltaic Power Systems Programme (PVPS) is one of the collaborative R&D Agreements established within the IEA. Since 1993, the PVPS participants have been conducting a variety of joint projects in the application of photovoltaic conversion of solar energy into electricity.

The mission of the IEA PVPS Technology Collaboration Programme is: To enhance the international collaborative efforts which facilitate the role of photovoltaic solar energy as a cornerstone in the transition to sustainable energy systems. The underlying assumption is that the market for PV systems is rapidly expanding to significant penetrations in grid-connected markets in an increasing number of countries, connected to both the distribution network and the central transmission network.

This strong market expansion requires the availability of and access to reliable information on the performance and sustainability of PV systems, technical and design guidelines, planning methods, financing, etc., to be shared with the various actors. In particular, the high penetration of PV into main grids requires the development of new grid and PV inverter management strategies, greater focus on solar forecasting and storage, as well as investigations of the economic and technological impact on the whole energy system. New PV business models need to be developed, as the decentralised character of photovoltaics shifts the responsibility for energy generation more into the hands of private owners, municipalities, cities, and regions.

IEA PVPS Task 13 engages in focusing the international collaboration in improving the reliability of photovoltaic systems and subsystems by collecting, analysing and disseminating information on their technical performance and failures, providing a basis for their technical assessment, and developing practical recommendations for improving their electrical and economic output.

The current members of the IEA PVPS Task 13 include:

Australia, Austria, Belgium, China, Denmark, Finland, France, Germany, Israel, Italy, Japan, Malaysia, Netherlands, Norway, SolarPower Europe, Spain, Sweden, Switzerland, Thailand, and the United States of America.

This report concentrates on the reliability of PV modules. The reliability of PV modules is described by theoretical models. We focus on available models and not in any case on the most important degradation mechanisms. Furthermore, statistical data of the PV module reliability in the field is presented and analysed. The importance of local environmental stressors, such as temperature, humidity, irradiance, wind, etc., influencing the reliability test methods is discussed.

The editors of the document are Marc Köntges, Institute for Solar Energy Research Hamelin, Emmerthal, Germany (DEU), Gernot Oreski, Polymer Competence Center, Leoben, Austria (AUT), and Ulrike Jahn, TÜV Rheinland Energy, Germany.

The report expresses, as much as possible, the international consensus of opinion of the Task 13 experts on the subject dealt with. Further information on the activities and results of the Task can be found at: http://www.iea-pvps.org.

Acknowledgements

This paper received valuable contributions from several IEA-PVPS Task 13 members and other international experts. Financial support is given by:

Bundesamt für Energie (BfE),

Chinese Academy of Sciences (CAS),

Austrian government, by means of the Austrian Federal Ministry for Transport, Innovation, and Technology (bmvit), represented by the Austrian Research Promotion Agency (FFG), under contract No. 853028,

Swiss Federal Office of Energy (SFOE),

U.S. Department of Energy with the National Renewable Energy Laboratory,

European Research Council under the European Union's Seventh Framework Programme (FP/2007-2013) to the ERC Starting Grant "Multi-field and multi-scale Computational Approach to Design and Durability of PhotoVoltaic Modules" - CA2PVM (Grant Agreement n. 306622),

French Environment and Energy Management Agency (ADEME),

and

German Federal Ministry for Economic Affairs and Energy (BMWi) under contract No. 0325786A, B, and C.

Supported by:

on the basis of a decision
by the German Bundestag

List of Abbreviations

Glossary	Description
AATR	Acetic acid transmission rate
Busbars	Wider screen printed bus bars on the front-side of crystalline silicon PV cells
c-Si	Crystalline silicon
Degradation mechanisms	A know physical or chemical mechanism that leads to degradation and failure.
Degradation mode	An observable mode of degradation that may involve a number of mechanisms and a degradation pathway among these.
Degradation path-way	A sequence of mechanisms or modes that are connected in a sequential or parallel set of pathways, and lead to accumulated degradation and failure
Encapsulant	A formulated polymer film, typically EVA, PVB, POE or TPU, used in the lamination process to produce a PV module. Also referred to as the pottant.
EPMA	Electron probe micro analysis
EVA	Ethylene vinyl acetate, a formulated polymer film used as an encapsulant in the lamination processing of PV modules
Gridlines	Fine screen printed silver lines (or fingers) on the front-side of silicon PV cells
HAc	Acetic acid
HALS	Hindered amine light stabilizer
KG	Köppen and Geiger
OTR	Oxygen transmission rate
PID	Potential Induced Degradation
PID-c	Polarisation or passivation form of potential induced degradation
PID-d	Delamination associated with potential-induced degradation
PID-s	Shunting form of potential induced degradation
POE	Polyolefin elastomer encapsulant
PV	Photovoltaic
PVB	Polyvinyl butyral
(Power) degradation rate	Usually assumed to be a linear rate and reported in % power loss per year, %/yr or %/a of PV modules or a PV systems
SEM	Secondary electron microscope
Stress level	The magnitude of the applied stress from a specific stressor
Stressors	Factors that apply different forms of stress to a PV module, such as temperature, humidity, irradiance, wind, snow, soiling, etc.
TPU	Thermoplastic polyurethane encapsulant
WVTR	Water vapour transmission rate

Definitions

Symbols and syntax

To indicate one of the endpoints of an interval is to be excluded or included from the interval, the corresponding square bracket notation described in International standard ISO 31-11 are used in this document:

$]a,b[=\{x\in\mathbb{R}|a<x<b\}$,

$[a,b[=\{x\in\mathbb{R}|a\leq x<b\}$,

$]a,b]=\{x\in\mathbb{R}|a<x\leq b\}$,

$[a,b]=\{x\in\mathbb{R}|a\leq x\leq b\}$.

Usage period of PV modules

There are several words used to name the time period a PV module is used in a PV system. We define the nominal service life or technical lifetime as the time the PV module is expected to be used in a PV system. The typical length of the nominal service life is expected to be 20 to 25 years. The real time period where a PV module is used in a system is named service life. The service life may vary from 0 up to 50 years.

Power loss and failure definitions

The determination of a power loss of PV system is done in various ways. In scientific studies sometimes the initial power of PV modules is available. In this case one can determine the power loss relative to the initial measurement. These studies are important for e.g. validating specific failure models of PV modules as done in Chapter 2.3.

In nearly all practical cases the initial power of a module is not known. In this case the current STC power is compared to the STC power on the nameplate of the PV module. This is the most common method to identify failure in commercial systems.

In the TASK13 IEA-PVPS T13-01:2014 report [1] the following definition for **PV module failure** is given:

A PV module failure is an effect that (1) degrades the module power and which is not reversed by normal operation or (2) creates a safety issue. A purely cosmetic issue which does not have the consequences of (1) or (2) is not considered as a PV module failure. A PV module failure is relevant for the warranty when it occurs under conditions the module normally experiences.

This definition is useful for a PV module manufacturer who is responsible for all failures which are caused by its product. This definition forms a good basis for all failures described in detail in the Chapter 2. A PV system operator also has to handle all kind of failures which cause a power loss in a PV system. He is also interested in failures caused by a lightning strike or by a catastrophic heavy snow load. To differentiate between these two different perspectives, of the module manufacturer vs. the system operator, we define a **PV failure** as any failure which causes a power loss or a safety failure in the PV system. Only light induced power degradations or instabilities which are incorporated in the nominal power rating of the modules are excluded from the definition of a PV failure. Again purely cosmetic issues are also excluded from a PV failure.

Executive Summary

In this report we present the current status and predictive ability for the power loss of PV modules for specific failure modes. The team describes PV module material interactions and incompatibilities among encapsulation materials and lamination processes so as to better understand PV module failures mechanism.

In order to model PV module degradation modes it is necessary to understand the underlying degradation mechanisms and processes on the molecular level. In most cases the encapsulant and backsheet films seem to play a major role in PV module degradation. Some failure modes like browning of encapsulants are directly related to the encapsulant film. But in most cases material interactions are the main root cause for PV module degradation. For example, acetic acid, which is a degradation product of EVA encapsulants, not only causes corrosion of the PV stringing and tabbing ribbons and the PV cell gridlines or fingers, but also promotes potential induced degradation and/or delamination. Furthermore, it accelerates the oxidation process of EVA itself. Also, the type of backsheet used in the PV module influences many degradation mechanisms by its barrier properties against water vapour, oxygen, and acetic acid. High concentrations of water vapour and acetic acid in the PV module accelerate nearly all degradation modes.

The literature review shows that PV module failure modes are well described in the literature, including their main driving factors. The review also shows that the right combination of the encapsulant and backsheet films can be beneficial in reducing failures. Nevertheless the studies also show that there are no common rules or acceleration factors which apply generally for all PV modules and can be used for modelling. On the one hand, the degradation modes depend on the bill of materials and components and are unique for each single PV module brand and model. On the other hand, there are typically several degradation modes and pathways activated simultaneously and these may have synergistic or antagonistic effects, making it challenging to correlate observed effects with single mechanisms.

For well-known PV module failure modes, modelling approaches to forecast the power loss are summarized from the literature. All these models are based on the principle understanding of the underlying process, but they are still only heuristic models which do not include the influence of material parameters. So the models are parameterized by the test results of whole modules and not on test results of the module components. To identify the impact of the various failures a survey on the impact of PV system failures in various climatic zones is conducted.

The results do not show a strong correlation of the observed failure occurrences and impacts with the Köppen and Geiger climatic zones. In the future larger datasets of observations may enable these insights, while additional factors which need to be considered for PV module failures may be identified. Independent of climatic zones some PV module failures stand out with a high power loss if a PV system is affected by the failure. In the rank order of impact, these failures are potential induced degradation, failure of bypass diodes, cell cracks, and discolouration of the encapsulant (or pottant) material.

This rank order of failure modes may be a result of the fact that for potential induced degradation, bypass diodes, and discolouration of the pottant material no appropriate tests exist in the standard IEC61215 design qualification and type approval test. Currently for all these failure types tests are in development, but they are not even included in the current revision of the IEC61215. Therefore, we recommend PV plant designers not only to check for an approved IEC61215 test for the PV module brands/models considered for use, but also for additional tests for PID (IEC/TS 62804-series), bypass diode test (IEC 62979, IEC/TS 62916). The UV-degradation test is slightly tightened in the current IEC 61215 compared to the former one, but there is still no pass/fail cri-

terion for discolouration. However, it is recommended to read the full protocol of an IEC 61215 test and look for discolouration remarks.

Besides PV module failure, the failure with the highest impact on the PV system is the soiling of PV modules in specific outdoor regions. The soiling also does not strongly correlate with the climate zones of Köppen and Geiger. Therefore, a special stressor classification for PV modules for soiling in the Middle East and North Africa regions is introduced. These classifications are derived by geographic information systems to allow a worldwide mapping of relevant stress factors for PV systems. In the future this stress factor mapping has to be expanded to other regions worldwide and for other stress factors than soiling.

1 Introduction

Currently plenty of PV module failures are known. For investors these failures are difficult to assess because there is little information how much impact and how often a specific failure mode occurs in real world PV systems. The lack of information adds an unnecessary uncertainty to the risk of investment. In this document we try to analyse this problem from three perspectives.

The first perspective is the view of a scientist, PV module expert or manufacturer. In chapter 2 we summarize PV module failure models. These models allow one to analyse the impact of specific well-known degradation modes and failures on the module power with a dependence on weather conditions. These models allow a manufacturer or a PV module expert to evaluate the power loss risk for specific known failures for a specific product. This information can be used to define the warranty criteria for the product. However, most of the failures have not been evaluated to this depth in literature. For these failures, data is summarized from the literature to explain the root cause mechanisms and, if possible, ways to simulate their impact on power production in the future. A framework is explained to model the power loss of multiple failures.

The second perspective is the view of an investor, banker or underwriter. We collect PV system failure data for four climate zones. These data allow analysing the occurrence of a failure relative to other failure types and its impact on the system power.

Finally, the third perspective is the view of a test institute and PV system planner. Here we explain how one has to modify testing methods for specific failure types to special regions. This allows adapting test methods for a given PV module to specific regional requirements.

2 Modelling of Known PV Module Failure

This chapter is directed to scientists and PV experts. The root cause analysis for many encapsulation-material related failures of PV modules is explained in the first subsection 2.1. In the second subsection 2.2 interaction between encapsulation materials and other module components are discussed. The next subsection 2.3 explains models simulating the time- and load-dependent power loss for specific failure types.

2.1 Description of material based failures

2.1.1 Photovoltaic Encapsulants: EVA, Silicones, POE

The most common crystalline silicon PV module design requires a polymeric encapsulant material to embed the solar cells and the stringing tabs between the glass front sheet and the backsheet or the rear glass sheet. The role of the embedding polymer is multiple. Its first purpose is to behave as a buffer layer to protect the brittle silicon cells from shocks occurring to the glass or the backsheet. For this, the elastic properties of the polymer are of critical importance. Its second role is to ensure the electrical insulation of the cells and the connectors to avoid short circuits. Besides these two properties, the main requirement of the polymeric material is to show a low absorbance in the active spectrum of the photovoltaic cells, in order to allow the cell to generate the highest possible photocurrent [2]. The conservation of these mechanical, electrical, and optical properties over time under the influence of UV exposure or temperature is of critical importance for the failure prevention of PV modules.

The dominant encapsulant polymer used in c-Si PV modules are based on EVA (Ehtylene Vinyl Acetate) co-polymers, even though silicones [Ketola08] have been used previously, and POE (Polyolefin elastomer) encapsulants [3], [4] are a focus of interest currently.

EVA, employed as an encapsulant for the lamination of PV modules, is a thermosetting polymer, which formulation is adapted for an exposure to photo oxidative stress. Common EVA formulations comprise, besides the polymer resin, of a crosslinking agent, an adhesion promoter, a UV absorber, and antioxidant agents. The crosslinking agent is a radical initiator - usually a peroxide - which decomposition under heat during the lamination will form free radicals, initiating radicals on the polymeric backbone. The formed radicals will in turn lead to the formation of covalent bonds between polymer chains. The usual additives and their function are listed in Tab. 1 [5] [6]–[9].

Tab. 1: Usual additives used in solar grade EVA formulations.

Function	Common examples
Crosslinking agent	Luperox (Lupersol) TBEC
	Luperox (Lupersol)
Crosslinking coagent	Triallylisocyanurate
	Triallylcyanurate
UV absorber	Cyasorb 531 (Chimassorb 81) Tinuvin 234

Function	Common examples
Hindered Amine Light stabilizer (HALS)	Tinuvin 123 Tinuvin 770
Primary antioxidant	Butylated hydroxytoluene (BHT)
Secondary antioxidant	Irgafos 168 Naugard P
Adhesion promoter	Silane A 174 / 2530-85-0

2.1.2 Auto-oxidation of EVA – Role of acetic acid

The dominant encapsulation material for PV modules currently is ethylene vinyl acetate copolymer (EVA). The aging behaviour and degradation mechanism of EVA and especially of formulated EVA (with stabilizer additives) as a PV encapsulation material are well described in the literature. The initial step of EVA degradation is the formation of acetic acid (HAc) followed by the oxidation and breakdown of the main polymer chain. The degradation rate is greater in an oxygen atmosphere [10]. Further degradation products reported in the literature are lactones, formed by intramolecular back-biting by the acetate group and the evolution of methane and the production of ketones and acetaldehyde. Furthermore, α,β-unsaturated carbonyl groups, hydro peroxides and anhydrides are formed during the oxidation process. Generally, their rate of formation and decay follow typical auto-oxidation kinetics [2], [10]–[15].

With increasing vinyl acetate content, the EVA degradation rate is enhanced [Sultan91]. An increasing vinyl acetate content results in a higher polarity and therefore higher solubility of the acetic acid in the polymer [14]. Additionally, the reduction in stability with increasing vinyl acetate content can be explained by the increased residual acetic acid content within the polymer arising from different processing steps. Formation of acetic acid occurs at temperatures from 120 to 150°C [11]. This temperature range is usually reached during polymerization and palletisation of the EVA copolymer, film extrusion, and also PV module lamination. The de-acetylation is not retarded by addition of free-radical inhibitors, and more importantly, is catalysed by acetic acid. The higher the amount of acetic acid, the faster the initial de-acetylation reaction, followed by the further oxidative degradation process.

As the EVA in a PV module is encapsulated with glass and backsheet films and the usually very volatile acetic acid cannot exit the PV module that easily, the presence of acetic acid in a PV module is a major drawback for the use of EVA encapsulants in PV modules. Hence, acetic acid is linked to several PV module failure mechanisms.

The acid has corrosive effects on cell metallization and the cell interconnect copper core and its tin coating. The copper core causes a brown discoloration of the EVA when it is directly exposed to EVA. Usually the tin or tin-based coating and solder material should protect the copper core of the interconnect ribbon, but it may not be robust enough to resist corrosion. This metallization, or interconnect, corrosion leads to an increased series resistance and therefore losses in module performance [2], [12], [15], [16]. Due to the long diffusion paths from the encapsulant to the backsheet, acetic acid can accumulate in front of the solar cells and lower the local pH value, leading to even faster corrosion [17].

Another cause of failure in c-Si modules is the potential induced degradation (PID) effect or degradation mode. Therein high system voltages cause leakage currents through the module's front glass and the encapsulation material. The resulting electrical potential between the frame and cells causes a detrimental effect on, and loss of, power output. Properties of the encapsulant like polarity, volume resistivity or water vapour transmittance rate (WVTR) strongly influence the PID effect. In addition the PID effect is significantly enhanced by the presence of acetic acid which eases the transport of Na+ from front sheet glass to the cells [18], [19].

By comparison, several studies on new polyolefin based encapsulants show that the lower polarity and lower WVTR values, in combination with the absence of HAc, can suppress the PID effect totally [18]–[20]. When using EVA as an encapsulant it is shown that backsheets with presumably high acetic acid permeation rates (AATR) reduce the sensitivity to PID and yellowing [17], [21], [22].

From all of the above mentioned research, it can be seen that HAc has a large role in degradation of PV modules. Therefore, for the lifetime of PV modules, it is important to understand the mechanisms of acetic acid formation within EVA, its deleterious effects during its time inside the PV module and its migration out of the module through the backsheet.

2.1.3 Browning of EVA

The most common and easiest encapsulant degradation mode to observe is the degradation of the optical properties caused by the discolouration of the encapsulant material. Since their introduction to the market the most common crystalline silicon PV modules are designed with ethylene vinyl acetate (EVA) as an encapsulating material. Discolouration of EVA in PV modules is expected to induce a power loss through a diminution of the short-circuit current of the module of up to 0.5%/yr [23], but the degradation rate due to this cause may reach about 10%/yr for modules with concentrators [5].

EVA based modules may show yellowing or browning over time in service or under UV exposure. This discolouration is mostly inhomogeneous and follows spatial patterns. These patterns depend on the type of module construction. Typically, for glass/backsheet modules the browning occurs in the central region of the cells with wide clear EVA areas, or "frames" around the cell edges, leading to what is at times referred to as doughnut ring patterns above each cell. Discolouration is rarely observed in the EVA between neighbouring solar cells [6]. For glass/glass module constructions, this EVA discolouration is more spatially uniform.

This yellowish or brownish appearance is caused by an increased absorption of light in the violet and blue range of the visible light spectral range. Besides the loss of light irradiance, or intensity, reaching the cells, the browning of EVA is not a safety issue in itself, but may reveal the presence of more worrisome failures modes. The yellowing or browning of EVA is more intense around hot spots or partially contacted cells, which is due to a local elevation of the temperature compared to the rest of the module.

It has also been shown, that the browning of EVA may show patterns of clearer stripes or points over some cells. The location of these patterns has been shown to correlate with the cracks on the cells. The supposed mechanism of this competitive discolouration is described below.

Photochemical [6] and thermo-oxidative processes [13] are identified as the main causes of the discolouration of EVA in PV modules as well as playing a role in delamination or embrittlement of the encapsulation material.

EVA polymer chains in the photovoltaic encapsulation materials are prone to chemical oxidation under exposure to UV or high temperatures and the different mechanisms of this degradation are known [24], forming among others coloured conjugated alkene or ketone by-products and releasing acetic acid as discussed above. In the presence of oxygen, further reactions such as chain scis-

sion or crosslinking may take place, resulting in a modification of the mechanical properties of the polymer. Nevertheless under UV-light irradiation at wavelengths above 300 nm, the degradation of non chromophoric polymers is likely to be initiated by chromophoric impurities which absorb UV-light and produce radicals that further react with the polymer [24]. The EVA polymer resin does not significantly absorb light in the UV-visible spectral region which is not absorbed by the glass front sheet. Thus, the cause of the fast discolouration of EVA is firstly not attributed to the UV-induced degradation of the polymer chains themselves, but to the degradation of stabilizer additives of the EVA compound [6]. This process can take place in the absence of oxygen.

During the lamination of the PV modules, the peroxide catalyst that serves as the crosslinking agent is depleted [25]. An inadequate or incomplete crosslinking of the polymer after a too rapid (short-time) lamination process may lead to residual (unconsumed) peroxide catalyst which can then take part in further UV-initiated photochemical reactions during the module service lifetime. A partially cured EVA shows faster discolouration under UV exposure than a totally cured one [6]. This type of accelerated browning is especially observed for EVA formulations containing a higher concentration of peroxides or containing coactivators absorbing light in the near UV range such as triallylisocyanurates, whose role is to accelerate the crosslinking reaction by forming free radicals without having to dramatically increase the peroxide concentration [7]. The type of peroxide itself has an influence on the formation of chromophores during lamination and subsequently on the discolouration rate of the EVA. Pern *et al.* [5] have compared two formulations differing only in the peroxide used, and have shown that a material with Lupersol 101 as the crosslinking agent shows a higher concentration of chromophores than a material with Lupersol TBEC, resulting in higher photostability of the latter. Primary and secondary antioxidants such as butylated hydroxy-toluene (BHT) [26][8] or phenylphosphites [6] are also known to participate to the formation of chromophores during the curing of EVA.

To avoid the absorption of UV light by the chromophores formed during the crosslinking and the subsequent degradation of the material, a UV absorber is added to the formulations and displaces the absorption cut-off of the materials towards the longer wavelengths [5]. Nevertheless the UV absorber itself is prone to UV-induced photo degradation, leading first to a decrease of the absorbance of the material, followed by fast browning as the material's chromophores are not protected anymore and undergo subsequent photo degradation. Furthermore, the degrading UV absorber may initiate further decomposition of the EVA chains and accelerate the discolouration [6]. To avoid this, a radical trapping stabilizer, also known as a hindered amine light stabilizer (HALS) is added to the compound. Its role is to prevent the photo induced oxidation of the UV stabilizer.

The schematic in Fig. 1 shows the evolution mechanisms of the browning process in EVA encapsulation material. HALS, under the action of UV and oxygen, eliminates reactive free radicals and stabilises the UV absorber [27][28]. The diffusion of oxygen through the module encapsulation material is possible in the case of glass/backsheet modules, as the polymer backsheet is breathable. This results in an inhomogeneous concentration of the UV absorber in front of the cells. Pern has shown that the concentration of UV absorber in a module exposed to UV decreases from the edge towards the centre of the solar cells [6]. This decrease is correlated to the intensity of the yellowing and can lead to characteristic cell-sized "rings" or "doughnuts" in the pattern of the browning. Therefore, it may be assumed that oxygen diffusion is the key parameter for the conservation of the UV absorber in the presence of HALS and the subsequent long-time protection against yellowing or browning of EVA in PV modules. In the absence of oxygen, the UV absorber is progressively depleted; the initially formed chromophoric impurities are absorbing UV and form chromophores with longer conjugation lengths, which progressively absorb in the longer wavelengths and lead to the yellowing of the material. This absorption of light increases with time, therefore the formation of chromophores is accelerated and the yellowing rate increases with time [5][7].

From all of the above mentioned research, it can be seen that in addition to the formation of HAc, the formulation, degradation by-products, and long-term behaviour of the added stabilizers (UV absorbers, HALS, antioxidants) play a large role in degradation of EVA. The optimized choice of stabilizers is therefore crucial to the long-term stability of EVA and consequently also the degradation over lifetime of PV modules.

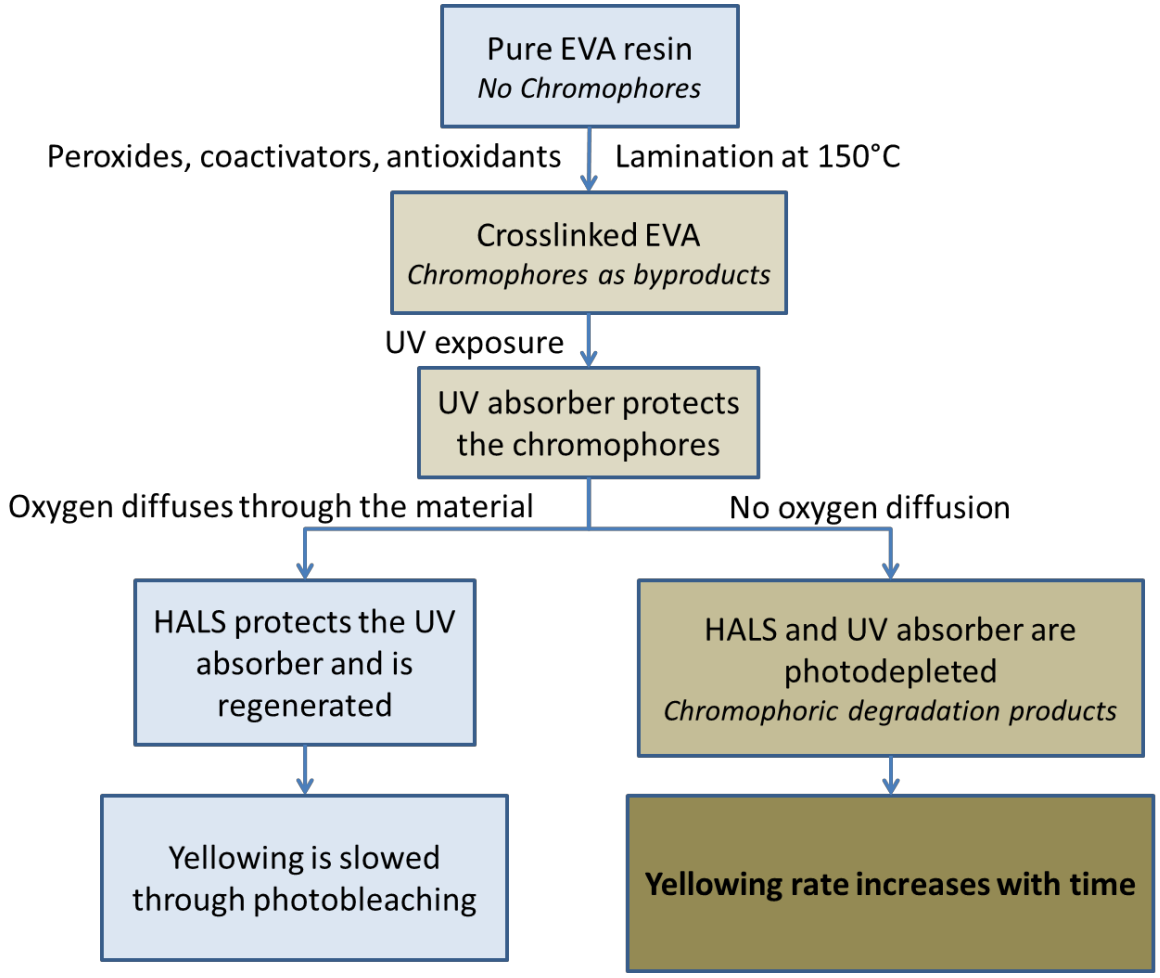

Fig. 1: Schematic diagram of degradation pathways of the yellowing process in an EVA-encapsulated PV module.

2.2 PV module failure modes related to material interactions

Many common PV module degradation modes are not the result of a single external stressor, but a combination of external stressors such as UV, humidity, temperature, and/or wind gusts. Internal factors such as the combination of the different materials used in a PV module may also affect the kinetics of degradation and the activated pathways [29], [30]. It is not only that certain module materials are incompatible with each other, but also that degradation by-products, such as acetic acid produced due to hydrolysis of the EVA encapsulant, can strongly influence individual degradation modes and pathways, for example interconnect or screen printed silver gridline corrosion [31] or cell PID-s. This chapter discusses the influence of material properties, combinations, and incompatibilities on PV module failure modes. Material interactions on relevant PV degradation modes and pathways and the influence of the lamination process on the long-term reliability of PV modules are also discussed within this chapter.

2.2.1 Influence of encapsulant-backsheet combinations on PV module degradation modes

Having the encapsulant and backsheet function together is important for the durability of the module package. Degradation modes influenced by the details of these two components include discolouration that may lead to transmission losses, delamination that facilitates moisture ingress, and corrosion of the metallization which is influenced by moisture and acidity in the encapsulant, (e.g. acetic acid from EVA). Degradation of the antireflective coating of the solar cells has been observed in some cases. Finally, thermal coefficient of expansion and mechanical properties of the encapsulation must be compatible with the balance of the module design.

EVA has been the most frequently used encapsulant. Polyvinyl butyral (PVB) has been examined as an alternative [32]. Various ionomers and a broad range of polyolefins such as polyethylene also exist on the market that can provide features such as higher electrical resistance. Common backsheet constructions include an outer fluoropolymer-based layer for UV durability, an inner PET layer for electrical insulation, and an inner ethylene vinyl acetate EVA layer for adhesion. (e.g. TPE (Tedlar[polyvinyl fluoride]/PET/EVA). Variants may contain metal (typically aluminum) foils as a moisture barriers, or use of other UV stabilizing materials with the polyester layer such that an outerlayer fluoropolymer is omitted. Alternatively, glass may be used on the backside of the PV module, motivated by its vapour barrier properties as is commonly used with bifacial cells.

Performance of these materials may differ depending on how they are used. Vapor barriers, while useful for keeping moisture out, may also inadvertently keep reaction byproducts, developed under light or heat, inside the module. This may lead to increased corrosion or to blister formation.

Moisture ingress at junction box penetrations and at the edge of the module are also possible. While certain polymer encapsulants may in themselves have desirable properties, their interfaces with the other materials in the module package must be carefully examined. Conventional qualification testing (IEC 61215) may not sufficiently elucidate any of these possible field-failure mechanisms.

Delamination has been observed between the encapsulant and the backsheet and within layers of the backsheet. The backsheet section in Tab. 9 chapter 3.4 shows an example of blisters in the backsheet occurring in Sanyo modules fielded in Tucson, AZ [33]. When such blisters are observed it may be because there is a vapour barrier, such as aluminum foil, used as one layer in the backsheet. E.g. the CO_2 gas generated as a byproduct of crosslinking within the laminate cannot escape and the resulting pressure results in delamination and pockets appearing as bubbles or blisters.

Relative water vapour transmission rates are needed to understand the environment within a PV module. With the exception of the ionomer encapsulant, it can be seen in Fig. 2 that moisture generally transmits much more rapidly through encapsulants than through backsheets when measured at 85°C [16].

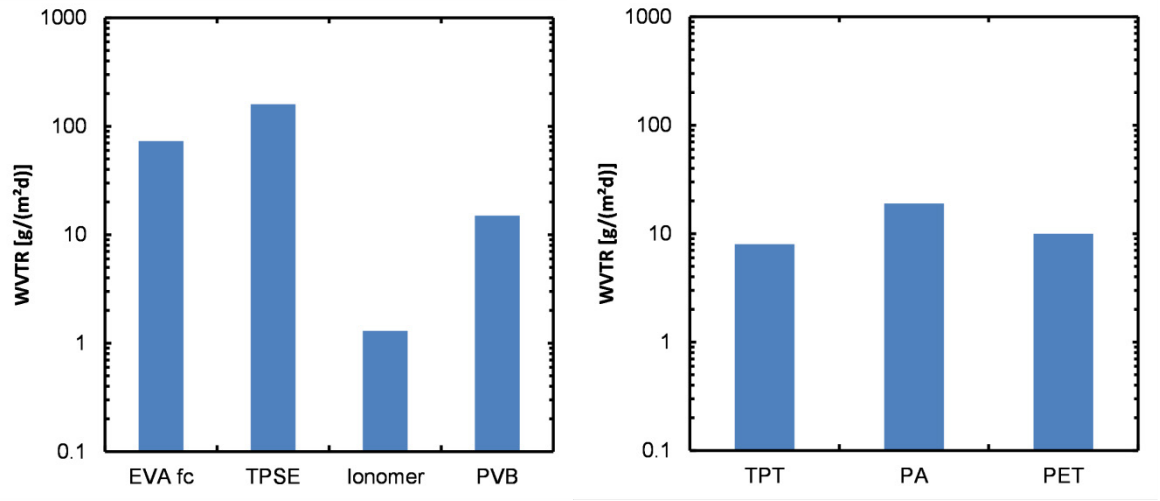

Fig. 2: Water vapour transmission rate (WVTR) through encapsulants, ethylene vinyl acetate (EVA), thermoplastic silicone elastomer (TPSE), an ionomer, and polyvinyl butyral (PVB), and through backsheets Tedlar-polyester-Tedlar (TPT) foil, a polyamide (PA) sheet, and a polyethylene terephthalate (PET) composite films. Adapted from [16].

Transmission of water vapour through the backsheet is nevertheless relatively rapid. In a one-dimensional calculation of moisture ingress into a glass/EVA/cell/EVA/backsheet structures, the concentration of moisture in the back-EVA as a function of time when exposed to constant environmental conditions starting with an initially dry specimen, is expressed as

$$C(t) = C_0(1 - exp(-WVTR_{backsheet}\, t/C_{sat,EVA}\, d_{EVA})), \qquad (1)$$

where C_0 and $C_{sat,EVA}$ are the initial and saturation concentration of the EVA and d_{EVA} is the EVA thickness. If d_{EVA} = 0.46 mm, $C_{sat,\,EVA}$(27°C)=0.0022 g/cm^3 the time in days to reach 50% of saturation is in Florida, USA for Polyvinyl fluoride (e.g., Tedlar), PVF = 0.0741, poly(ethene-co-tetrafluoroethene) (e.g. Tefzel), ETFE = 0.223, PVF/Polyester = 0.457, and PET = 1.78.

In PV modules, an important question is the rate at which the moisture arrives at the front of the cell and contributes to corrosion damage of the screen-printed Ag cell metallization, the interface with Si and other metallization such as the solder bonds. Using a 1-D model for the lateral transport of moisture and a finite-element analysis using meteorological data from Miami, the concentration of dissolved water as a function of distance from the edge is shown in Fig. 3. This analysis is for a glass/glass module construction, recalling that moisture ingress through backsheets is much faster.

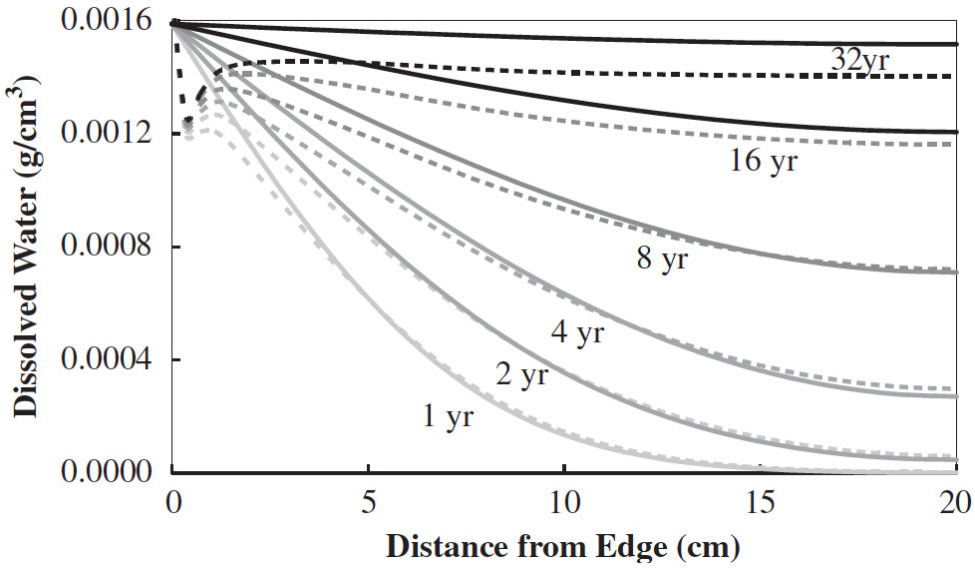

Fig. 3: One-dimensional model of moisture ingress in double-glass laminate construction using EVA. Solid lines and dotted lines are achieved at using two different methods. T = 27:1 °C and RH = 71.2% (the average conditions for Miami) [34].

Simply using moisture barrier materials is insufficient because issues such as adhesion and transport of moisture at interfaces and openings must be considered. Mobil Solar/ASE America type 300-DGF/50 modules produced for a period of several years around 2001 have frequently been seen in the field exhibiting delamination, Fig. 4. These are glass/glass construction and from the literature and visual inspection, these modules had a specific ionomer encapsulant [35] that has proven to have insufficient adhesion. Delamination occurred frequently over the junction boxes and at the edges. Corrosion in these modules was facilitated by delamination, which permitted direct exposure of cell materials to moisture, in the form of liquid water, from the environment. It can be seen that glass/glass construction does not necessarily eliminate moisture ingress into the modules, which can also be understood in view of the results in Fig. 3.

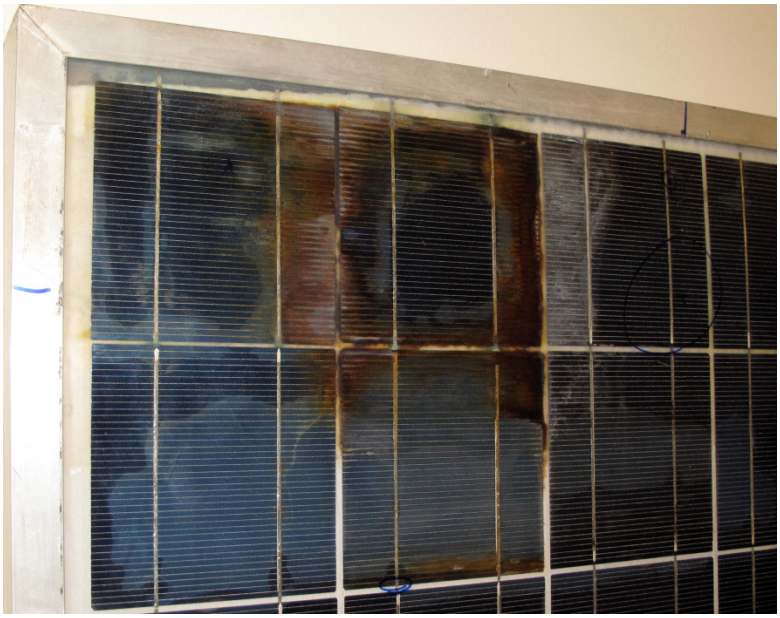

Fig. 4: Glass/glass module with specific ionomer encapsulant type that has proven to have insufficient adhesion, showing delamination and corrosion.

2.2.2 Lamination process related quality issues

Currently in the PV market, EVA is undoubtedly the dominant encapsulant material in use. Thus this chapter is focused on the typical lamination process of c-Si PV modules with EVA encapsulant. For EVA encapsulants, the PV modules are typically laminated on flat-bed vacuum-bag laminators. Different laminator manufacturers provide various designs to achieve high production throughput and good quality control, such as large-area laminators, stack laminators, multiple-stage laminators, etc. Yet, they all share the same working principle.

Both the selection of packaging materials and the lamination process are crucial for the reliability of PV modules. Compared to the packaging materials, the effect of the lamination process is relatively poorly studied. In the relevant field of research, especially among module manufacturers, the focus is commonly on the evaluation of the effect of the lamination process on the encapsulation quality of PV modules. Yet, there are not many publications that intend to prove, either qualitatively or quantitatively, the dependence of the module reliability on the encapsulation quality.

After module lamination, the manufacturers generally perform a series of technical control evaluations to ensure the production quality of PV modules. From those controls, they obtain the following quality factors that are used to judge the quality of the manufactured series of modules:

- Gel content
- Adhesion strength of the neighbouring module components
- Voids formation
- Cell breakage
- Cell/interconnection swimming
- Glass breakage
- Visual defects (discolouration, milkiness, …)
- Residual thermal stress

Those encapsulation quality factors are influenced by one or multiple steps of the module lamination process. There are essentially 3 steps in PV module lamination, namely the preheating step, the curing step and the cooling step. The 3 steps are all crucial for the resulting module encapsulation quality.

At the start of the lamination process, the module layup is placed into the lower chamber of the laminator automatically or manually. During the preheating, the layup is heated gently from room temperature to about 60-80 °C with the heating rate of ~5-10 °C/min. While it is heated up, both the lower and the upper chamber is evacuated to ~ 1 mbar. The purpose is to remove the trapped air within the module layup. There are several problems that could occur if an inappropriate preheating process was adopted. Glass warpage could occur in the case that the layup is placed onto the heating plate directly, without short metal pins acting as lifters. If that occurred, the cell and interconnection may swim in the laminate due to premature and non-uniform softening or melting of the EVA films. The use of pin lifters can also alleviate the probability of glass breakage upon membrane pressing by providing better control of the EVA film softening and melting. At the end of preheating, the EVA encapsulant has to overcome its melting/softening temperature. If the preheating is inadequate and the membrane is pressed down before the EVA is softened, the probability of cell breakage is increased due to the mechanical stress transmitted through the EVA. Schulze et al. [36] showed that the EVA is softened above 60-70 °C, and after that its stiffness can drop by nearly one order of magnitude. Felton [37] shows that the probability of cell breakage is also affected by the cell thickness. Another problem may be the loss of additives occurring during the preheating. It was shown by Li [38] that at 80 °C the silane adhesion promoter already escapes from the EVA. This suggests that a excessively long heating time will cause the loss of significant amount of additives like silane primer. This leads to poor interfacial adhesion strength in the PV module.

One major function of the preheating step is to evacuate the trapped air within the module layup. If the evacuation is insufficient, the entrapped air will not leave the layup fully. This will lead to the formation of air pockets in the laminated module. The air pocket is located at the interface of the neighbouring module components. It is an aesthetic defect and may lead to further delamination during module deployment. In the malfunctioning laminator, the membrane may press onto the module layup unintentionally during the preheating. This can be due to the membrane material problem or the inefficient pumping in the upper chamber. The early membrane press during preheating can cause the poor air evacuation and result in the formation of air packet in the module. The preheating step is also capable of removing the pre-absorbed moisture in the packaging materials including EVA, especially in the case of poor storage condition. If the preheating is too short, the moisture cannot be removed sufficiently and will then contribute to the formation of voids in the laminated PV module, as discussed in [39].

After the preheating step, the metal pins are retracted and the module layup contacts the heating plate. After that, the lower chamber maintains the vacuum level while the pressure in the upper chamber ramps up to typically 1 bar. This effectively results in 0.1 MPa (1 bar) membrane pressure applied onto the module layup. The pressure improves the heat transfer from the heating plate to the layup and leads to faster heating rate of the layup. Its temperature ramps up quickly from 60°C-80°C to the desired curing temperature ranging from 140°C to 170°C, depending on the formulation of the EVA encapsulant. The major objective of the curing step is to allow the EVA to be cured to the required gel content. The curing reaction is influenced by the curing agent/co-agent used in the EVA, the temperature and the time. The curing of EVA encapsulant starts at the onset temperature of about 110-130 °C.

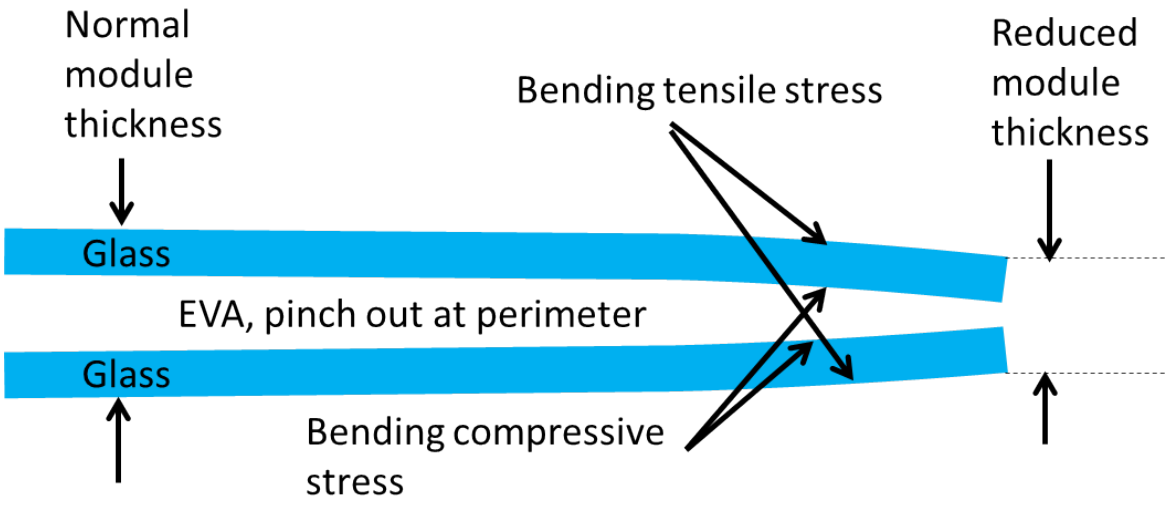

Fig. 5: Sketch on a module with "lamination pinch-out" and the resulting stress in the module. Image redrawn from [40].

A lamination pinch-out at the module edge occurs as a result of the stress concentration at the module edge from the rubber membrane, as shown in Fig. 5. This leads to the bending of the outer skin that is in contact with the membrane during the curing step. In the case of a glass-glass module, the upper glass is observed to be bent at the edge after lamination. This results in very high local stress around the module edge. Cording [40] calculates that the stress from the lamination is 50% of the design modulus of rupture for annealed glass. This greatly enhances the probability of glass breakage during lamination or the module deployment, considering the additional load that will be applied like wind or snow load. Moreover, the bent glass has the tendency to return to its original shape after lamination and results in a large peeling stress between the glass and the EVA. This will cause encapsulant delamination. Once the delamination takes place, with

the help of moisture and other stresses, it will start to propagate towards the module centre. Furthermore, in both glass-glass and glass-backsheet modules, the lamination pinch-out causes a reduced encapsulant thickness along the module edge. To solve this problem, it is recommended to apply proper frames around the module during lamination. The framing should be placed close to the PV module and as thick as the module layup.

For a given EVA encapsulant, the degree of cure is determined by the temperature and the duration of the curing step. The desired gel content is at least 70% or 80%, depending on the materials and manufacturers. If the temperature and the duration are poorly controlled during the lamination process, the EVA can be either under cured or over cured. Both conditions have detrimental effects on the module's reliability, which will be detailed in the following section. Under cured EVA can lead to additional encapsulation quality problems. The formation of voids (or air pockets) in the EVA layer can occur during the module cooling step. This occurs mostly at the edge and the corners of glass-glass modules. It is due to the evolution of the dissolved volatiles in EVA or local material shortage [39]. The under cured EVA also contains large amounts of unreacted peroxides, which may accelerate the degradation of EVA during field deployment. Moreover, the under cured EVA leads to insufficient adhesion strength between EVA and neighbouring module components and can exhibit haze (ASTM D1003-13) five times higher than the fully cured EVA [41]. For certain EVA encapsulants, this could lead to visible milkiness in the modules. The over cured EVA can also lead to other encapsulation quality problems. Voids can be formed in the EVA layer as a result of the excessive amount of volatile organic compounds (VOCs) released in the curing reaction. An ultra-long curing step leads to the formation of photo-excitable chromophores that results in accelerated discolouration of the EVA encapsulant during the module aging [2], as previously explained in Section 2.1.2. Also the higher stiffness in the over cured EVA increases the stress level of the thermal stress and the stress under mechanical loading [36].

Insufficient flow of EVA encapsulant may occur due to either a too low lamination temperature or too short curing time. This leads to incomplete wetting of the EVA on the surface of the neighbouring components, especially the cells and the interconnections due to their complex surface geometries. This poor wetting will cause the formation of voids at the interface. It will also cause deterioration of the adhesion strength between the EVA and other module components. In the case of an unnecessarily high lamination temperature, a few encapsulation quality problems may occur. The curing reaction progresses so fast that the EVA crosslinks and becomes too viscous before it completely wets the surfaces. Furthermore, the residual thermal stress in the module, after cooling down to room temperature, is proportional to the lamination temperature. Eitner et al. [42] showed that in the cooled module, the backsheet stays under tension, while the cells are subject to compression. The neighbouring cell gap is also reduced by 175-130 µm when the module cools down from 150 °C to -40 °C. This means higher lamination temperatures will increase the residual thermal stress in the module and pose threat to the cells and interconnections during field deployment.

After the curing step, the lower chamber is vented to 1 bar. After that, the module is removed from the curing chamber and cools either uncontrollably in the air or in a controlled cooling press. The temperature - pressure - time (T-P-t) profile of both processes are shown in Fig. 6.

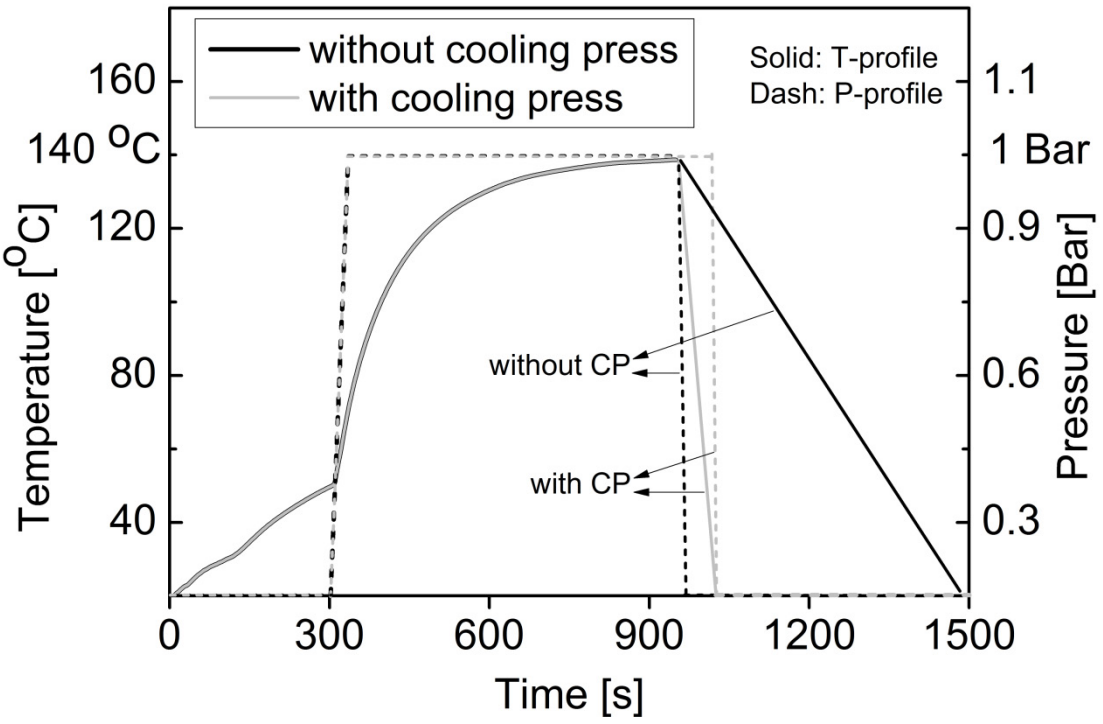

Fig. 6: Temperature and pressure profiles of the EVA encapsulation process of PV modules with cooling in air and accelerated cooling under pressure.

The differences between both cooling processes lie mainly in the following two aspects: i) a higher and controlled module cooling rate; ii) application of a controlled 0.1 MPa (1 bar) pressure throughout the module cooling process. EVA is a nearly amorphous material with a small degree of crystallinity. The difference in the cooling rates will definitely influence its resulting crystallinity and other material properties. Thus, the encapsulation quality of the modules is also affected by the cooling step in the following aspects. Li shows that by applying pressure during cooling and using a higher cooling rate, the residual normal stress in the Si solar cell in the encapsulated module after cooling can be reduced by as much as 22±2 to 27±3% depending on the EVA gel content [43]. The peeling strength between the EVA and the glass can be enhanced by over 10%, thanks to the application of pressure during cooling [43]. Due to the quenching of the growth of the crystalline phase in the EVA, the haze of the EVA is reduced by 50% when the accelerated cooling is applied [44]. However, as the crystallinity is low in any case, there is no clear effect on the total transmission through the EVA encapsulant. In the case of air cooling, during the cooling step, the module temperature can remain at or above the onset temperature of curing reaction for 1-5 mins. During this time, the gel content of EVA can further develop. Thus the cooling step also has an effect on the EVA gel content, which is more pronounced for under cured EVA.

2.2.3 Influence of the lamination process on the reliability

Currently there is a lack of literature that establishes the quantitative relationship between module quality and module reliability. However, there exists a qualitative description of how the encapsulation quality factors could affect the module reliability. Several studies have investigated the influence of poorly crosslinked EVA in PV modules on the long-term reliability of PV modules. At NREL several studies on the creeping behaviour of uncured or partially cured EVA in PV modules was done [45]–[47]. They found that even PV modules with uncured EVA are not likely to creep significantly in most environments and mounting configurations, partially due to post-crosslinking of EVA during operating conditions, partially due to temperature gradients over the

PV module with colder zones at the edges of the PV modules restraining creep. Post-crosslinking of EVA under operating conditions was also found in another study [48], [49]. They also found that poorly crosslinked PV modules with degree of crosslinking values below 50% showed discolouration of the soldering ribbons in the middle of the cells after exposure to accelerated aging tests. In contrast, all test modules with high degree of crosslinking values above 80% did not show any discolouration effects at the ribbons. These discolouration effects observed with the modules with short lamination times upon accelerated ageing can be explained by the surplus of still reactive peroxides in the modules which can react either directly with the surface of the soldering ribbons or with degradation products of the EVA like acetic acid and subsequently lead to a corrosion of the soldering material. Surprisingly, for none of the modules investigated by Hirschl et al. a relevant change in the electrical power output could be detected after the various ageing treatments, although optical changes on the backsheet and the connector ribbons surfaces were observed. This is in good agreement with findings from Morlier et al., who reported that the curing state of EVA influences the material's stability towards oxidation when exposed to damp heat ageing [50]. Materials with high amounts of curing agents showed lower stabilities [51]. Nevertheless, the decrease of the module performance over testing time did not depend on the initial degree of crosslinking. However, a recent study investigated the correlation between the crosslinking conditions and potential induced degradation effect in crystalline silicon PV modules. They found that PV modules encapsulated by EVA with higher degree of crosslinking showed lower susceptibility to PID due to higher volume resistivity [52]–[54].

Novoa [55] developed a model that can evaluate the debond energy and the debond growth rate in function of *T* and *RH*. They showed that lower EVA elastic modulus due to under curing will lead to lower debond energy and higher debond growth rate. This suggests the higher probability of delamination for under-cured EVA [56], [57]. Jensch et al. [58] showed that the phosphite-containing UV absorber can react with silane to produce silanephosphate during the lamination process. A long lamination process can lead to poor initial adhesion between EVA and glass. Novoa [55] also showed that very high elastic modulus of the over-cured EVA may sharpen the debonding tip, reducing the ability of EVA to accommodate the stress, and thus lead to higher debond growth rate.

In some cases, cell swimming (lateral motion) during lamination can cause short circuits between the neighbouring cells. In this case, a significant loss in the module power output is immediate. Cell/string swimming results in additional stresses in the interconnection and the cell. This will cause higher probability of interconnection failure upon cyclic thermal stress and harm the module reliability. Furthermore, the cell swimming is also regarded as a visual defect of the modules.

Voids are categorized into 2 types: Type-I the air packet located at the interface of the neighbouring components; Type-II the voids located solely inside the EVA encapsulant layers. Both void types arise from different causes during the module lamination. Their impacts on module reliability are also different. The Type-I voids are often large in size, above 1 cm in diameter. If they are located at the front-side of the PV cell, they will reduce the incident light arriving at the cell front and hence the module power output. The Type-I voids also act as a reservoir for in-diffused moisture and accelerate the delamination initiating from the voids. They will accelerate the hydrothermal degradation of the packaging materials and the cells. Dhere et al. [59] showed that the formation of Type-I voids also accelerate potential induced degradation (PID) of PV modules. The Type-II voids are typically smaller, with diameters of about 1 mm. They are embedded inside the EVA encapsulant layer. If a high concentration of this kind of voids are formed at the cell front, the short-circuit current and the power output of the module is expected to be lowered. Yet, in the case that the density of the voids is low or the voids are not located on top of the cells, the effect on the module electrical performance is immeasurable. The Type-II voids themselves pose small risks for module reliability, especially when the EVA is cured sufficiently. Li [60] showed that there is no impact of the Type-II voids on the module reliability in the 3000 hours of damp heat test. In modules with under-cured EVA, under conditions like damp heat, the combination of moisture

ingress and the lower viscosity of EVA at elevated temperature allow further growth of the Type-II voids. When the voids grow to contact the interface of EVA with neighbouring components, they will accelerate the delamination and harm the module reliability.

The mismatch of the coefficients of thermal expansion for different module components is the origin of the residual thermal stresses in the laminated module. At the curing step, the module components are in a nearly stress-free state. When the module is cooled down to room temperature, as the materials contract differentially, the residual stresses start to build up inside the module. The thermal stresses are normally invisible after lamination. Only in the case of glass-backsheet modules, as the backsheet contracts more than the glass, the whole module bends towards the backsheet. This leaves the glass in the contraction and bending stress and the backsheet in tensile stress. At the module edge, there will be stress perpendicular to the glass/EVA interface and act as a peeling force. In this case, the high thermal stress can cause the initiation of the delamination from the module edge and undermine the module reliability. The author in [61][62][42] studied thermal stresses in laminated modules. Eitner et al. [42] finds out that the cells exhibit the lowest coefficient of thermal expansion (CTE) and consequently stay under compression with up to -74 Mpa stress at -40 °C. The high stress at the cell/EVA interface could lead to cell cracks causing module reliability problems under mechanical loading and make cells more prone to snail trails. These high residual stresses can also cause delamination at both glass/EVA and cell/EVA interfaces and harm the module reliability.

2.2.4 Materials and potential induced degradation

To better understand the cause of PID effects it is good to consider the PV system, panel, and cell level separately. On the module level, the strongest factors influencing PID are the interaction of the encapsulation material, glass, and frame resulting in certain electrical leakage current paths. Furthermore, material properties, production processes as well as module layout contribute to the occurrence and rate of PID-s, see [1].

When using EVA as an encapsulant it was shown that backsheets with presumably high acetic acid permeation rates (AATR) reduces the sensitivity to PID-s and yellowing [17], [22]. Not only acetic acid itself, but also moisture ingress after delamination of PV modules, in turn leads to corrosion of metallic contacts and increase in series resistance (R_s) [63]. Therefore, laminate design in terms of composition of different materials has a strong impact on PID-s induced cell degradation.

Properties of the encapsulant, such as its polarity, volume resistivity or water vapour transmittance rate (WVTR), strongly influence the PID-s effect. As the sodium from the glass has to move through the encapsulant, there is a strong influence of the type of encapsulating material on this ionic current flow. Therefore, one possible way to reduce PID-s effects caused by ionic current flow through the encapsulant is to choose the most suitable encapsulating material. EVAs with high volume resistivity guarantee strong PID-s resistance [64], since higher volume resistivity reduces ion mass transfer from the front-side glass to the PV cell, which results in a less conductive encapsulation material and a lower leakage current [65]. But, high temperatures reduce the resistivity of EVA and seem therefore to be a critical factor [64]. Furthermore, PID-s is significantly enhanced by the presence of acetic acid which eases the transport of Na^+ from glass to the cells [18], [19]. However, if material substitution is to provide protection against PID-s effects, than the key parameter is its volume resistivity. Also, one should identify materials with low WVTR since moisture ingress needs to be reduced. In fact, other encapsulants that can be considered as an EVA alternative have been proposed, such as: PVB, TPU, TPO, silicone or ionomers. But, regarding polarity, water vapour transmission rate (WVTR), optical, and electrical properties, polyolefins and ionomers are the most promising materials which can overcome PID-s related problems [65], [66]. However, ionomer is normally used as a blocking ionic diffusion layer between glass and EVA and not as a substitutive encapsulant material [65] since it is claimed to fully suppress the PID-s effect by capturing the ions [19]. By comparison, several studies on new polyolefin based encapsulants

showed that lower polarity and lower WVTR values in combination with the absence of acetic acid (in respect to EVA) can suppress the PID-s effect totally [18]–[20]. An overview of volume resistivity of some encapsulant materials is shown in Fig. 7 and can also be found in the work of Berghold and co-workers [67].

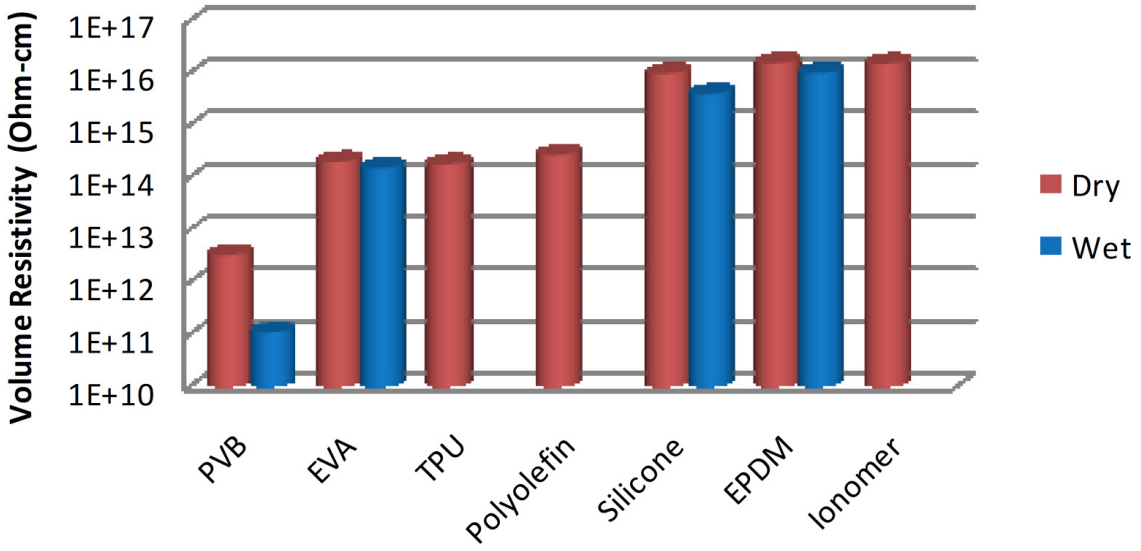

Fig. 7: Volume resistivity measured using alternating direct current (DC) polarity +/- 700V. "Wet" samples are immersed in water at 40°C [68].

Environmental factors such as humidity and temperature also influence the PID-s effect. Humidity forms a film on the front glass, which becomes electrically conductive after a percolation threshold of about 60% connectivity has been reached [69]. Possible sources for moisture ingress were already discussed above (delamination, reduced adherence in between anti reflective coating (ARC) and glass …). The effect of temperature on PID-s effects, on the other hand, is kind of peculiar. Some experiments [70] showed that increased temperature not only leads to faster PID-s because of increased leakage current, but it also plays an important role in the regeneration process in a panel. Activation energies for recovery processes have been estimated to 0.7 eV [71]. However, temperature is indirectly influencing PID-s effects since other failure modes that are leading to PID-s effects (delamination, corrosion, hot spots, bubbles, as well as permeation of water, acetic acid and atmospheric gases …) are temperature dependent processes.

2.2.5 Materials and Snail Tracks

Snail Tracks (also called Snail Trails) are a visible defect which is caused by discolouration of the silver paste of the front side metallization of silicon solar cells. In a PV module the effect looks like a Snail Track and it occurs at the edge of the solar cell and along usually invisible narrow cell cracks. The discolouration itself is reported to have no influence on the performance of the PV module. But the cell cracks, visualized by the snail tracks, can reduce the PV module power.

In several studies it was shown that the choice of EVA via its additive composition and the type of backsheet determines the susceptibility or resistivity to snail-track formation [72]–[74].

Meyer et al. report that water vapour coming through the backsheet is claimed to dissolve silver particles which migrate into the encapsulation on top of the grid finger, where a chemical reaction within the encapsulant film results in the typical observed colouring. Mini-modules encapsulated with an EVA containing a high level of silicon containing additives (silane based adhesion promoter) were consistently protected against the development of snail trails. Phosphite containing additives (peroxide decomposers) on the other hand increased the susceptibility [72], [73].

Recently Kim et al. [74] proved this discolouration happening due to the formation of silver acetate, where silver acetate was synthesized by silver carbonate originating from the reaction of Ag ions and carbon dioxide and acetic acid that originated from the degradation of EVA.

2.2.6 Materials and corrosion of interconnection and silver grid

One major concern for durability of PV systems is corrosion of the metallic components within a module since this can reduce the power output by increasing the series resistance of the electrical interconnects [75], [76]. Since corrosion is known to be accelerated by the presence of water, the characteristics of encapsulants and backsheet materials with respect to moisture ingress and corrosion are becoming more and more important for the long-term durability of PV modules [77]–[80].

Therefore, the importance of the permeation properties of encapsulants and backsheets, as well as design of PV module (materials) were already studied by several authors [15]–[17], [79], [81], [82]. Increased corrosion of solder on the silver busbars of the silicon cells was observed near delamination and near cell edges, due to higher availability of water vapour.

Degradation of ethylene vinyl-acetate (EVA) may accelerate metallization corrosion in different ways [83]. During degradation of EVA, acetic acid is released which may lead to a corrosion of the solder bonds, which is visible as green Cu acetate patterns [84]. The acid has corrosive effects on cell metallization and the cell interconnect copper core and its tin coating [77]. The copper core causes a brown discoloration of the EVA when it is directly exposed to EVA. Metallization corrosion leads to an increased series resistance and therefore to losses in module performance [2], [12], [15], [16], [63]. Due to the long diffusion paths from the encapsulant to the backsheet, acetic acid can accumulate in front of the solar cells and lower the pH value leading to even faster corrosion [15], [17].

2.2.7 Materials and delamination

The primary function of the EVA is to serve as the structural adhesive in the PV module. Thus, poor EVA adhesion with other module components weakens the structural integrity and the mechanical strength of the PV modules, which impairs the module reliability upon mechanical loading. Yet, currently, there is no quantitative requirement on the minimum adhesion strength of each interface in the PV modules. The adhesion strength is prone to the stress like moisture, heat, UV radiation and chemical interactions.

Delamination and cracked cell isolation are relevant failure modes for long time field exposures of PV modules, leading to power losses higher than 10% according to Fig. 3.1 in [1]. However, delamination has also been reported in 5% of the failures of PV modules recorded in the first two years after delivering [85], presumably due to imperfect manufacturing.

Regarding the adhesion strength of EVA to other module materials, influencing the ability of the encapsulant to resist against delamination and provide optimal sealing, peeling tests by pulling the backsheet away from glass [86], or by pulling Titanium beams bonded to the glass with an EVA interlayer [55] have been proposed, possibly with different peeling angles. Inspection of the tested specimens shows delamination along the interface between the encapsulant and the glass with a resulting rough surface [86], or also with delamination along the Titanium beam and the EVA interface [55]. From the diagram relating the peeling force per unit width to the peeling extension obtained from 90° peeling tests of a backsheet from a rigid glass substrate [86], insight into the adhesive behavior of the polymer can be developed.

UV exposure alone can also cause the loss of adhesion and subsequent delamination [58], [87]. Jentsch et al. studied the chemical origin of the loss of adhesion of EVA encapsulant under UV exposure. The decomposition of UV absorbers results in the formation of benzoic acid and a phenol product. This acid catalyses and accelerates the debonding of EVA from the glass. The author's

question whether UV absorbers and phosphide should be used in EVA encapsulants intended for long lifetime PV modules.

The thermo-visco-elastic properties of the encapsulant [88][89] also have an important role on the peeling adhesion, since the Young's modulus expressing the adhesive stiffness, E/h, is strongly temperature-dependent, see Fig. 8 from [88]. Experimental results in [55] also report that the critical crack opening for complete delamination is temperature-dependent. As a result of these dependencies, peeling tests in [55] and [90] show that the peel strength and also the adhesive energy G_c of the EVA/glass interface decays almost linearly from 25°C to 50°C, with a drastic drop for a temperature higher than 60°C, when the EVA becomes very soft, see also Fig. 8. Hence, for a proper evaluation of the adhesion between EVA and glass testing should be done at application relevant temperatures and not just at room temperature.

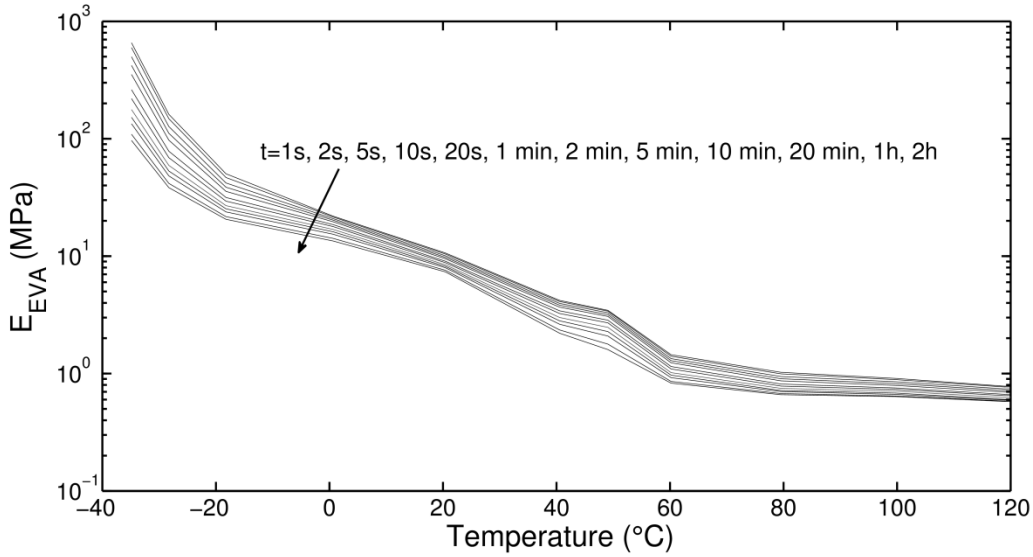

Fig. 8: The temperature dependency of the Young's modulus of EVA [88].

Exposure of the PV module to ambient moisture is also a reason for encapsulant degradation. EVA is permeable to vapour diffusion [34], [91] whose infiltration can cause oxidation phenomena on the solar cell surface and then significant power losses [92]. Moreover, the kinetics of debonding is also affected by ambient moisture with a decrease in the adhesive energy [93][55]. Peeling tests in [55] conducted at an ambient temperature of 30°C and with different relative humidity (RH) have shown failure at the Titanium beam-EVA interface with a reduced adhesive energy with increasing humidity levels.

2.3 Influence of failures on PV module power

The most important failure types of PV modules have been described in the previous TASK13 report "Review of Failures of Photovoltaic Modules" [1]. In this section models to describe the degradation rate of the modules caused by a certain failure mode are introduced.

In a PV module various parts are combined into one product. Even for equal parts like cell interconnect ribbons, solar cells and bypass diodes one has to expect a variation of initial quality of the parts. For some failure types, one part can lead to a full power loss or safety fault of the module. This is the case for connectors, cables, backsheet, junction box and glass. These parts may not only lead to power loss of the PV module, but also to a power loss of the whole string in a PV array. Other parts like the potting material, frame, cells, cell interconnect ribbon, string interconnect, bypass diodes and glass coating may fail partly without a total power loss of the module or

the PV module string. Furthermore, the bypass diodes are able to prevent a total power loss of a module, e.g. if a substring of the module is defect.

For this reason a full framework is needed to represent the power loss of PV modules. Thomas Friesen presented in the report of the "Performance Plus" project such a framework based on a one diode model [94]. The easiest way is to simulate the module with an electrical model and describe aging mechanisms for each part of a component. Fig. 9 shows such a framework. The elements of the framework should have a distribution of initial values to cover realistic conditions. To represent the distribution a Monte Carlo simulation with the distribution of initial values can be done.

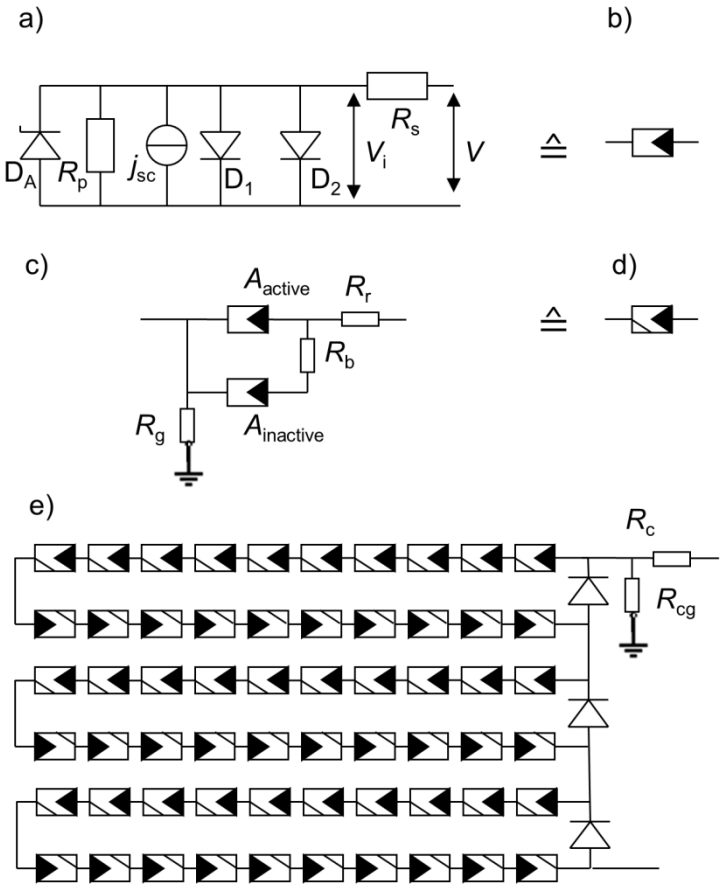

Fig. 9: Electrical framework for aging modelling of PV modules.

In the literature various aging models for module components are described. These can be used to model the behavior of parts of the framework. Aging mechanisms influencing the light intensity can be modeled by reducing the initial current j_{sc} of the current source in the cell. The aging of cell interconnect ribbons result in an increase of the ribbon resistance R_r. Cell breakage effect the break resistance R_b and the parallel resistance R_p of the cell. A potential induced degradation affects also the parallel resistance R_p of the cell.

Besides material parameter and material dependent aging models input parameter for the climatic conditions are needed. For modeling of PV module failure in many cases the knowledge of the internal loads like temperature, chemical conditions, radiation, and mechanical loads in/on the PV module are needed. These can be measured or taken from publications on typical climatic zones as reported by Herrmann [Herrmann11]. One very important part is to convert the external loads to internal loads of the module. Koel et al. describe a method how to calculate the module temperature depending on the temperature of the environment, the insolation on the module and the wind speed [Koehl11], see also part 2 of the energy rating standard IEC 61853-2:2016

[IEC61853-2]. With these methods the external loads can be transferred into a module temperature. Furthermore, a variation of initial material parameters has to be known to start the simulation. The variation can be implemented by a Monte Carlo simulation.

In the following chapter the aging of material parameters are described for several degradation mechanisms.

2.3.1 Influence of EVA browning on PV power

According to the previous observations from chapter 2.1.3, the relevant parameters for a model prediction of the yellowing of EVA in a PV module are numerous: the concentration of peroxides and antioxidants in the EVA compound, the temperature profile and the length of the lamination process, the transmission of the module glass front panel in the UV range, the intensity of the sun irradiation, the temperature of the module, the size of the cells, and the permeability of the polymer backsheet or edge sealing [95], [96]. The power loss caused by the yellowing also depends on the quantum efficiency of the cells in the spectral range of the absorption of the chromophores. The module parameter affected by the yellowing of the encapsulant is the short-circuit current density J_{sc}. The short circuit current is expressed as the integral of the product of the external quantum efficiency (*EQE*) and the incident light spectral intensity $I(\lambda)$ reaching the cells over the absorption range of the solar cells [97]:

$$J_{SC} = q \int_0^\infty I(\lambda) EQE(\lambda) d, \qquad (2)$$

where q is the elementary charge and λ the wavelength. Thus, considering the external losses, the absorption of the encapsulation $A(\lambda)$ in front of the cells, and the reflection of the incident light on the front panel $R(\lambda)$ of the modules, the short circuit current is expressed as:

$$J_{SC} = q \int_0^\infty I(\lambda)(1 - R(\lambda) - A(\lambda)) EQE(\lambda) d. \qquad (3)$$

Thus there is a linear correlation between the photocurrent generated at a given wavelength and the absorption of the EVA at this wavelength. To our knowledge there is no model which describes the evolution of the absorption of the encapsulant $A(\lambda)$ as a function of the aforementioned influencing factors.

EVA discolouration is a continuous changing failure over the modules service life. Some modules show a faster, other a slower yellowing process.

Obvious browning is the sign that a module started to degrade; modules showing a slight browning may not show detectable power losses. Typically, mean yearly degradation rates due to yellowing are about 0.5%/yr [1] and may reach up to 1%/yr in hot and humid or moderate climates [98]. Nevertheless power losses of up to 10%/yr have been observed for mirror enhanced photovoltaic modules installed in desert environments [5]. Some studies [99], [100] report constant degradation rates while others suggest that this degradation rate increases with time over larger time spans [101], [102]. This increase is due to the broadening of the EVA discolouration from only yellow blocking light at short wavelengths to the brown. Typically short circuit current losses of 10% are observed over the first decade of exposure for modules prone to yellowing [99], [100].

To sum up, the power losses induced by the yellowing of the encapsulant follow initially a constant loss rate and this degradation rate increases with time as the EVA absorption coefficient increases and more photo degradation occurs, leading to faster degradation.

It was suggested by Pern that the yellowing reaches a saturation value as the UV absorber that is involved in forming the chromophores is depleted over time (see 2.1.3) [5]. Although it has not been experimentally verified, and other systems with photo degradation do not show a saturation of the yellowing process [103], Pern suggests that the power loss over time induced by the yel-

lowing of the encapsulant follows a sigmoid curve showing an initiation phase, a linear decrease of power and ultimately a saturation as the yellowing reaches its maximum.

2.3.2 Influence of delamination on PV power

Delamination is an important cause of peak power loss in PV modules. It can occur at any of the interfaces within the PV module, e.g. glass/EVA, cell/EVA, silver gridline/EVA, ribbon/EVA, interlayer of the polymeric backsheet, etc. The major drivers for the delamination are the stress exerted at the interface from residual thermal stresses or from external mechanical stress applied on the module and the deteriorated interfacial bonding as a result of the attack from heat, UV and moisture. After delamination, new interfaces are created, i.e. glass/air and air/EVA in the case of glass/EVA delamination, EVA/air and air/cell front in the case of cell front/EVA delamination. The increase in reflection can be calculated using the Fresnel's equations. For the interfaces of glass/air and EVA/air, the interfacial reflectance is about 4%. This reflection loss causes a drop in P_{max} via the reduction of the short-circuit current [75]. Furthermore, the delamination is associated with other drivers of module degradation. Moisture diffusing into the EVA can condense in the delaminated region and accelerate the propagation of the delaminated region [34]. The delamination also forms a pathway for faster moisture ingress into the modules. When delamination occurs at the cell surface, corrosion of metallic components will take place by the moisture condensation, acetic acid produced by EVA and the oxygen arriving at the interface [63], [104]. Delamination can accelerate the moisture ingress and facilitate moisture condensation. Therefore, the corrosion is accelerated by the delamination.

Due to the optical loss and corrosion-induced series resistance increase, cells in the delaminated area will produce less current. This is the origin of current mismatch. If the mismatch is significant, it will trigger the bypass diode and cause further power loss of the PV module [105].

Park et al. studied a 25-year-old module with partial delamination and EVA discolouration [75]. They show that the main origin of the P_{max} loss is the current drop due to the increased reflectance by the air gap in the delaminated region and the reduced transmittance of the discoloured EVA. The total current loss in the part with delamination and discolouration is 3.8 times higher than those without. Van Dyke et al. investigate the cause of degradation of a field-deployed PV module based on EFG-Si [63]. Delamination and discolouration are observed mostly around the module edge. In the first 3 years of deployment, the module power P_{max} had dropped by nearly 20%, while the short circuit current I_{sc} drops by ~ 5%. The degradation is explained by the delamination, moisture ingress, and the subsequent corrosion on the electrical contacts in the module. The delaminated area causes cell mismatch and further results in local heating. The high temperature in the delaminated and discoloured area promotes faster moisture ingress, delamination, and corrosion. Sánchez-Friera et al. analyses the degradation of a PV system after 12 years of exposure [104]. A power loss of 11.5% is observed. It is found that the loss in module power P_{max} is mostly due to the loss in the short circuit current I_{sc}. They attribute most of the degradation to the delamination at the cell/encapsulant interface. This delamination further accelerates the degradation of the antireflective coating on the cell front and the corrosion of the metallic components contacting the cells. Moreover the delamination will cause a power loss due to the cell electrical mismatch in the module.

A number of studies have been carried out to develop a detection method for the delamination in PV modules. Sinha et al. [106] proposes a method and analysis based on pulse infrared thermography. This fast and non-destructive method is able to detect the delamination and estimates the delamination thickness. Voronko et al. utilizes both Pulse Thermography (PT) and Scanning Acoustic Microscopy (SAM) to detect the defects including delamination [107]. They show that the presence and position of delamination and voids can be detected non-destructively by both techniques. The SAM can offer better resolution on small defects.

Loss of adhesion and delamination can occur upon the exposure to heat and moisture [108][109] [110]. In the accelerated testing, the delamination is often triggered by damp heat. Wu et al. studied the reduction of peeling strength between EVA and backsheet in different damp heat test conditions [110]. They show that the peeling strength reduction depends strongly on the temperature and relative humidity of the test condition. A humidity dose model is proposed by assuming the surface relative humidity of the backsheet as the driving force and an Arrhenius-based model with the temperature as an accelerating factor. It is shown that the correlation between the peeling strength and the humidity dose follows an exponential model with activation energy of ~63 kJ/mol. Peike et al. studied in detail the degradation mechanism of the encapsulated c-Si solar cells after 2000 h of damp heat [84]. They show that both emitter and antireflective coating remain intact. The degradation is caused by the increased series resistance due to the corrosion of the solder bond and the gridline. More in-depth study shows that the entrapped acetic acid produced by EVA is responsible for the corrosion of the joint between the screen printed silver busbar or gridline and the cell surface as shown in chapter 2.3.5.

Due to the important role of moisture in the delamination process, studies have been carried out on moisture ingress into PV modules. Kempe et al. [34] used finite-element analysis to model the moisture ingress with actual atmospheric data. It shows that the moisture can ingress significantly into impermeable module packaging through the module edges during life time. The moisture in the module can condense and increase corrosion rates. Due to the residual shear stresses in the module, the condensed water is more likely formed at the interface between EVA and cell/glass. This could cause accelerated corrosion and enhanced interfacial delamination. The delamination will provide more rapid pathways for further moisture ingress. Meitzner and Schulze al. [111] point out that the determination of the moisture uptake for different PV encapsulants requires more care. The conventional method assumes the validity of the Henry's Law. However, for materials with significant interaction with the dissolved water molecules, it is no longer valid. They show that for materials such as PVB, the ENSIC model is more valid. This finding is valuable for the simulation of moisture ingress into PV modules. Park et al. [112] develop a degradation model for the degradation induced by moisture condensation (MC) in the PV modules. The moisture condensation often occurs in the field-deployed modules in certain climates. They show that the MC-induced degradation rate is 1.45 times compared to the damp heat degradation at 85°C and 65%rh. It is also shown that the MC frequency in the modules depends on the encapsulant type, where the polyolefin type shows much higher frequency than EVA and silicone.

Detection methods for the moisture distribution inside the PV module have also been studied. Carlsson et al. [113] developed a moisture-sensing technique by measuring the AC resistance of a porous TiO_2 film deposited on the glass substrate. It is proved that this sensor can use be used for measuring the moisture concentration in the aged PV modules. Rashtchi et al. [114] used FTIR to study the water absorbed in the EVA encapsulant. They find that the water molecule is not interstitially located in EVA, but they are bonded to one or two C=O groups by hydrogen bonding. They claim that this is a promising way of providing depth-resolved water concentration distribution in the EVA layer in PV modules.

Novoa et al. [55] developed a mechanics-based technique to evaluate the debond energy and growth rates in the function of temperature and relative humidity. They show that the debond energy decreases from 2.15 kJ/m^2 to 1.75 kJ/m^2 for the EVA/glass laminate when temperature rises up from 25°C to 50°C. The debond growth rate of EVA is enhanced by 1000 times with merely 10°C increase of temperature or 15% increase of RH. This shows that the delamination is accelerated by module temperature and moisture ingress. They derive an equation showing the debond growth rate in function of explicit debond energy, relative humidity, and temperature, based on a fracture kinetics model for the visco-elastic debonding in PV module. By the best of our knowledge there is no model in the literature describing the resulting power loss caused by delamination.

2.3.3 Influence of cell cracking to PV module power

Current modelling of the influence of cell cracking of crystalline silicon solar cells is based on determining the maximum electrically detached cell area caused by a cell crack. An electrical stimulation of the solar module reveals the expected power loss [115]. However, most detected cell cracks do not separate a cell part electrically from the cell, especially not for the whole service life of the PV module.

Paggi et al. reported [116] the mechanical stress of cells in PV modules with a PET front sheet. A compressive thermo-elastic residual stress builds up in the solar cells after module lamination. Therefore, solar cells cracked after the lamination stage tend to show low electrical resistances across the cell crack. The further application of mechanical bending induces a tensile stress state in the solar cells which, superimposed to the compressive residual stresses, progressively compensates them, and leads to an increase in the crack opening which finally induces electric insulation along the crack line. In electric models with a distributed series resistance [Breitenstein13], the effect of deformation on the electric response can be taken into account by the introduction of an additional localized resistance in correspondence to the point where a cell metallization finger intersects a crack, dependent on crack opening [117].

The important question is how long does a cell cracks need to separate cell parts electrically from each other. Käsewieter [118] showed in a bending test of module laminates that the silver front side metallization cracks immediately with the crack in the silicon. However, as the mechanical load vanishes the front side metallization reconnects nearly without any additional contact resistance. In contrast the aluminum rear side metallization does not immediately isolate with the first cracking of the silicon. The rear side metallization shows a fatigue cracking behavior. The electrical crack resistance increases slowly by the number of cycles. After a certain cycle the electrical contact through the back metallization shows a random contacting and isolation. To our knowledge it is not known which critical parameter influence the time of electrical degradation of the rear side paste along cell cracks.

A second aspect of cell cracks is rarely addressed in the literature. Cell cracks reveal along the crack path a defective silicon surface. Along this surface a drastically enhanced recombination current flows across the depletion region [119]. This recombination current can be described by an increased saturation current of the diode with ideality factor 2 for each cracked cell [120]. For simplification this parallel diode can also be simulated as parallel resistance. This recombination current reduces especially the low light efficiency of PV modules. If each cell in a 60 cell module is cracked and all cell cracks do not lead to an separated cell area, the power loss of the module is typically below 2.5 % of the nominal power at standard test conditions [115].

To our knowledge a model which describes the power loss depending on weather conditions is not yet available. Morlier et al. [Morlier15] set up simulation of the PV module power loss with the electrical framework for PV modules shown in Fig. 9, and a distribution of cell cracks measured in one exemplary PV-system shown in Fig. 10. However, the time and climate dependent evolution of the system power is simply modelled by a change in crack resistance. The time dependent influence of the climate on the crack resistance is not yet known. It is also not known which cell/module production factors influence how long the conductivity across a cell crack is sufficient for the power generation.

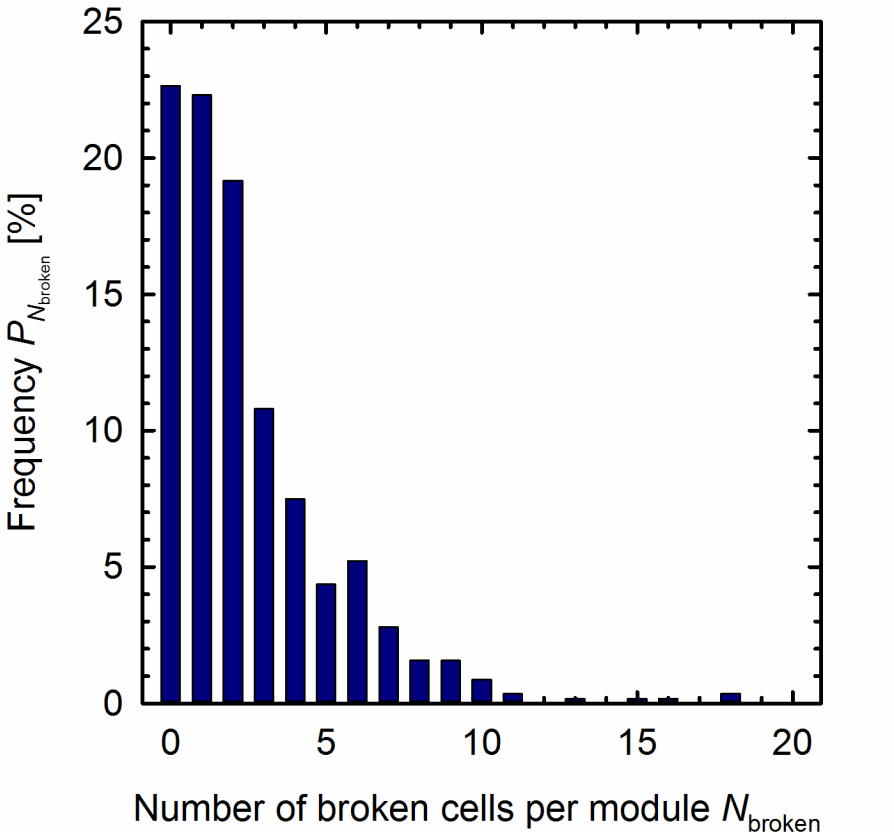

Fig. 10: Typical distribution of cell cracks per module in a PV-system.

Flash testing and two-diode model fitting of the dark I-V curve of modules undergoing cell breakage can be used to show fundamentally the causes of power loss. In a stress test involving mechanical loading, thermal cycling, and humidity freezing of 60-cell multicrystalline modules, I_{mpp} is found to degrade most severely among the flash test-determined parameters [121]. Using the metrics introduced by King [122], I_{mpp}/I_{sc} ratio decreases greatly, indicating degrading junction properties (shunt or recombination currents) and the effects of mismatch in current output of the cells. This is consistent with cell breakage, which causes both recombination pathways that defeat the cell junction and various extents of the active cell circuit area removal. To a lesser extent, but becoming more important with increased damage to cells, the V_{mp}/V_{oc} ratio decreases, indicative of series resistance.

With an approximate 10% relative decrease in module power when cell cracking is induced, series resistance increases modestly. This is best measured using a combination of light and dark *IV* curves [123] or light *IV* curves [124] at two intensities. Using such analyses, for the 10% module power loss, series resistance increase is 0.5 Ohm cm^2, responsible for a 2% absolute drop in fill factor and about 2.6% of the observed 10% module power loss. As the number of interconnecting bus ribbons increase on the cell, the series resistance and mismatch losses are reduced because the current collection ability is maintained to a greater extent despite the cell cracking.

Dark *I-V* curve analysis shows further the multiple mechanisms associated with the cell breakage. Due to fractures penetrating the cell junction, second diode parameters that describe the junction quality show degradation, ideality factor n_2 and pre-exponential J_{02} increase. First diode parameters associated with the minority carrier lifetime n_1 and pre-exponential J_{01} also increase, resulting from the creation of unpassivated semiconductor surface area at the new crack interfaces [121].

Typically PV systems are very inhomogeneously affected by cell cracks. Fig. 10 shows typical distributions of cell cracks over a PV system. Furthermore, isolated cell parts due to cell cracks de-

crease the current at the maximum power point. These two facts lead to a power loss in a PV system which is not equal to the sum of power losses of the single modules.

To simulate the maximum expected power loss due to cell cracks in a PV system one has to know the distribution of cell parts which might get isolated due to the cell cracks. This distribution can be measured by electroluminescence or UV fluorescence measurements [Koentges14]. For the distribution of isolated cell parts given in Fig. 11 a Monte Carlo simulation is done to calculate the expected power output distribution of strings composed of PV modules with this distribution of cell part isolations. The resulting worst case power distribution of 20 strings with 20 modules is shown in Fig. 12. This distribution should be asymmetrical. However, for medium cell crack occurrence like it is shown in Fig. 10 the resulting string power distribution can still be fitted by a Gaussian distribution. In the simulated case the mean power loss of the strings is about 12% after complete isolation of all cracked cell parts.

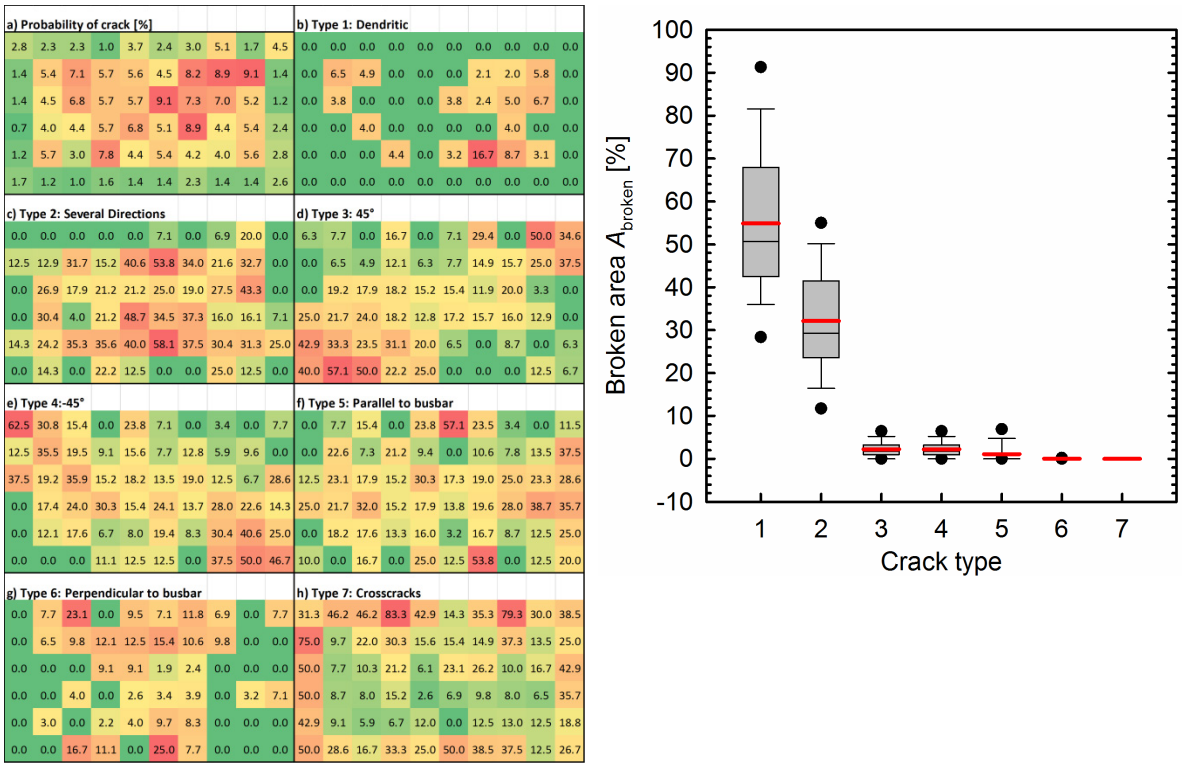

Fig. 11: The distribution of the isolated cell parts is described with these two graphs. The left graph shows the distribution of various cell crack classes over the measured modules. The right graph shows the distribution of the broken area for the seven crack classes.

Currently there is no method to identify if existing cell cracks will lead to a power loss or not. It may appear curious that PV modules with lots of cell cracks keep their power much longer than PV modules with only some cell cracks, because in the first case the cell cracks do not lead to high crack resistances, but in the second case the crack resistance increase within a short period and lead to a high power loss caused by only some cell cracks.

As already mentioned the development in the market tends to move to more than three busbars per cell or even to multi wire approaches. This will reduce the risk of power loss, because only small pieces can detach from their corresponding busbar. However, the current cells and the cell interconnection schemes reach high fill factors in the module. Therewith the I_{mpp} gets closer to the I_{sc}, and therefore already small detached cell pieces can cause a power loss. The allowed detached cell fraction $A_{inactive}$ without impact to the module power is given by the inequation [115]

$$\frac{A_{inactive}}{A_{total}} > \frac{(I_{sc}-I_{mpp})}{I_{sc}}. \qquad (4)$$

For a modern high efficiency module (*FF*~79%) this relation means that only ~5% of the total cell area A_{total} may be detached compared to former modules with much lower fill factor (*FF*~73%) where 8%-10% cell area loss has no effect on the module power.

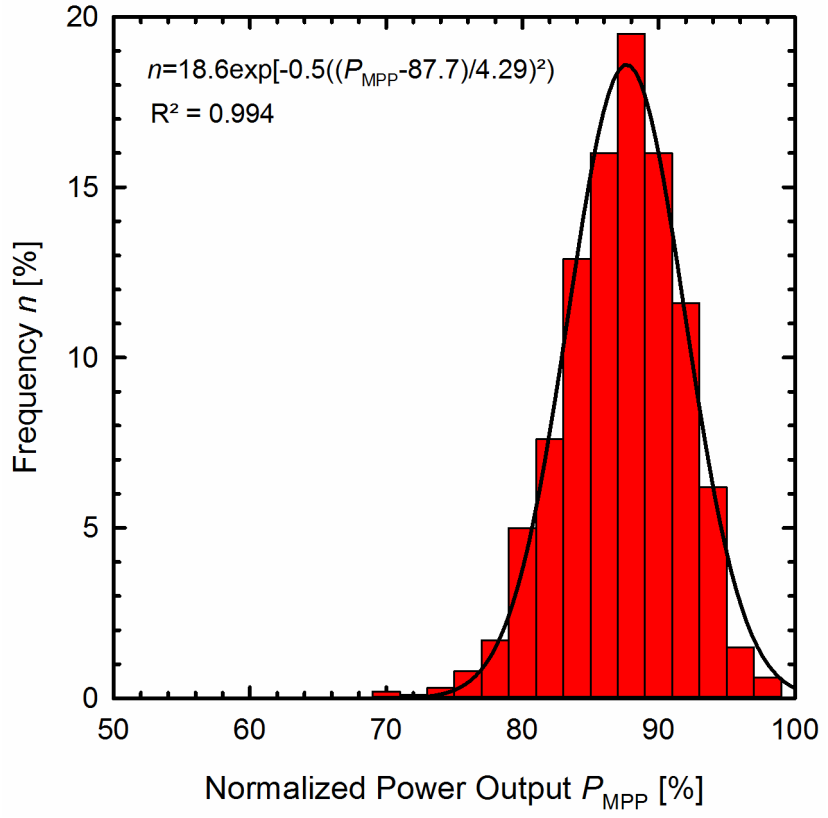

Fig. 12: Power output distribution of PV module strings with cell cracks. The power output is normalized to the power of a defect free string.

2.3.4 Influence of the potential-induced degradation by shunting on the PV power

The difference of potential between the cells and the support structure of the module drives a leakage current that can lead to a power degradation. We differentiate two failures modes for crystalline silicon cells, the PID-p (for **p**olarisation or **p**assivation) and the PID-s (for **s**hunting). The PID-p is a temporary and reversible degradation of the passivation layer which reduces the performance due to a surface recombination increase [125]–[127]. The PID-s is due to leakage current involving ionic flow of Na+ from the glass, encapsulant or cell surface into the cell, diffusing into silicon stacking faults and shunting the cell [128]. The sodium incorporation in the Si surface degrades primarily the *FF*, the V_{oc}, and lastly the I_{sc}. A part of this degradation is non-reversible, and another part is reversible with thermal treatments and/or reversal of the voltage bias between the active cell circuit and the grounded module face [129]. PID-s seems to be the main PID problem in the field due to the large market share of conventional n+/p silicon solar cells and is discussed in this section.

We previously listed factors influencing the PID-s effect in Table 6.2.1 in [1]. A complete model of the PID-s could contain more parameters than typically available. We focus in the following on a review on phenomenological models where parameters have to be determined from fully manufactured modules. There is no model based on material parameters of the module components

available in literature yet. There are empirical models that link the environmental stress to the *IV*-curve parameters of given modules.

In typical PID tests high voltage between the cells and the frame of the module is applied. For indoor tests the module terminals are short circuited to have uniform cells potential. The environment can be natural outdoor conditions or indoor controlled conditions.

Numerous PID papers (e.g. [127], [129]) describe specific experiments and their effect on the power, on the leakage current and on the visualization of the degradation made by EL, EBIC, EDX, or STEM, but without extracting power degradation models.

A model of the leakage current has been described by Hoffmann [69], depending on humidity, temperature, and both temperature and humidity. Indeed measuring the leakage current is crucial to assess the stability, the uniformity and the continuity of PID-s tests. But up to now, the leakage current has not been clearly linked to the power degradation for crystalline silicon modules [69], [130], [131]. Higher conductivity of the silicon nitride and increased metallization area leading to reduced sodium transport to the silicon and recovery behaviour of PID-s [129] are some of the explanations for the lack of a relationship between leakage current and PID-s power loss.

The typical shape of the time dependent power loss for the PID-s effect appears to be a sigmoidal function of the time (Fig. 13). First the degradation is slow, then fast and then stabilizes at a certain power depending on the applied voltage.

We focus on three empirical models of the PID-s effect. The first model by Hattendorf et al. describe the power degradation [131] and recovery [132]. The second model by Taubitz et al. describe the shunt resistance degradation and recovery [133]. The third model by Hacke et al. describe the power degradation for crystalline silicon [134] and for thin-films [135]. All models are based on indoor experiments with PV modules. The Taubitz and the Hacke thin-film model have been compared to outdoor tests.

All models assume that the PID-s depends on the applied voltage (system voltage) *U* between the cells and the frame, the module temperature *T*, the ambient relative humidity H, and the time *t*.

The model of Hattendorf is based on a matrix of indoor experiments where modules are exposed to varying voltage, module temperature, and ambient humidity. The conditions are varied to determine the model parameter for the module power P_{mod} equation:

$$P_{mod}(U,T,H,t) = \mathrm{P}_{ini}[1 - p(t)]. \qquad (5)$$

The initial module power is P_{ini}. The function $p(t)$ symbolize the power loss due to environmental influence:

$$\mathrm{p(t)} = p_{\infty} \frac{1-e^{-\frac{t}{\tau_1}}}{1+e^{\frac{1-t_0}{\tau_2}}}, \qquad (6)$$

$$p_{\infty} = \lim_{t\to\infty} p(t). \qquad (7)$$

To determine the model's parameter the power degradation is measured as function of the time with the system voltage *U* as parameter and fixed humidity *H* and temperature *T*. The saturating power p_{∞} is extracted by fitting Eq. (6) to the measured data as shown in Fig. 13.

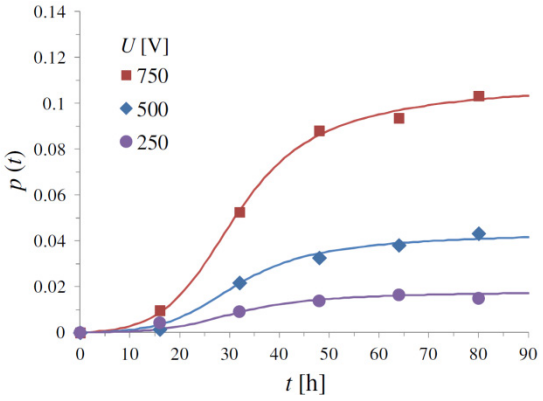

Fig. 13: Power degradation as function of the time with the system voltage as parameter. Reprinted from Hattendorf 2012 [131].

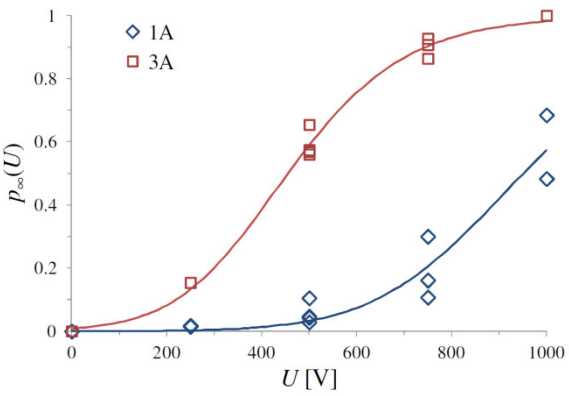

Fig. 14: Final power value as a function of the applied voltage with the module type as parameter. . Reprinted from Hattendorf 2012 [131].

The coefficients of the following equations parameters are extracted by fitting the determined saturating power as a function of the system voltage (Fig. 14), with humidity *H* and temperature *T* as parameters:

$$p_\infty(U) = \left(1 + e^{\frac{U-U_0}{\Phi}}\right)^{-2}, \qquad (8)$$

$$a(H) = \frac{H_0}{H}, \qquad (9)$$

$$b(T) = e^{-\frac{T-T_0}{\vartheta}}, \qquad (10)$$

$$t_0(T,H) = a \cdot b \cdot t_0', \qquad (11)$$

$$\tau_1(T) = b^2 \cdot \tau_1', \qquad (12)$$

$$\tau_2 = \tau_2'. \qquad (13)$$

The model has 6 free parameters: t'_0, U_0, Φ, τ'_1, τ'_2, and ϑ. The parameters H_0 and T_0 are scaling parameter. The parameter H_0 = 41.39 g/m^3 and T_0 = 323.15 K have been chosen, corresponding to a relative humidity of 50%rH and a temperature of 50°C. The parameters $a(H)$ and $b(T)$ are acceleration functions. For $T = T_0$ and $H = H_0$ they are equal to 1, therefore τ'_1, τ'_2 are the time constants under these conditions. The parameter τ_2 remains constant for a given module. These parameters are to be extracted by the least square method for each type of modules.

The PID-s regeneration process is activated by switching off the system voltage. The regeneration rate increases with increasing temperature. Hattendorf modeled the power regeneration by the following extending equations [132].

$$P_{mpp}(t) = P_{ini}\{1 - p_0[1 - r(t - t_0)]\}, \qquad (14)$$

$$p_0 = p(t_0), \qquad (15)$$

$$r(t) = (1 - p_0)\left(1 - e^{-\frac{t}{\tau_3}}\right) + p_0\left(\frac{2}{1+e^{-\frac{t}{\tau_4}}} - 1\right), \qquad (16)$$

$$r(t) = r_1(t) + r_2(t), \qquad (17)$$

$$\tau_3(T) = \tau_3' \cdot e^{-\frac{T-T_0}{\theta_3}}, \qquad (18)$$

$$\tau_4(T) = \tau_4' \cdot e^{-\frac{T-T_0}{\theta_4}} \qquad (19)$$

Considering Eq. (5) and assuming the degeneration process is being stopped, and the regeneration is starting at some point in time called t_0, $p(t_0)$ gives the value of the PID-s pre-damage. The regeneration model has 4 free parameters τ'_3, τ'_4, ϑ_3, ϑ_4. The parameters are determined by fitting the above mentioned equations to experimental results. The fit of the regeneration Eq. (14) to experimental results is illustrated with different p_0 as parameter in Fig. 15. An example of the $r(t)$ regeneration function is illustrated in Fig. 16, with a visualization of its two components $r_1(t)$ and $r_2(t)$.

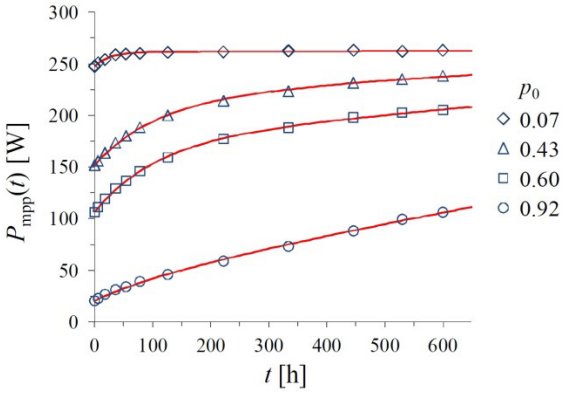

Fig. 15: Temperature-driven regeneration of four full-size modules measured at T = 70°C and H = 50% without voltage applied. The modules are equal in terms of constitution, but differ regarding PID-spre-damage. The curves are mean square fits by Eq. (14) and (16). The parameter p_0 is comprised between 0 and 1 and represent the PID-s pre-damaged level. Reprinted from Hattendorf 2013 [132].

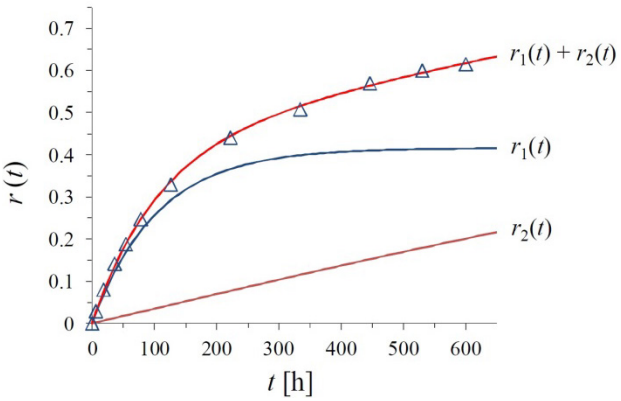

Fig. 16: The regeneration function r(t) and its two components. The graphic relates to the identically marked curve in Fig. 15 (p_0 = 0.43). Reprinted from Hattendorf 2013 [132].

The Taubitz model is based on indoor controlled tests and outdoor tests on identical single cells mini modules. The system voltage U applied to the module is the same for all tests (-1000 V). Fig. 17 shows three phases which have been defined to describe the module shunt resistance behaviour with a sequenced applied voltage. Under bias voltage and high relative humidity, the module is in the shunting phase (S-phase). When bias and/or humidity stops, the shunt degradation slow down in a transition phase (T-phase), and then regeneration starts (R-phase). The transition and regeneration is modelled by two equations.

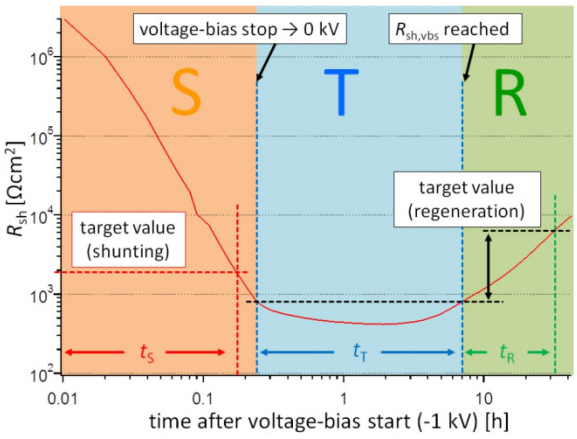

Fig. 17: Evolution of the shunt resistance with sequenced applied voltage. Reprinted from Taubitz 2014 [133].

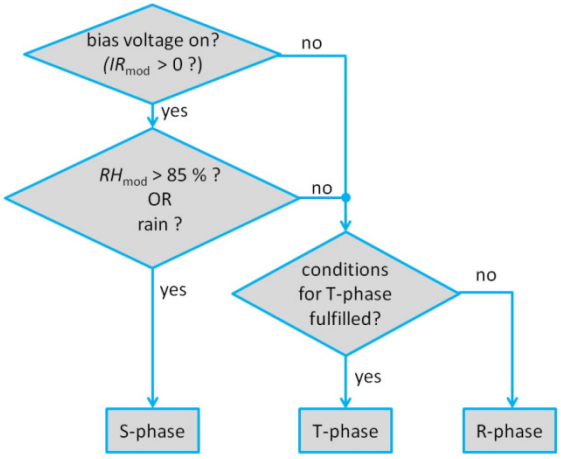

Fig. 18: Phase assignment process. Reprinted from Taubitz 2014 [133].

The shunt resistance in the 3 phases is modelled by three equations. The shunt resistance in the shunting phase is modelled by

$$R_{sh}(t) = a_s \cdot e^{-\frac{t}{b_S \cdot T}}, \qquad (20)$$

for the regeneration phase by

$$R_{sh}(t) = c_R + a_R \cdot e^{\frac{t}{b_R \cdot T}}, \qquad (21)$$

and for the transition phase by

$$R_{sh}(t) = a_T(T) \cdot (t + b_T \cdot T) + c_T\,. \qquad (22)$$

The constants a_S, a_R, $a_T(T)$, $b_S(T)$, $b_R(T)$, $b_T(T)$, c_R, and c_T have to be determined for each specific module type. Some of them are dependent on the module temperature T. The constants are determined by measuring the times t_S, t_T, and t_R for reaching certain target values as given in Fig. 17. The models phase is assigned by the process described in the Fig. 18.

The exponential function in Eq. (20) implies that this model cannot describe the stabilization of the degradation seen in the Hattendorf experiments.

This model has been compared to outdoor experiments with quite a good correlation (Fig. 19).

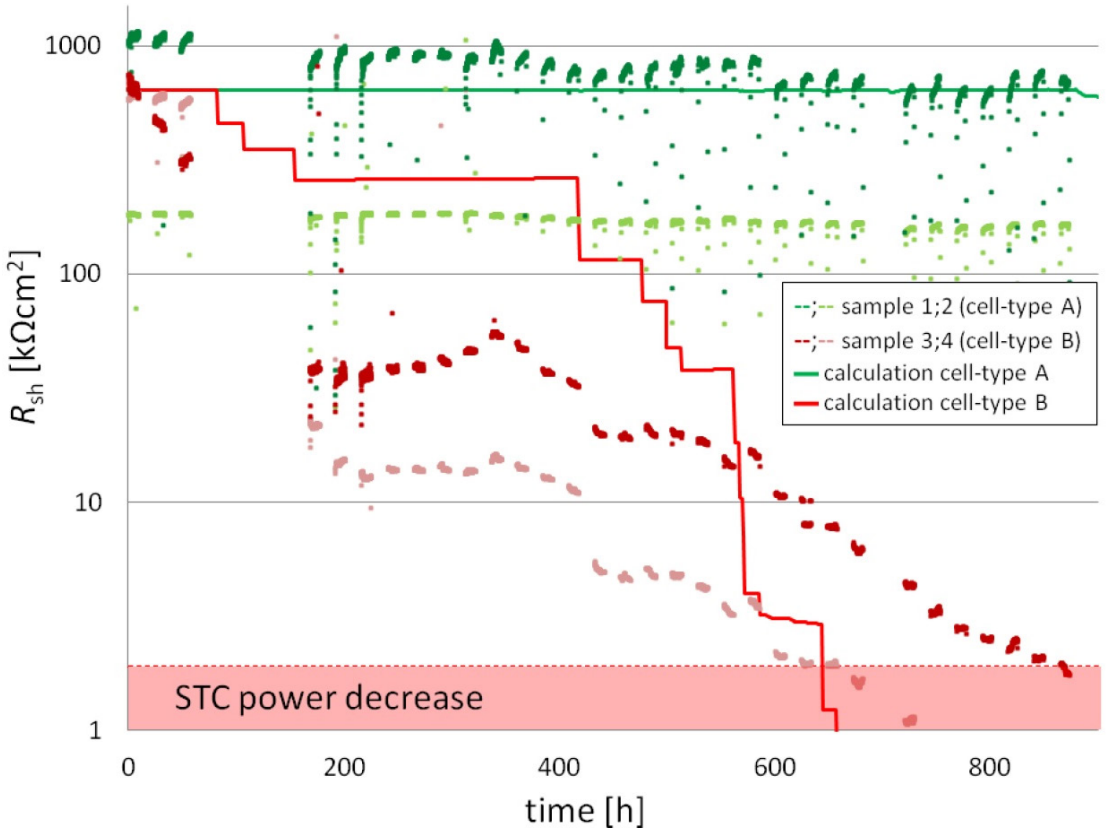

Fig. 19: Measured and modeled R_{sh} evolution. Reprinted from Hacke 2016 [135].

However, the mathematical link between the R_{sh} model and the impact on the real power degradation is not quantified by Taubitz.

The parameters of the Hacke model [134] are extracted from indoor tests and do not comprise regeneration modeling. For the determination of the parameters a fixed system voltage (-1000 V) is applied to 20 identical c-Si modules while varying temperature and humidity levels.

The equation chosen to fit the power degradation of c-Si modules is:

$$\frac{P_{max}}{P_{max_0}} = 1 - A \cdot e^{-\frac{E}{kT}} \cdot H^B \cdot t^2 \quad . \qquad (23)$$

The constants *A* and *B* are determined by fitting the Eq. (PIDHACKE) to experimental results. The parameters have to be determined for each module type. This parabolic model is applicable to the beginning of the degradation phases of PID-s, as it can fit the beginning of a sigmoid and does not describe the stabilization phase of the sigmoidal curve. This model is applied by Annigoni [136] to aim for outdoor power prediction of c-Si modules for various climates.

Similar modeling to predict PID occurrence in thin-film modules in the field using accelerated tests can be performed [135]. A progression of potential-induced degradation (PID) mechanisms is observed in CdTe modules, which is dependent on the system voltage level, temperature, and moisture ingress. This degradation includes shunting [137], junction degradation, and two different manifestations of series resistance increase [135]. Considering the PID mode that occurs first, shunting, an exponential model based on module temperature and relative humidity (*H*) is fit to the PID rate for multiple stress levels of a CdTe module in chamber tests and validated by predicting the observed degradation of the module type in the field (Fig. 20). The exponential model, close to the derivative of the c-Si (23), shown to be applicable in higher relative humidity regime is of the form:

$$\frac{d}{dt}\left(\frac{P_{max}}{P_{max_0}}\right) = A_0 \cdot f(U) \cdot e^{-\frac{E_a}{kT}} \cdot e^{H \cdot B} \quad , \qquad (24)$$

where E_a is the thermal activation energy, A_0 is a pre-exponential, *f(U)* expresses the voltage dependency, not detailed here, *B* is the exponent associated with the relative humidity *H* (taken in percent), *k* the Boltzmann constant, and the *kT* product in units of eV.

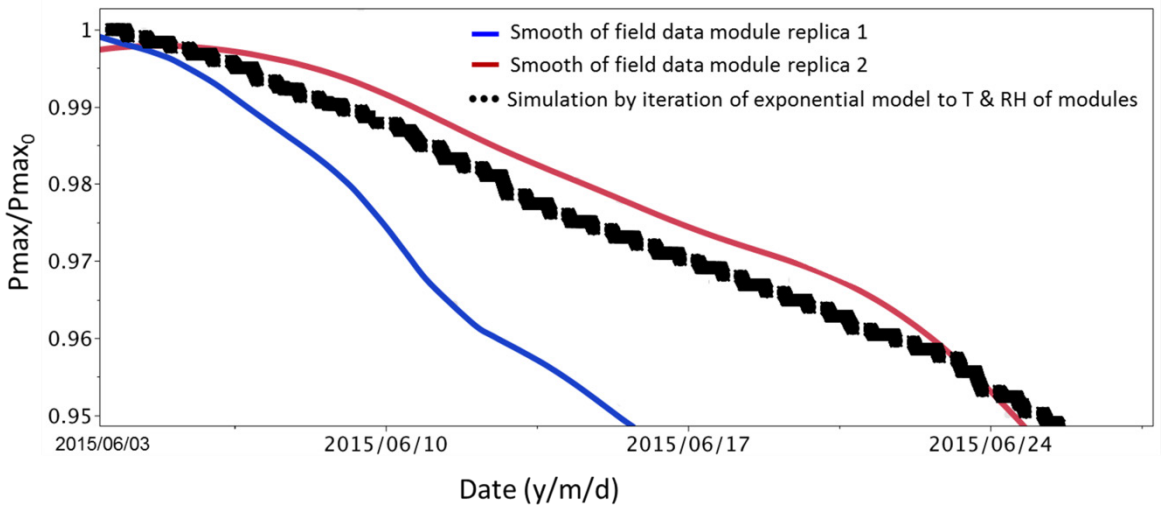

Fig. 20: Iteration of the chamber test-derived exponential model to 20-s interval data for CdTe module temperature T and surface humidity H in Florida and its correspondence to the measured module power P_{max} for two fielded replicas.

The degradation predicted by the exponential model was validated by observing a match with the experimental degradation rate of this module type in the field (Fig. 20), which also exhibited shunting as evidenced by significantly reduced low light performance compared to STC performance. Success is also attributable to slow or minor thermally activated recovery in this module type when unstressed, unlike c-Si, where recovery must be considered [133]. For Cu(In,Ga)Se_2 also a reversible PID mechanism being triggered by negative system bias exist [138]. The PID degradation in CIGS modules degrades the fill factor, the open circuit voltage and increases the series resistance of the module. However, in this case a recovery of the module power is possible [139], [140].

The Hattendorf model is built with indoor tests on c-Si modules under several system voltages. It is based on sigmoid functions that describe the degradation and the regeneration of the power, and it provides methods to extract its parameters. There is no link with outdoor tests, but a simulation of an outdoor application has been presented. The sigmoidal function fully describes the evolution of the power until its stabilization. It also shows evidences that the PID power degradation saturation level is a sigmoid function of the system voltage. That means modules which work fine with 1000 V system voltage could totally fail with 1500 V.

The Taubitz model is built with indoor tests on c-Si single cell modules under a fixed system voltage. It is mainly based on exponential equations that describe the degradation and regeneration of the shunt resistance. The model results have been correlated with outdoor tests results. The exponential functions cannot describe the stabilization of the degradation and the regeneration. The shunt degradation is observed long before it impacts on the power. This kind of study should be continued to establish the link with the power degradation.

The Hacke models are built with indoor tests on c-Si and thin-films modules under a fixed system voltage. Their equations only describe the beginning of the degradation of the power, with a parabolic function for c-Si and a linear function for TF. However, the TF modelization allows making a correlation with results in the field.

For degradation rate modelling for PID-s, the most complex component is to understand the recoverable and unrecoverable components, which can vary depending on module type and the stress level as determined or moderated by the weather. PID-s is the most deleterious system voltage stress effect that manifests in the relatively short term, and it is the most often modelled. However, a number of other related degradation mechanisms associated with electrical potential, including electrochemical corrosion, series resistance losses, gas evolution, and delamination associated cathodic reactions named PID-d [141][32][33][135] remain long-term durability issues that still need to be better modelled.

Details of the influence of weather, module surfaces being wet or dry, coatings, soiling, encapsulants, PID-s resistance at the cell and encapsulation levels, and their interaction remain areas for further study. Furthermore, the intrinsic parameters of the module are absent in these models. Resistivity of the glass and the encapsulant are missing, refractive index of the ARC on the cell is missing, yet these parameters play an important role in the PID-s. A new matrix of experiments could be built using a standard PID test applied to modules with a variation of these additional parameters.

2.3.5 Influence of the silver grid corrosion on the PV power

In this section, the degradation process induced by hygrothermal stress on screen printed silver metal busbars or gridlines of the solar cells is described. These screen printed silver conductors are formed from paste that contains glass frit and conductive silver particles. The screen printed paste is fired during cell processing to form an ohmic contact with the silicon wafer [Paretkar16]. The hygrothermal degradation of this metallization has been observed at the late stages of module nominal service life.

As shown in the electroluminescence (EL) image of Fig. 21(a), a dark area in the central region of each PV cell is frequently observed in PV modules subjected to exposure in outdoor conditions over 20 years. In addition, the spreading of the EL dark area in the peripheral region in each PV cell is also sometimes observed; see Fig. 21(b). While the different distributions of the EL dark area may depend on differences in the configuration of PV cells/modules, it has been elucidated that the root cause of the decrease in EL brightness is moisture that penetrates from the ambient into the PV module. It has been suggested that moisture penetrated into a PV module becomes a basis for the hydrolysis of EVA. EVA is the most popular encapsulant used in crystalline silicon PV modules. Acetic acid (HAc) is produced by hydrolysis of EVA, and this acid corrodes some metal parts, and it attacks the silver gridline interface with the silicon on PV cells, which is a crucial current path for photovoltaic electric current. Indeed, the continuously increasing HAc content within the EVA of PV modules exposed for long-term in the field has been reported by Shioda et al. and Masuda et al. [142], [143]. This increasing HAc content is also found when PV modules are exposed to elevated hygrothermal stress levels for 2000–3000 h [142], [143].

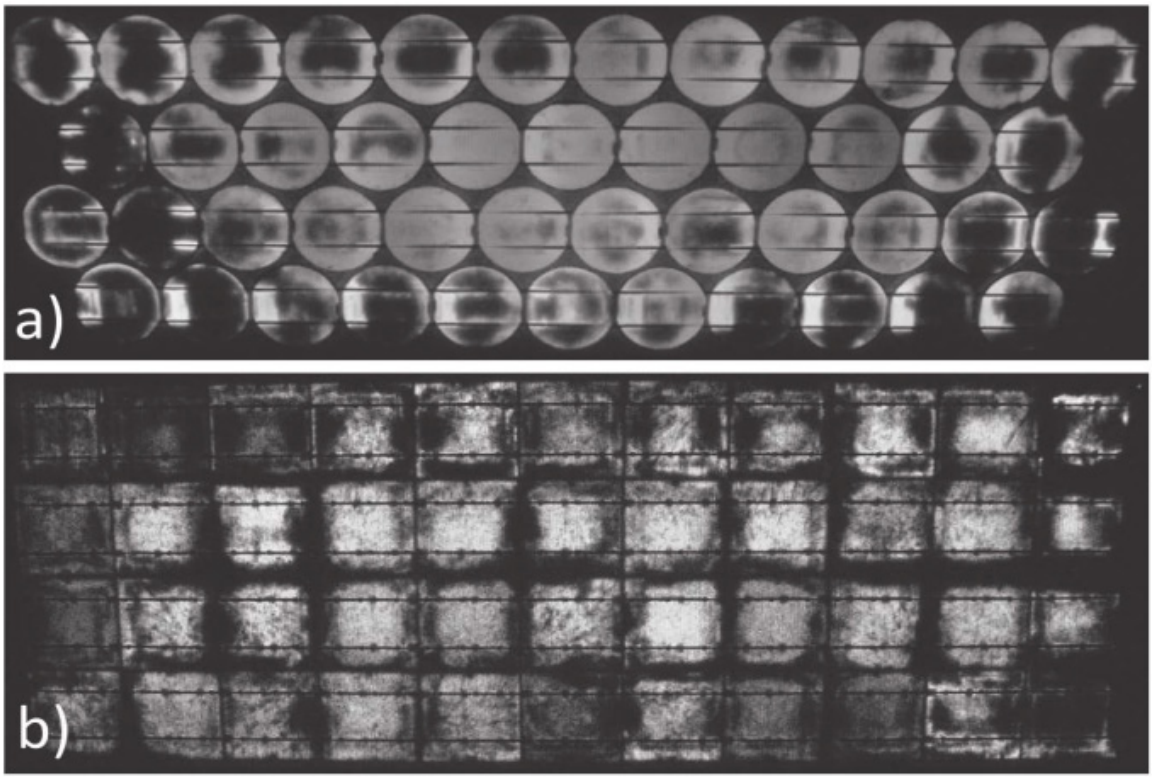

Fig. 21: EL images of PV modules exposed at Cfa climate in Köppen climate classification in Japan over 30 years.

Kraft et al. proposed a degradation mechanism related to the corrosion of silver gridlines [144] based on previous investigations of damp heat-induced degradation [84]. Kraft et al. demonstrated the dissolution of the glass layer underneath the silver gridline metallization by the immersion of PV cells into aqueous HAc solution. This proposal accurately explains the previous observations gathered when the PV cell area with high series resistance is correlated to the dark EL area. These signals seem to be a crucial "aging signature" which can be observed in the PV module.

The gap evolved by the dissolution of the glass layer underneath the silver gridlines of the PV cell may be monitored by the alterations of capacitance and/or impedance under alternating current (AC) loading conditions (Fig. 22). Experimentally, PV cells soldered with cell interconnect ribbons are mounted in a chromatography chamber filled with HAc vapour (Fig. 23). The humidity in the vapour over the saturated aqueous salt solution of the closed cabinet is self-adjusting [Carr49]. This exposure system has been applied in previous work of Kempe et al. [Kempe07]. As a reference, PV mini-modules (ca. 4 W, 180 x 180 mm²) are assembled with the same type of PV cell plus extra EVA, backsheet, and glass. A damp heat test for these PV mini-modules is conducted at 85˚C / 85% relative humidity for 3000 h. The electrical characteristics of PV cells and PV mini-modules are periodically assessed by a solar simulator and an EL image analyser. The characteristics of the AC impedance are evaluated by an LCR meter with frequency scanning function [145].

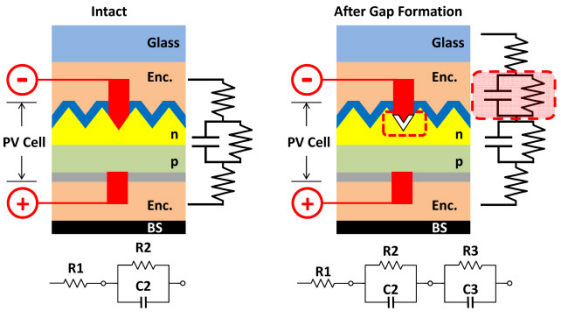

Fig. 22: Evolution of AC equivalent circuit by the formation of gaps underneath the silver gridlines.

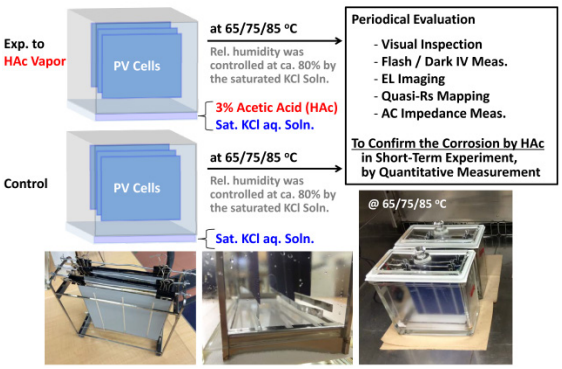

Fig. 23: Experimental setup for the exposure of bare PV cells to HAc vapour.

Bare c-Si PV cells promptly degrade by the exposure to the hygrothermal vapours over saturated KCl solution containing 3% HAc according to the exposed duration. However, the degradation is not observed under hygrothermal stress without HAc vapour. The degradation profiles obtained at higher temperatures are divided into 2 phases by the PV characteristics. Firstly, the P_{max} rapidly declined with decreasing *FF* after a short time-lag (Phase I). Thereafter, the gradual reduction of P_{max} with declining I_{sc} (Phase II) is observed (Fig. 24). These degradation phases may be independent of each other, since their activation energies, calculated using an Arrhenius equation, are slightly different (Fig. 25).

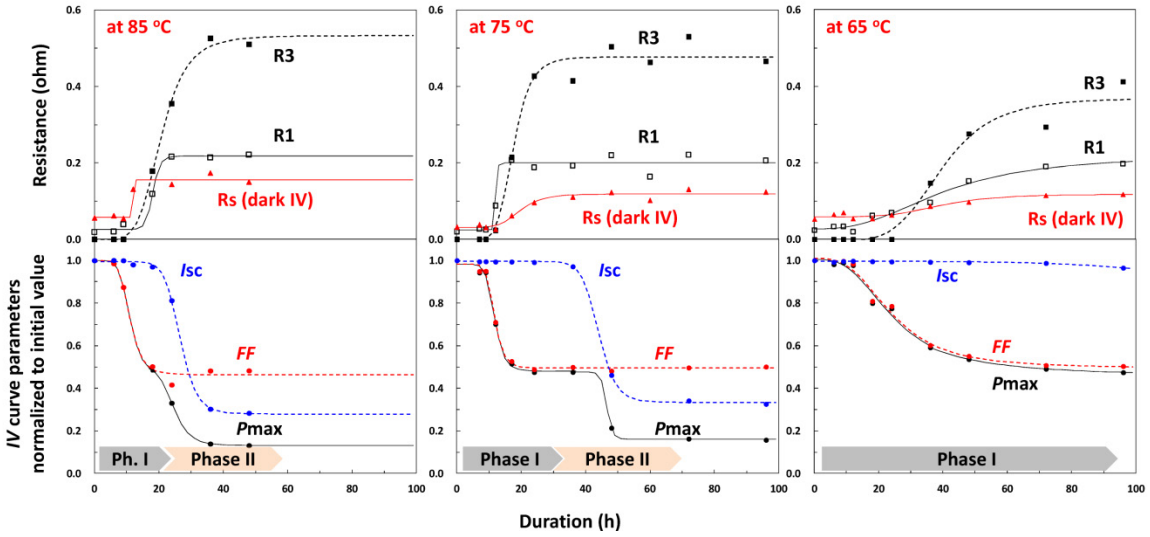

Fig. 24: Phase transition of cell parameter during exposition of PV cells to HAc vapour.

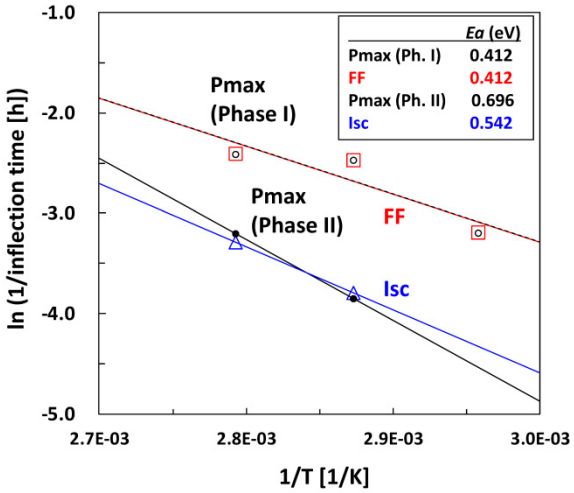

Fig. 25: Arrhenius plot and activation energies for I/V curve parameter during the degradation of PV cells exposed to HAc vapour.

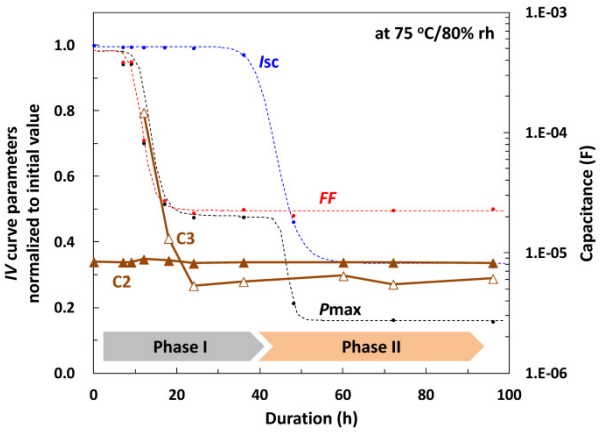

Fig. 26: Development of novel capacitor C3 during degradation of PV cells exposed to HAc vapour.

It is worth noting that in Phase I, the development of a new capacitance C3, with higher capacitance than that of p-n junction (C2) is identified by AC impedance spectroscopy (Fig. 26). The increasing series resistance (Rs, R1) is also detected in the dark *IV* curve and AC impedance spectrum. The resistance (R3), associating with the newly formed capacitor (C3) rapidly increases through Phase I. During Phase I, the distinguishing transition of EL images is observed, from a nebula-like image characterized by a bright cloud-like area and EL bright points being semi-uniformly distributed in the lower EL brightness background, to a constellation-like image where the bright points sparsely remain only on finger electrodes under the dark EL background (Fig. 27).

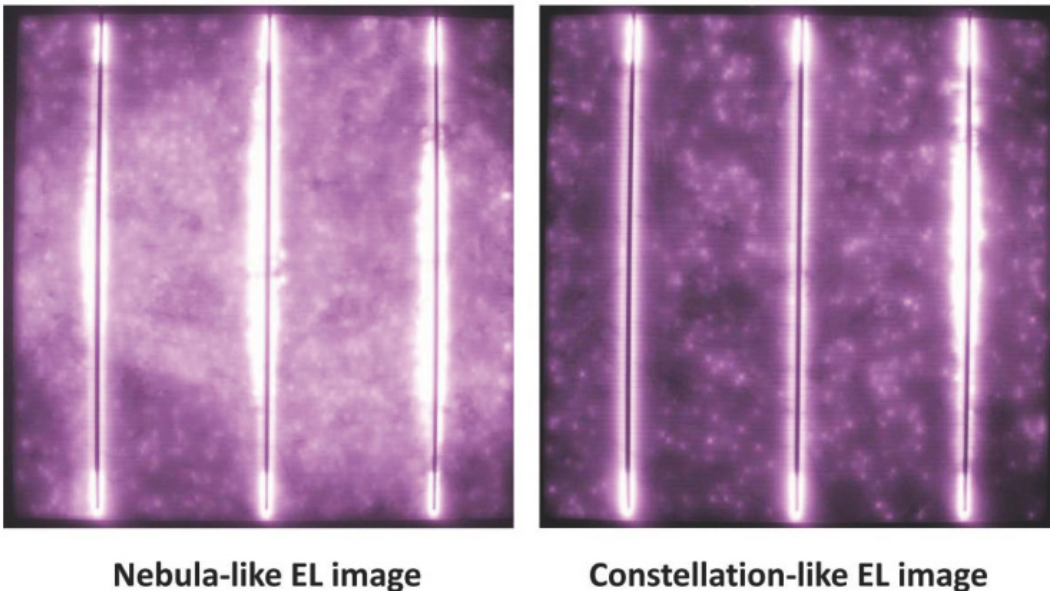

Fig. 27: Evolution of EL image during degradation of PV cells exposed to HAc vapour.

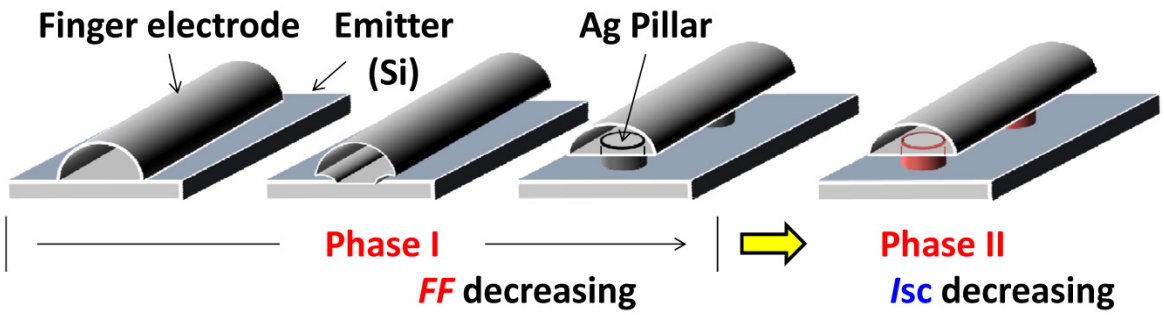

Fig. 28: Putative degradation process of c-Si PV cells exposed to HAc vapour. The red colour of the Ag Pillar in phase II indicates a change of contact properties to the underlying silicon.

These results suggest that the gap underneath the silver gridlines and busbars grows during phase I, although the direct contacts of Ag and emitter surface by Ag pillars seem to remain (Fig. 28). In Phase II, the series resistances Rs and R1, the newly developed impedance consisted of capacitance C3 and the resistance R3 and *FF* stay nearly constant (Fig. 24). It should be noted that I_{sc} is decreasing with the evolution of the EL image to complete dark cell areas where the EL emission is limited to only near the cell interconnect ribbon. From these results it is assumed that an addition of a forward-directional diode and/or increased resistivity occurred at the Ag pillars. It has been understood that the current path between emitter and silver finger consisted of two routes (direct contact via Ag pillars and electron tunnelling via nano-Ag colloids dispersed in glass layer [146], [147]). Therefore, it is assumed that the FF reduction during Phase I is induced by dissolution of glass layer-contained nano-Ag particles. In Phase II, the decrease of I_{sc} and the change in blocking characteristics in reverse bias as shown in Fig. 29 suggest that the electric properties in the contact of the Ag pillars are changed, although the precise mechanisms have not been elucidated. Indeed, the gaps formed by the dissolution of Pb-containing glass layer are clearly confirmed in Fig. 30.

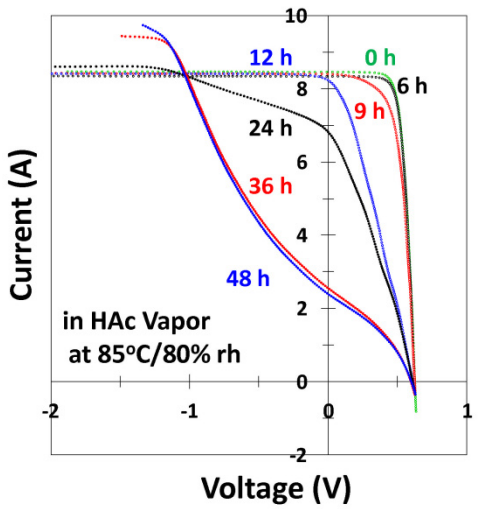

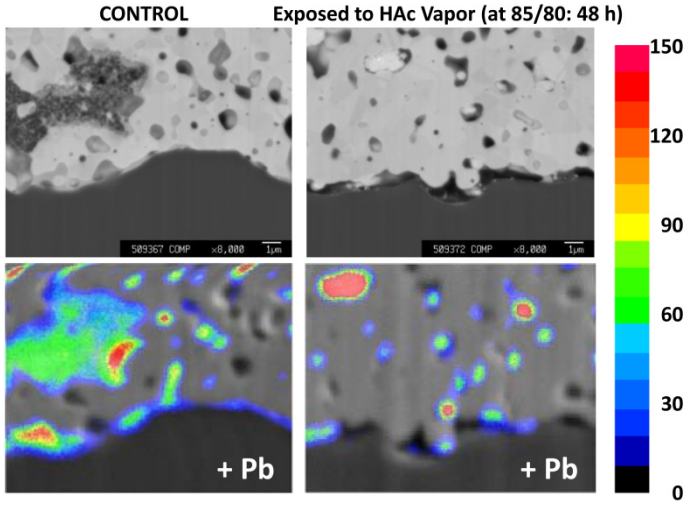

Fig. 29: Evolution of I-V-curve in PV cell exposed to HAc vapour at 85˚C/80% rh. The cell starts to lose its diode blocking characteristic in reverse bias after 24 h.

Fig. 30: Upper images: SEM images of cross sectional view a front silver paste/silicon interface. Lower images: Overlay of secondary electron microscope (SEM) and electron probe micro analysis (EPMA) images of the same sections. In the left side images of a control sample, on the right samples exposed to HAc vapour for 48h at 85°C are shown.The colour levels (ppm) indicate the concentration of Pb observed with EPMA.

A similar progression in phases of the *IV* and AC impedance parameters with those obtained in PV cells subjected to HAc vapour are observed in the laminated PV cell encapsulated in a conventional module architecture, see Fig. 31. The ingress of moisture onto the PV cell within the PV module progresses from the periphery to the central area on a PV cell in a constant humidity damp heat test [148]. The degradation caused by the diffused moisture is observed around the peripheral area of the PV cell at first, and it is subsequently induced at the central region under the damp heat condition [84], [143]. Because of lateral non-uniform degradation phases occurring even in a one cell module, the electrical signal from each region with different degradation phases may combine and lose their own characteristic feature(s) such as the development of R3 and C3, when the signal is obtained from a whole PV cell signal. However, the phase transition of every signal on a PV cell (within a PV module subjected to damp heat testing) can be actually detected. Therefore, it is indicated that the degradation process identified on a bare PV cell exposed to HAc vapour, which seems to be spatial-isotropically degraded, is able to be captured as an "aging signature" even in a PV cell laminated in PV module, which seems to be spatial-anisotropically degraded under the damp heat stress.

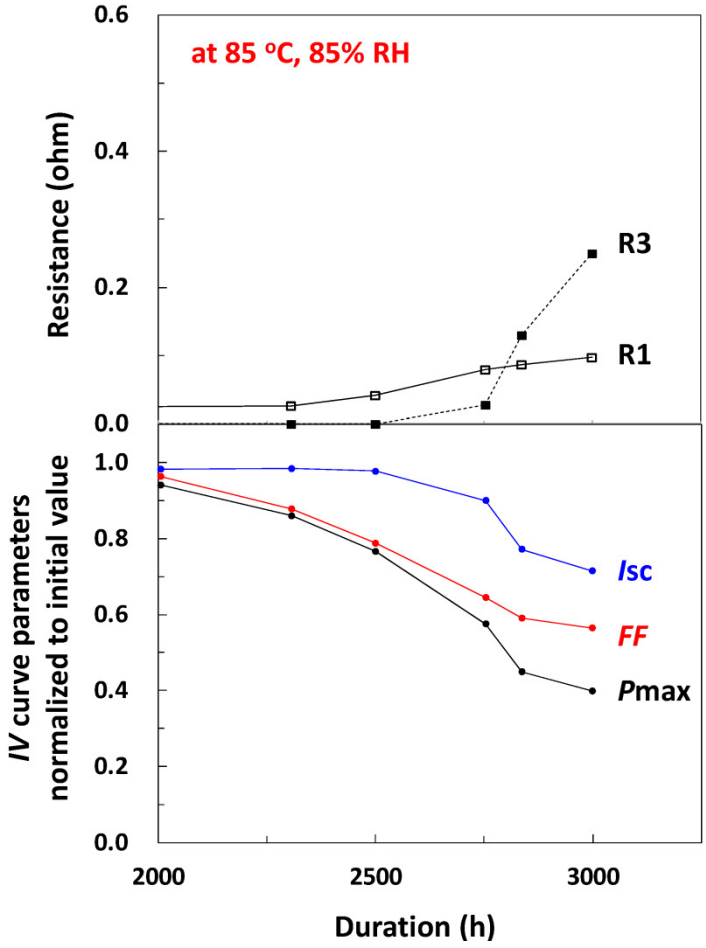

Fig. 31: IV-curve and AC impedance parameter of a PV mini-module as function of the damp heat stress duration.

The activation energies for *FF*-reduction and *FF*-associated power-loss estimated in this study (0.41 eV) are lower than those calculated from whole power-loss in PV modules subjected to damp heat stress (0.49 eV and 0.51 eV in [149] and [150], respectively). In contrast, that for Isc-reduction or Isc-related power-loss determined above (0.54 eV - 0.70 eV in Fig. 25) is larger than the activation energies observed in PV modules. Because power-loss in PV modules consists of *FF*- and I_{sc}-associated power-loss, it is assumed that the activation energy for power-loss in PV mod-

ules is a complex function of those for *FF*- and I_{sc}-associated power-loss. Therefore, it is suggested that the degradation in PV cells exposed to HAc vapour has a similar failure mode with that in PV modules under damp heat stress conditions, since the averaged activation energy (0.52 eV) for *FF*- and I_{sc}-associated power-losses in PV cells exposed HAc vapour is very similar to that for whole power-loss in PV modules during damp heat stress test.
The acceleration factor between power-losses observed in PV cells exposed to HAc vapour at 85˚C (Fig. 24) and in PV module under damp-heat stress conditions (Fig. 31) is roughly estimated 100. And, the acceleration factor between power-losses in damp heat conditions and in tropical climate conditions has been estimated to be 23 [149], [151]. From these estimations, ca. 2300 times acceleration is induced by the direct exposure of PV cell to HAc vapour as compared to outdoor exposure of a PV module installed in tropical climate conditions. However, there are some problems for simple application of this acceleration factor for a lifetime prediction method under outdoor climate conditions, as follows; 1) the amount of liberated acetic-acid within PV modules is strongly affected by the details of moisture ingress and elimination through the backsheet and edge seal (if present). Although the time required for the moisture to reach the centre of the PV cell front side in a PV module is about 2000 - 3000 h even under damp heat stress condition [152], [153]. This time is not considered in the direct exposure of PV cell to HAc vapour. 2) In addition, the generated HAc is not uniformly distributed in the PV module, since its amount in each region within PV module depends on the concentration of moisture in each respective portion [154], [155]. Therefore, the anisotropic degradation observed within the PV cell area of a PV module under damp heat condition and in the field is not reflected in the exposure of PV cell to HAc vapour. 3) The combined effects of temperature and humidity on the hygrothermal degradation of PV modules have not yet been completely resolved. It has not been elucidated whether the time to failure of PV modules under hygrothermal conditions are determined by the exponential corrosion model or the power law model [149], [151], [156]. Since this “aging signature” detected in PV modules in an accelerated test would be easily identified also in PV modules exposed outdoor over the long-term, the signature will be available as an index to estimate their degradation level/phase induced in the installed environment. Especially, it is assumed that the parameters specified from the AC impedance spectrum will be valid since these parameters are not convoluted with other mechanisms caused by light-irradiation in PV cells (e.g., discolouration of the encapsulant).

2.3.6 Influence of dust soiling on PV power

Soiling of PV modules is not a typical module failure mode such as cell cracking or delamination, since it does not negatively impact the long-term reliability of PV systems, but instead it is a usually reversible effect, which can be mostly removed by cleaning. Soiling of PV modules can have various origins such as algae growth on the module surface, air pollution or dust accumulation (dust soiling). In a sense also snow load on PV modules can be regarded as soiling. All these effects cause PV power losses due to reduced optical transmittance, which accumulate to energy yield losses in a certain time period. These energy losses can be quite significant [157], [158], in the order of 5 – 20% over the course of one year, depending on the location of the PV module and is known to be dependent on the angle of incidence [159].

With regard to modelling of PV energy yield losses caused by dust soiling the following factors must be considered:

- Dust accumulation rate: It is a site specific parameter and depends on the local climate (i.e. seasonal variation of dust density, frequency of rainfall), the nature of topography or surrounding vegetation and the mounting conditions of PV modules (i.e. inclination, height above ground). Dust soiling is always the balance of dust accumulation and dust removal. Cementation of dust at the module surface can occur for periodical wetting (dew formation) and drying-out cycles.

- Adhesive effects at the module surface will impact the soiling rate. Adhesion is influenced by the surface structure of the module (coating, roughness) and the chemical and physical properties of dust particles.
- Long-term operation will lead to abrasion effects at the glass surface, which normally will reduce optical transmittance and PV module output power. Abrasion can be either caused by sand storm (environmental abrasion, sand blast) or damage from periodical cleaning, which will be required for economic operation in desert climate.

An overview of latest results and ongoing research on dust soiling and dust mitigation was reported in a workshop on soiling effect of PV modules [160]. A discussion on the background of international collaboration on dust soiling also must mention the activities of the "PV Quality Assurance Task Force (PVQAT)", where task group 12 is working on the various aspects of soiling and dust [161]. Finally, a comprehensive literature collection on dust and soiling is given in [162].

Fig. 32 illustrates the various factors, which impact dust soiling of PV modules. The photo also shows that specific Operation & Maintenance (O&M) measures, such as periodic cleaning, will be required to ensure economic operation of PV power plants in desert regions.

Fig. 32: Factors influencing dust soiling of PV modules in desert regions: 1 Climatic impact, ambient dust concentration, 2 Glazing characteristics, adhesion effects, non-uniform soiling, 3-Installation conditions, 4-Surrounding environment, dust particle characteristics. Photo: TÜV Rheinland Group

A commonly used experimental method to monitor site specific dust soiling is the use of two irradiance sensors (encapsulated calibrated crystalline silicon cells), of which one is cleaned daily and the other is naturally soiled. The transmittance loss due to dust accumulation is given by the ratio of daily sums of solar irradiation, measured by both sensors (soiled/cleaned). This ratio is defined as Daily Soiling Loss Factor (DSLF). As an example, Fig. 33 shows the time evolution of DSLF for a location in Arizona, which is measured for a patterned (micro-structured) front glass without anti-

reflective coating. The two years monitoring data reveal that optical transmission loss caused by dust soiling can be subject to a large variation. The ratio of annual sum of solar irradiances, measured with soiled and clean sensor, defines the Annual Soiling Loss Factor (ASLF). The resulting annual transmission loss is given by (ASLF - 1) x 100%. Due to higher frequency of rainfall, the annual transmission loss was -1.2% in 2015 compared to -3.6% in 2014 [163]. It must be noted that these results only give an indication of local soiling loads, but cannot be directly transferred to yield estimation of PV modules or PV power plants. Dust soiling effects on module and systems scale depend on a number of additional factors such as edge effects caused by the module frame (non-uniform dust accumulation). Furthermore, the surface structure of the front glass and potential coatings may result in different DSLF values [164].

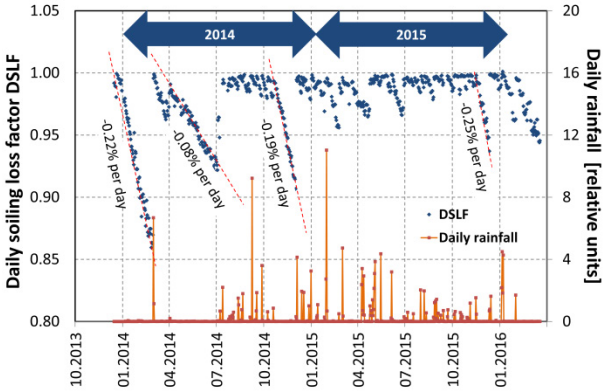

Fig. 33: Time evolution of Daily Soiling Loss Factor (DSLF) at a location in Arizona desert.

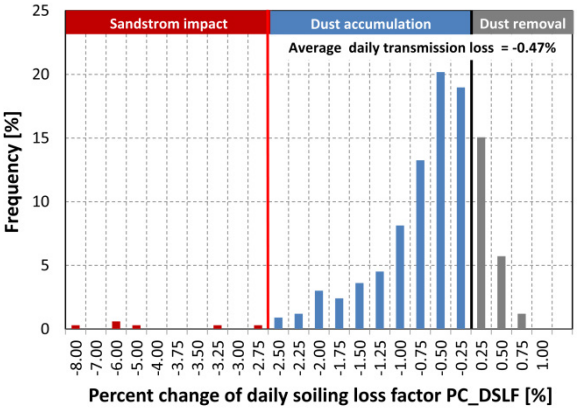

Fig. 34: Dust soiling characteristic of a location in Saudi Arabia.

The impact of dust soiling at different locations can be compared by means of the dust soiling characteristic, which is represented by the frequency distribution of the daily percent change DSLF (PC_DSLF) and can be positive or negative depending on whether the dust accumulation or dust removal effect is larger. As an example Fig. 34 shows the characteristic for a test location in Saudi Arabia. The distribution curve is typically bell-shaped and can be divided in the sections explained in Tab. 2.

Tab. 2: Sections of the dust distribution as shown in Fig. 34.

Section	PC DSLF [%]	Explanation
I	< -2.5	Heavy dust accumulation, sand storm impact
II	[-2.5 .. 0[	Typical dust accumulation
III	[0 .. 0.75[	Dust removal by wind or other effects
IV	> 0.75	Dust removal by rain or cleaning

In this example, the great majority of days in the year (>95%) falls in section II and section III, which can be referred to as the definition of a cleaning cycle. In this range the average value of PC_DSLF is -0.47%, which means approx. -3.3% accumulated dust soiling per week. If weekly cleaning is applied, the average annual transmission loss is -1.4%, which means approx. +2% increase of energy yield, if uniform soiling across the PV array is assumed. Furthermore, the diagram shows SLF changes due to sand storms. In this example -8% worst case DSLF change is observed.

Keeping soiling loss in desert regions below 2% may require weekly cleaning of the entire array. Nowadays, the majority of PV power plants in deserts are manually cleaned as shown in Fig. 35However, this means a high cost factor, especially if transport of water is required. Manual wet cleaning is effective, but personnel must take reasonable care in case of thin-film modules not to cause hot-spot damage due to partial shading.

Fig. 35: Manual cleaning of a PV array. Photo: TÜV Rheinland Group

Automatic cleaning devices offer a number of advantages: Dry cleaning with brushes can be flexibly applied and variations in the cleaning process are under better control. Today, various types of cleaning devices are commercially available. Systems connected to guide rails using a rotating brush/air pressure or cleaning robots, which autonomously can move across the array. But, large-scale application has still not been realized. An obstacle may be that harmonized standards for product qualification are missing, which describe the mechanical reliability, the abrasive impact on glass, and the cleaning efficiency.

Some PV glass manufacturers offer glass types with anti-soiling coatings. These can be divided in hydrophobic types (droplet of water forms a spherical shape) and hydrophilic types (droplet spreads and is wetting a large area). The effectiveness of anti-soiling coatings is a subject of current research. General findings are published in [165]. The anti-soiling coatings showed a tendency for easier cleaning. After cleaning the transmittance values recovered almost to their initial values, even after the harsh dew soiling test.

Regarding module failures caused by dust soiling, the predominant failure mode is abrasion of the module surface, which can be either caused by natural weathering (sand blasting) or frequent cleaning. Abrasion of the PV glass surface is not a type of defect which would normally will affect the reliability of PV power plants or lead to safety risks, but it will cause performance losses due to deterioration of optical transmittance. Depending on the installation conditions and the frequency of sandstorms, abrasion effects can also occur on the rear side of the PV module. For polymeric backsheets weathering effects are more pronounced compared to PV glass, which might result in safety and reliability risks. For quantifying abrasion effects the short-circuit current of a PV module, which is correlated with the optical transmittance, is a suitable parameter. It is measured in +/-85° Angle of Incidence (AoI) range as described in the standard IEC 61853-2 [166]. As an example Fig. 36 illustrates the change of the angular characteristics of solar glass during a blowing

sand test according to MIL-STD-810G. After 120 minutes of exposure the entire AR coating was abraded. The data also reveal that transmittance loss at normal incidence can be partially compensated by better angular response for large AoI.

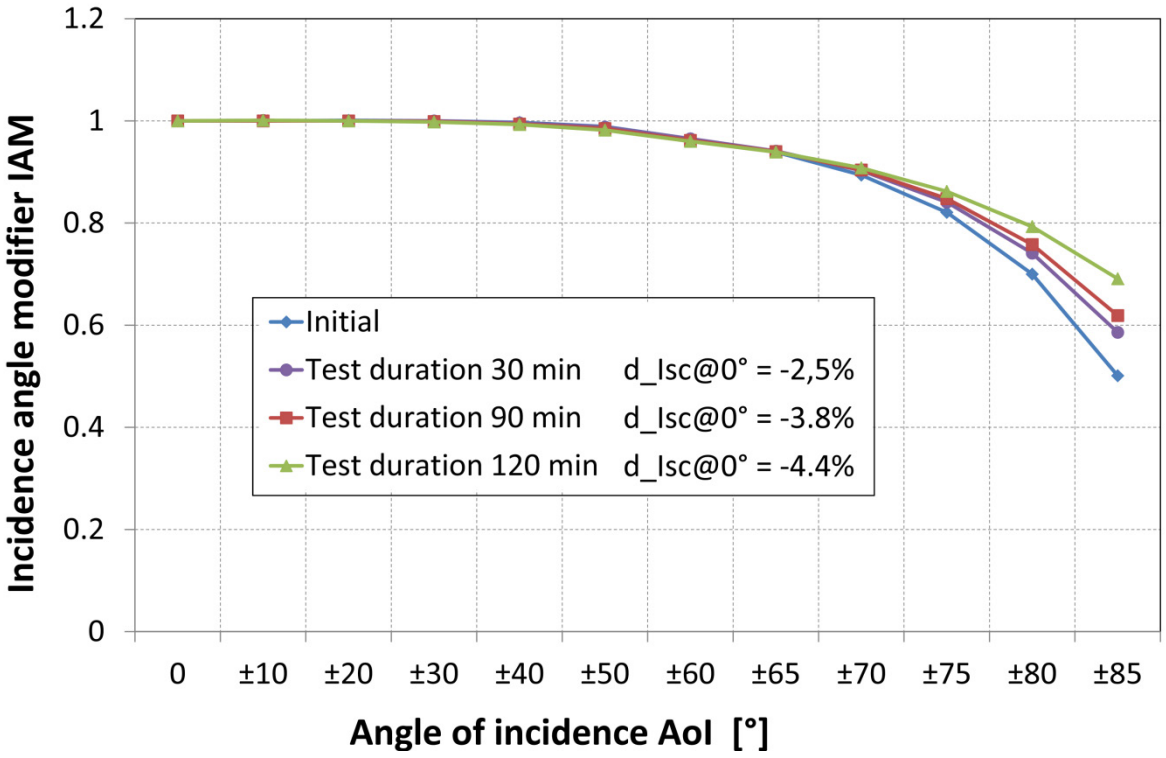

Fig. 36: Change of the angular characteristic of a PV module with AR coated glass caused by blowing sand test in accordance with MIL-STD-810G.

A commonly used test requirement for PV module qualification testing is that maximum power deterioration shall not exceed -5% [167]. This requirement shall also apply for PV modules to be qualified for desert regions. So far, results from laboratory testing show no evidence that long-term abrasion of a glass surface will lead to a higher than -5% performance loss.

Abrasion of the module surface can be analysed by accelerated testing in the laboratory. The current standard test, IEC 60068-2-68, MIL-STD-810G, DEF-STAN 00-35 EN 1096-2, ASTM D 986-05, offer a wide range of test conditions (Sample orientation, particle size, sand concentration, exposition area) and test severities (air velocity, test duration, temperature). Because of that, the comparability of test results between test laboratories is currently not given. This makes harmonization of testing an urgent topic so that benchmarking of various products will be possible.

For automatic cleaning devices we face the same situation that harmonized procedures for product qualification testing are not available. Today, several research groups are working on that topic [160]. These procedures consist of alternating cycles of artificial soiling and cleaning.

2.3.7 Influence of biological soiling on PV power

While soiling on PV module is often considered in terms of dust or soil containing silicates, carbonates and various oxides [168], there is also a large portion of materials that are biological in origin contained within the soiling material. Biological components including sub-aerial biofilms [157], bird droppings [159], fallen leaves, resin from trees, pollen, and the growth of moss [169] or lichens can all contribute to the total soiling. The contribution of organic matter to the total soiling has been measured to be in the order of 42% after a 6 month period and 58% after an 18 month period in a tropical environment [157]. The biological components are one contribution to

the larger soiling effect and in most instances would be measured as part of the total soiling. As such, the degree of biological soiling can be measured using similar methodologies.

A major contribution to biological soiling of PV modules is from sub-aerial biofilms. These are microbial communities that can grow on the surface of the PV module, at the interface between the front sheet cover glass and the atmosphere [170]. Biofilms formed on solar collectors, including flat plate PV modules, can reduce the portion of light that is transmitted through the cover glass by absorption and scattering. Studies have shown that sub-aerial biofilms can block up to 70% of transmission and scatter radiation between 250 nm and 1800 nm [170]. This is largely in the wavelength range where PV modules operate.

While organic matter is only one portion of the total soiling, it can be particularly detrimental to the performance of a PV module. One reason for this is that many of the components (algae, fungi, heterotrophic and cyanobacteria) forming sub-aerial biofilms containing photosynthetic pigments and will block or absorb portions of the visible spectrum [170]. For example, a species of microalgae, Chlorella sp., is a type of green algae and has been found in the sub-aerial biofilms grown on PV modules in a tropical climate [157]. Microalgae contain a number of pigments and chlorophylls which absorb strongly in the visible spectrum. The absorption and scattering coefficients [171] and cross sections [172] of one example of a green alga, Chlamydomonas Reinhardtii, is shown in Fig. 37. A biofilm comprising of this, or similar, microalgae could block a large portion of the light incident upon the PV module in the range where the PV module is most efficient. Under outdoor growth conditions with appropriate nutrients and salinity, microalgae such as Chlorella can double in biomass in one to two days [173]. While this growth rate is not likely on the glass surface of a PV module, it is worth noting these microorganisms can grow rapidly under the right conditions.

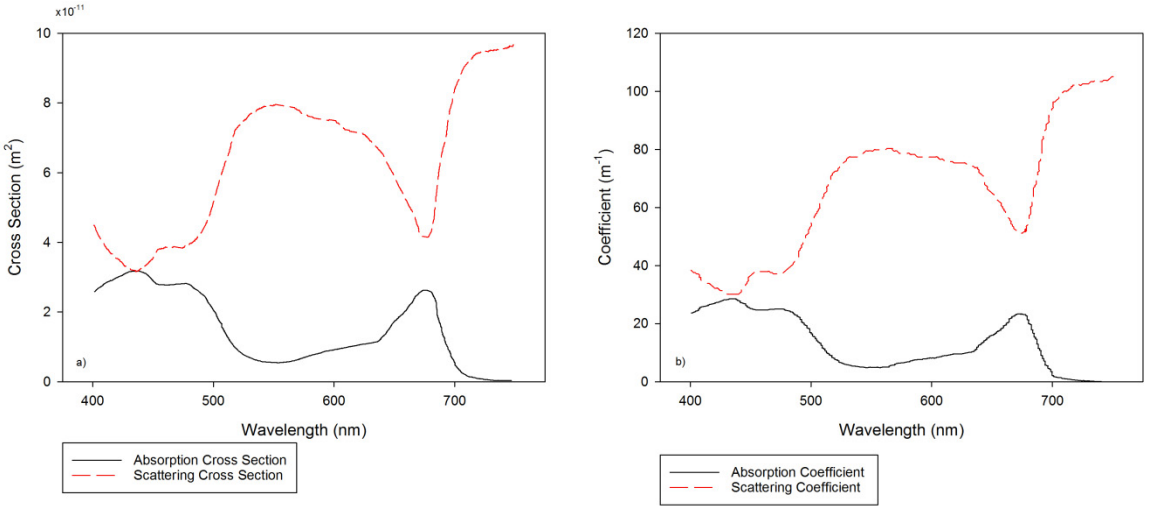

Fig. 37: a) The absorption and scattering cross section of C. Reinhardtii [172] *and b) the absorption and scattering coefficients of C. Reinhardtii with a cell density of 0.0898 kgm-3* [171].

Due to their absorption spectra, sub-aerial biofilms can be a major contributor to soiling, particularly as they are not easily removed by rainfall in self-cleaning events. It has been shown that rainfall is effective at cleaning larger loose particles, including pollen of approximately 60 µm in size, from PV modules [169]. However, smaller particles tend to have a larger influence on the performance of PV modules than larger particles [174]. These smaller dust particles in the range of 2–10 µm, are not cleaned as effectively by the same rainfall [169]. Microbial films and biological cells are of a size that would be classified as 'finer particles". As such they are very effective at absorbing and scattering light, and they tend not to be removed by rainfall events [157]. Sharakawa et al. noted a range of colonizers on the surface of PV modules. These were dominated by fungi

throughout the 18 months of measurement. However, the proportion of Chlorella and Ulothrix in the biomass increased throughout the study. The range of microorganisms showed a wide diversity initially, but tended to reduce in diversity over time as those microorganisms could better adapt to the environment.

Sub-aerial biofilms can also contribute to overall soiling in other ways. They can provide a surface for further dust to adhere to, exacerbating the module soiling level. This can lead to the growth of plants of a larger scale including moss and lichen. Sub-aerial biofilms also pit and etch glass, which can directly reduce transmittance of solar irradiance to the module [170]. As a result of their large contribution to soiling and the promotion of further soiling, some studies indicate an anti-fungal agent should be included in the cleaning regime for PV modules [157].

The effect of this additional absorption and scattering by sub-aerial biofilms can be modelled as additional terms in the equations relating to short circuit current as outlined in subsection 2.3.1 in Eq. (3):

$$J_{SC} = q \int_0^{\infty} I(\lambda)(1 - R(\lambda) - A(\lambda) - A_B(\lambda) - S_B(\lambda))EQE(\lambda)d. \quad (25)$$

Where $A_B()$is the absorption by the sub-aerial biofilms present on the surface of the PV module and $S_B()$ is the scattering of light from the surface of these films. The absorption (κ_λ) and scattering ($\sigma_{s,\lambda}$) coefficients of a range of green algae, including Chlorella sp. can be calculated from experimental measurements of the average absorption and scattering cross sections of different microalgae [172]:

$$\kappa_\lambda = C_{abs,\lambda} N_T \, , \quad (26)$$

$$\sigma_{s,\lambda} = C_{sca,\lambda} N_T \, , \quad (27)$$

Where $C_{abs,\lambda}$ and $C_{sca,\lambda}$ are the experimentally measured values of average absorption and average scattering cross sections of microalgae in suspension (m^2) [Lee2013]. N_T is the cell density, or total number of cells per m^3 of solution.

Biofilm formation is likely to occur in areas with high humidity [Sayyah2014], that is, regions with a tropical climate. For example, Sào Paulo [Shirakawa2015] has conditions with significant variation in day and night time temperature, allowing condensation to form on the modules. This condensation acts as a source of water and can promote the growth of significant biofilms [Shirakawa2015]. The diversity of microbial life on PV modules has also been investigated in the Mediterranean environments (Valencia, Spain) where a wide range of heat and radiation adapted species were found on the solar modules [Darwish2015]. While this study did not comment on the effect on the PV module performance it is clear that microbial communities are abundant on PV modules.

Larger scale biological effects can also contribute significantly to PV module soiling. Resin particles from pine trees can stick to the module surface and trap larger dust particles [169] and the sap from gum trees is known to be a problem [175]. The other main contributor on PV soiling is from bird droppings. Bird droppings (Fig. 38) can have a much higher impact on performance than soiling due to dust and other biological based soiling [176]. Bird droppings are fairly opaque and can entirely block transmission of light to the PV module. Additionally, the affected sections of the module remain shaded until they are manually cleaned [174]. These are not easily washed away by rainfall [177] and as such, performance losses due to bird droppings are not fully restored after rainfall events [159].

In severe cases, the occurrence of bird droppings can cause hot spots where the affected cell acts as a load for the remainder of the string [174]. The presence of bird droppings, or other larger

biological soiling such as moss (Fig. 38) and lichens produce uneven coverage of soiling [177] and this acts as localized shading on the module. As such, the impact can be modelled in a similar way to a partially shaded PV module.

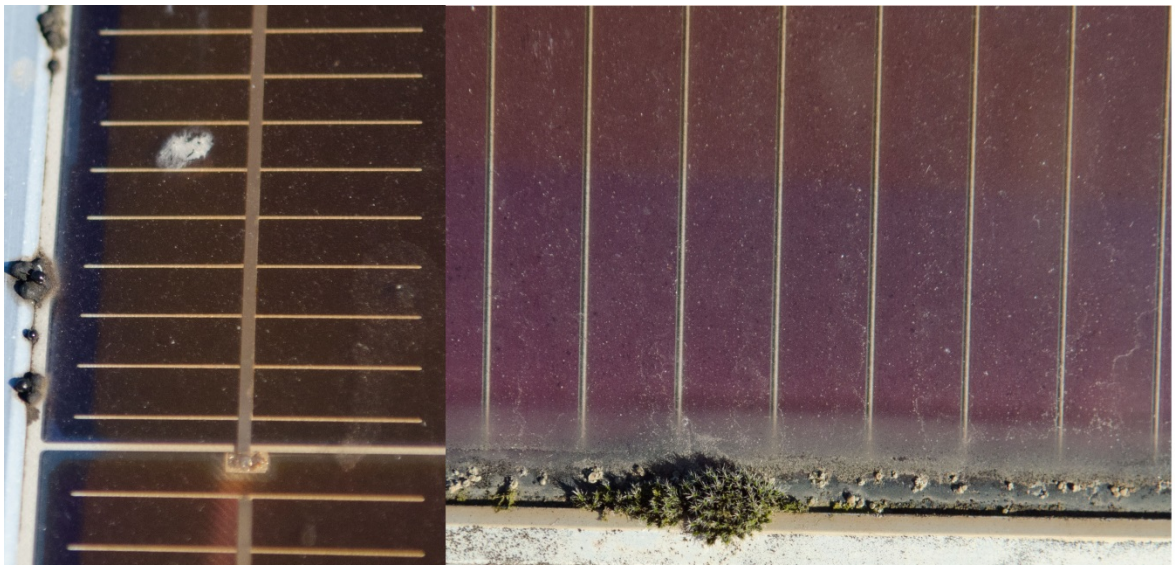

Fig. 38: Example of bird droppings (left) and moss (right) on a PV module.

Manmade structures such as solar arrays can provide good nesting sites for birds. For example, birds have been known to nest behind the heliostats in large solar thermal systems [178]. These problems tend to occur near populations of birds and include urban areas [174]. However, this type of biological soiling tends to have a higher impact on remote area power supplies or standalone PV systems, particularly offshore systems, where cleaning is impractical [179]. Lamont and El Chaar (2011) commented that birds tend to nest or rest on offshore platforms, leaving behind droppings and nests which can detrimentally affect PV performance.

In summary, biological soiling is one component of the total soiling affecting a PV module. However, it can be particularly detrimental due to the optical absorption characteristics and the particle size. The contribution and growth of biological soiling is very location and climate dependent, but can largely be modelled as part of the contribution to general soiling and dust formation. Measurements have shown that the decrease in transmittance to the solar cell as a result of the soiling is approximately the same as the reduction in power output from the cell [169]. As such, this can be modelled by reducing the initial current j_{sc} of the current source in the cell. Very dense soiling, such as large clusters of bird droppings, can be also be modelled as a reduction in current. In addition, the uneven shading may cause some further issues. This can be modelled as a PV module under non-uniform irradiance.

3 Database on Module Failure Modes and their Impact on the PV Module Power

We designed a survey format to collect failure data of PV systems for various climate zones. The goal of the survey is to evaluate the possible different impacts of the failures for Köppen-Geiger climate zones [180] and give recommendations for test methods depending on the climate zone.

In Chapter 3.1 existing surveys on PV system or PV components are reviewed. Chapter 3.2 introduces the survey format used in this publication. The analysis of the survey is presented in chapter 3.3.

3.1 Review of other field failure databases

With the rapidly expanding number and size of PV systems [181] being produced and installed in the field, it is becoming increasingly important to develop an understanding of their reliability and performance. As such, it is essential that we quantify the types, locations and frequency of failures in PV systems installed in the field. This will ensure information on the reliability and occurrence of faults is available to advise the industry and consumers on best practices in the choice of system components, manufacture, and maintenance of PV systems.

Globally, there has been much data collected on the conditions of PV systems and modules after they have been deployed in the field for a number of years. Yet, these surveys or studies are often conducted on isolated systems and generate relatively small datasets. To establish good statistics on the occurrence of field failures of PV modules it is essential to produce large datasets. These datasets must also include a variety of technologies from different manufacturers and climatic zones. Including this range of data will allow links between technologies, locations and failure modes to be determined. An example of this correlation is the tendency for PV modules installed in regions with relatively high ambient temperatures and dry climates to show more severe yellowing of the encapsulant than in other locations [182].

The data so far collected can only account for a small fraction of the total number of systems installed. This drives the need for a survey which can collect comprehensive data that samples a significant portion of number of installed PV systems globally. Although such a survey does currently not exist, there has been a number of smaller scale surveys that have been conducted. This review aims to show the types of PV system surveys that have been conducted to date and the type of data they collect. This information has been used for the development of the PV Failure Database described in 3.2. Therefore, the database will allow using a great number of results from primary surveys.

The studies that have been published and are publically accessible can be classified into three main sub groups. Group 1 are surveys where the data acquisition is done by experts, group 2 are surveys where the data acquisition is done through voluntarily reporting by people which are partly non experts and group 3 pertains to long-term outdoor measurements. There are variations and exceptions to these main groups such as case studies of individual locations and small arrays [183]. Each of these three main variants is discussed in more detail below, with key differences and advantages highlighted. Each type tends to be identifiable in part by the equipment and methodologies used for data collection. However, there are some overall trends that become apparent, such as the increased usage of a formalized visual inspection sheet or module condition report that originated from NREL [184] and TASK13 in the report “Review of Failures of Photovoltaic Modules” [1].

3.1.1 Expert data acquisition

This group of studies is performed by researchers or industry groups, experts in the field, going to the sites and collecting data or conducting surveys. The data that is collected may include a variant of visual inspection [182], [184]–[187] which in some cases is a variation of the visual inspection sheet produced by NREL [184]. This visual inspection is then often backed up by more technical approaches such as IV tests and infrared imaging [188], [189]. The specific equipment used by the researchers varies from study to study with the availability of different measurement equipment.

The All India Survey of Photovoltaic module degradation conducted in 2013 [182] is a good example of this category of study. In this study researchers went into the field and surveyed the condition of PV modules. Measurements of the electrical parameters of the PV modules were coupled with a visual inspection derived from the NREL visual inspection sheet. The All India Survey observed socio-economic factors as well as correlated the faults and data with the different climatic zones covered by the survey. They found that discoloured modules tended to correlate with hot and dry climates, while corrosion was most common in hot and humid zones.

This type of of study can be effective as they can be conducted on the same system over a number of years to give a chronological progression of field failures and faults. The PVRessQ! field survey of PV system failures [188] collected many data points from AIST which show a steady increase in the number of failed modules (of the 1080 installed). The data in this survey included visual identification of faults as well as IR and *IV*-measurements.

Many smaller scale case studies and inspections of PV modules in the field also fall into this category and include studies from Africa [190], Asia [191], Kenya [185] and Australia [183]. Some studies focus on the PV module in great detail [192] while other studies are more focused on the performance of the PV system and record less details on faults within the PV module [193].

The core advantage of this type of survey or study is that they tend to be delivered and implemented by experts in the field with access to the appropriate equipment for electrical and optical measurements. This produces a high quality peer-reviewed dataset. However, although large data sets exist [188], the number of PV systems covered in these studies is generally smaller than other types of studies. These are likely costly to implement due to the time required to take detailed measurements and the costs of the measurement equipment.

3.1.2 Voluntary reporting

Surveys and studies that fall into this category are conducted by the owner/operator, installer, regulator, end user of the PV system or industry groups and the data is reported back to a central agent. This is typified by the person(s) involved with the PV system voluntarily reporting data. The data that is collected tends to centre around visual inspection of the modules and system components [194], but may also include infrared measurements or IV tests in some situations [195], [196]. In this type of survey the type of system or module fault can be collected and may be verified by photographic evidence in some cases. The results of only a relatively small number of this type of survey or study are publically available.

Examples of this type of study include the 1000 roofs program in Germany where data was self-reported by end users. The studies collected data on the type of system fault (inverter and PV module) as well as the occurrence of the faults over a number of years [196]. They found that the PV module (referred to in their study as “solar generator”) was responsible for a proportionately larger number of reported faults than the inverter and other system defects [196].

Other surveys are targeted at a broader customer base, such as the consumer survey in Australia conducted by a consumer advocate group. This survey has 700 respondent advocates and captured data on system information, brands, reliability, and costs. The results of this survey indicate

that 25% of the owners had problems with their system, 12% of which were problems with the inverter [197]. This survey provides limited technical detail, but does provide a good snapshot of the overall reliability of PV systems in Australia. Another study conducted in Australia is targeted specifically at the faults occurring within the PV systems. The PV Fault Reporting Portal (PVFRP) is a web based system open to owners, operators, installers, and inspectors [194]. This portal allows respondents to self-report information on which part of a PV system has failed and relies primarily on visual inspection by the end user of the PV system.

The major advantage of these self-reported data sets is that they can potentially reach a very large audience if widely publicized. This allows a significant amount of data to be collected from a broad geographic region by a crowd-sourced or citizen-science approach. However, the data require further validation because the people collecting the data are not experts in the field. For example, interpretation of "severe or minor discolouration" in a module is a fairly subjective term. This can be mitigated by appropriate instructions in the survey.

3.1.3 Long-term outdoor measurements

The third group of field fault studies is conducted by a researcher driven project on a relatively small-scale system in long-term outdoor test areas [122], [198]. These tend to be very technical and detailed studies where researchers inspect PV modules and record measurements including IV curves, infrared images, spectral response of the module, optical microscopy, and scanning electron microscopy. These are often accompanied by a detailed visual inspection.

The core advantage of these studies is that they provide extremely detailed technical data of high quality. However, they are generally examining small systems or dataset of specific case studies and the scope of these projects can be limited. These provide great technical detail, but are not collecting information on the frequency of occurrence of field failures on a larger scale.

3.1.4 General trends from the data that has been published

A meta-analysis of the data collected in the surveys and studies described above shows the categories of information that have been collected. Although not an exhaustive survey of all case studies on PV systems, this does highlight likely questions and areas of focus for the new survey.

Tab. 3: Proportion of studies that have collected varieties of general PV system information. Percentages indicate the proportion of the studies identified that collected this information, i.e. 100% indicates all identified studies included this information.

Group	Manufacturers (brands)	System size or module rating	Costs	Performance degradation
Expert data acquisition	67%	92%	58%	58%
Voluntary reporting	67%	100%	33%	100%
Long-term outdoor studies	67%	67%	-	67%
Total	67%	89%	42%	63%

As seen in Tab. 3, the three groups of studies all tend to collect similar information in regards to system configuration, manufacturers of the components and the overall degradation of the per-

formance of the system. Many datasets are less concerned with the capital costs associated with the system as they vary widely and have dropped dramatically over the last decade [181]. As such, information on costs rapidly becomes out of date. Information that is worth including in the future surveys are the manufacturer, the nominal system power and a focus on the overall degradation of the system.

Tab. 4: Proportion of studies that have collected information on faults in the components of PV systems. Percentages indicate the proportion of the studies identified that collected this information, i.e. 100% indicates all identified studies included this information.

Group	Data Acquisition System	Inverter	Junction Box	PV Module	Other	AC Disconnects
Expert Data Acquisition	8%	33%	42%	83%	42%	8%
Voluntary Reporting	-	100%	67%	67%	100%	-
Long Term Outdoor Studies	-	33%	-	100%	-	-
Total	5%	42%	37%	84%	42%	5%

Tab. 5: Proportion of studies that have collected data on specifics of PV modules and the methodology used. Percentages indicate the proportion of the studies identified that collected this information, i.e. 100% indicates all identified studies included this information.

Group	Module Certification	Visual Inspection	Visual Inspection derived from NREL/TASK13	IV Test	IR Record	Details on Types of Fault
Expert Data Acquisition	25%	75%	25%	50%	42%	50%
Voluntary Reporting	33%	67%	33%	-	33%	67%
Long Term Outdoor Studies	-	100%	-	100%	100%	100%
Total	21%	79%	21%	53%	47%	63%

The meta-data analysis on which components are containing faults in Tab. 4 indicate that many surveys focus on the PV module itself with slightly lower occurrences of data collected on the balance of systems. Interestingly there are few studies on the reliability of the associated data acquisition systems, which are important for long-term reliability measurements on PV systems. These are likely to develop faults, particularly in respect to sensor boxes, over long periods of time. From Tab. 5 it is apparent that the majority of the studies include a variation of a visual inspection, with many more recent studies using visual inspection sheets derived from NREL/TASK13 [184][1]. More studies use a visual inspection rather than an IR or *IV* test which makes sense as it is the test that requires the least equipment costs to implement. It is recom-

mended that future surveys also focus on visual inspection so as to ensure as wide a user base as possible can complete and return information on PV field failures.

There have been many studies conducted on faults in PV systems, and these can be placed into three main types. Each of these types of surveys has its own advantages that are worthwhile incorporating into a new field failure database. The technical details from accelerated lifetime testing and long-term outdoor measurements provide a solid understanding of the mechanisms of PV faults. This information is routinely published in high quality scientific publications and is worth integrating into a larger database. To reach as wide an audience as possible the data collection and reporting should be driven by the end users rather than researchers and experts being dispatched to the site. This allows data to be collected on numerous systems and from a range of climate zones and locations, potentially as part of normal reporting in PV maintenance work or system monitoring. Data entry into the database (or survey form) must be straightforward so that data entry is not an onerous task. However, there also needs to be sufficient detail in the survey and database so that the fault and its significance can be identified. The collection and processing of this information from a large number of PV systems will be able to advise industry and consumers on best practice in the choice of system components, manufacture, and maintenance of PV systems.

3.2 Description of the PV system failure survey

We designed a survey format to collect failure data of PV systems for various climate zones. The goal of this survey is to evaluate the possible different impacts of the failures across various climate zones and give recommendations for test methods depending on the climate zone. For this work we use the climate groups defined by Peel based on Köppen and Geiger (KG) A Tropical, B Arid, C Temperate, D Cold (continental), and E Polar for classification of climatic zones. We rename and regroup the zones to Hot and Humid (A), Hot and Dry (B), Moderate (C), and Cold and snow (D&E) [180].

The survey is implemented in a Microsoft Excel 2010 spreadsheet. The format of the survey is shown in Fig. 39. The survey and an description of the survey can be downloaded from the IEA PVPS internet home page [199], [200]. The list of possible choices is given in Tab. 6. The survey is segmented into three sections. In the first section “PV system basics” basic data of the PV system is collected. In the second section one must specify the amount of the above specified system one has inspected. The third section allows specifying for each part of the total system to give a detailed analysis of the found failures and the therewith related power loss and safety issues.

The survey is designed to collect data from PV experts, scientific publication, system owner, installer, manufacturer, and internet surveys. By noting the source in the survey, the quality level of each dataset is recorded. This allows the survey to access a greater pool of data.

The climatic zone, way of data collection, the module type, and other things are collected in the database. However, to get results out of the database the categorization must be as robust as possible.

To fill in new data into the survey sheet one has to load the survey sheet into the excel program and choose the worksheet “PV_system_survey”. Scroll to the upper left corner of the worksheet if the cursor is not already there. Click the button “New form” to generate a new input mask. A new mask appears, and the focus automatically jumps to the new mask with a name “PV_system_survey (X)” where X stands for a number. Now one can start to input the data. To delete a table one can press the button “Delete form” then the current visible table will be deleted. To duplicate a table, e.g. the next input is very similar to the one which is already in the database, navigate to the table to be copied, and click on “Copy form”. This generates a new mask with the exact same data. Herein one can edit the form as necessary.

New form | Copy form | Delete form | Survey version 14 October 2016

PV system basics | Goal of this survey | How to start ? | Other questions

System ID:		PV module type		
Source of data		Inverter type		
Country		Mounting system type		
Climate zone		Grounding of substructure & module frames/conductor		
Special stress		Other system component		
Kind of system		Nominal system power	[kWp]	
Orientation		Date of system start	[MM/YYYY]	
Inclination		Date of failure documented here	[MM/YYYY]	
Comment if a field is orange				

Integral data

	Following failure specifications are based on investigated percentage of					
Total system power loss [%]	Inverter [%]	Cable and interconnector [%]	PV module [%]	Mounting [%]	Other [%]	Comment

Failure specification for 0 **% of the system**

Failed system part	Failure 1 specification	Power loss 1 [%]	Failure 2 specification	Power loss 2 [%]	Safety failure 1	Safety failure 2
Inverter	No failure	No detectable loss	No failure	No detectable loss	No failure	No failure
Cable and interconnector	No failure	No detectable loss	No failure	No detectable loss	No failure	No failure
PV module	No failure	No detectable loss	No failure	No detectable loss	No failure	No failure
Mounting	No failure	No detectable loss	No failure	No detectable loss	No failure	No failure
Other system component	No failure	No detectable loss	No failure	No detectable loss	No failure	No failure
Comment if a field is orange						

Fig. 39: The survey is implemented in a Microsoft Excel worksheet. For each PV system five separate failure specifications are available. For most of the input fields a preselection is available. The list of possible preselection is given in Tab. 6.

The **System ID** is a category that enables the contributor to identify the source of its own data input and avoids repeated input of the same data. The **System ID** should de-identify the contributor and not enable other people to identify the source of the data. Furthermore, the **System ID** can be used to address questions from the TASK13 team to the contributor of the data set. The **system ID** will be exchanged in the public version of the database with an arbitrary number. If the current input is extracted from a scientific publication the **System ID** has to be used to fill in the reference of the paper in the IEEE format style. The source of the data must be specified in the category **Source of data**.

Tab. 6: List of possible preselection of the survey shown in Fig. 39.

Source of data:	System owner; Installer; Expert; Manufacturer; Scientific publication; Internet survey; Other; Unknown
Country:	List of all 206 sovereign states
Climate zone:	Hot and humid (A-climate); Hot and dry (B-climate); Moderate (C-climate); Cold and snow (D&E-climate); Other; Unknown
Special stress:	*Island, coastal region (10 km); Agricultural environment; Other; Unknown*
Kind of system:	*Free standing commercial; Roof top commercial; Facade/roof integrated commercial; Free standing test system; Roof top test system; Facade/roof integrated test system; Tracked system commercial; Tracked test system; Other; Unknown*
Grounding of subst. of mod. frames/cond.:	*Non/non; Grounded/non; Grounded/conductor +; Grounded/conductor -; Non/conductor +; Non/conductor -; Other; Unknown*
Orientation:	*-90° (east); -67,5° (east-southeast); -45° (southeast); -22,5° (south-southeast); 0 (south); 22,5° (south-southwest); 45° (south-west); 67,5° (west-southwest); 90° (west); 112,5° (west-northwest); 135° (northwest); 157,5° (north-northwest); 180° (north); -157,5 (north-northeast); -135 (northeast); -112,5 (east-northeast); East/west; Tracked; Other; Unknown*
Inclination:	*90 (horizontal); 80; 70; 60; 50; 40; 30; 20; 10; 0 (zenith); Other; Unknown*
PV module type:	*Monocrystalline Si; Multicrystalline Si; CdTe; CIGS; a-Si; a-Si; Multijunction a-Si; Organic; Other; Unknown*
Inverter type:	*Central inverter with trafo; Central inverter without trafo; String inverter with trafo; String inverter without trafo; Module inverter; Resistor; Single module analyser; Other; Unknown*
Mounting syst. type:	*Clamps; Rail system at short sides; Rail system at long sides; Backrail; Roof integrated; Facade integrated; Delta support; Other; Unknown*
Other component:	*Power transformer; Main DC cable; Main AC cable; Battery; Optimiser; Other electric/electronic parts; Other mechanic parts; Other; Unknown*
Inverter failure:	*No failure; Complete failure; Partial failure; Interconnect failure; Failure due to external fire; Failure due to internal fire; Theft/vandalism; Other; Unknown*
Module failure:	*No failure; Delamination; Defect backsheet; Defect junction box; Junction box detached; Frame breakage/bown/defect; Discolouring of pottant; Cell cracks; Burn marks; Potential induced shunts (often named PID-s); Potential induced corrosion (often with thin-film modules); Disconnected cell or string interconnect ribbon; Defective bypass diode/wrong dimensioned; Corrosion/abrasion of AR coating; Glass breakage; Isolation failure; CdTe: back contact degradation; Hail -> glass breakage/cell breakage; Snow load -> deformed frame/glass- /cell-breakage; Storm -> deformed frame/glass-/cell breakage; Direct lightning stroke -> defect glass/frame and defect bypass diodes; Animal -> bite/corrosion/dirt; Biofilm soiling; Dust soiling; Humidity corrosion/silver finger corrosion; Failure due to external fire; Failure due to internal fire; Theft/vandalism; Other; Unknown*

Mounting failure:	*No failure; System design failure; Overload of structure; Material failure; Indentation/damage of the roof; Clamp detachment/improperly installed; Failure due to external fire; Failure due to internal fire; Theft/vandalism; Other; Unknown*
Interconnect failure:	*No failure; Connector does not fit (e.g. different manufacture); Connector corroded; Defect combiner box; Defect string fuse; Animal bite/other animal issue; Isolation failure; Wrong interconnection; Failure due to external fire; Failure due to internal fire; Theft/vandalism; Other; Unknown*
Power loss:	*No detectable loss;]0%-3%];]3%-10%];]10%-20%];]20%-30%];]30%-40%];]40%-50%];]50%-60%];]60%-70%];]70%-80%];]80%-90%];]90%-100%];]20%-50%];]50%-100%]; Other; Unknown*
Safety failure:	*No failure; Fire/burn mark failure; Electrical isolation fails; Mechanical failure; Other; Unknown*

In the following subsections we give three examples how to fill in the survey format.

3.2.1 Simple standard roof top system

To input a simple standard roof to system simply go through the fields, and choose from the drop down lists the input. For a typical roof top system choose in the category **Kind of system** the item *Rooftop commercial*. In the category **Orientation** choose one system orientation which is closest to or the mean of the system orientation. There is one special item for *west/east* oriented systems. Roof top systems with various orientations which differ from each other more than ±22.5° must be split into two systems. For each orientation a table has to be filled in. The inclination of the photovoltaic modules must be filled in the category **Inclination**. Choose the closest inclination item. For systems with various inclinations of the photovoltaic modules, for each inclination a table has to be filled in if the inclination angle varies more than ±10°.

3.2.2 Large system with components of various types

For large systems with components of various types, for each part of the system with one equal set of system components one failure survey should be filled.

If one type of failure causes a variety of power losses the failure should be split up into several parts. E.g. there are 10% of the total amount of PV modules with PID-s failure. Five percent points have a power loss of]3%-10%] 3 percent points]10%-20%], and two percent points]20%-30%]. In this case the PV failure survey should be filled in as shown in Fig. 40. If all of these PID-s modules have an additional failure the failure may be added as failure 2. However, it is not possible to include various distributions of different failures. Therefore, it is recommended to focus on the failures with the highest impact to the power loss.

If only 1% of the total amount of modules is examined in a large system consider that in the section “Failure specification for X% of the system” the failure specification is relative to the total nominal power of the system and not relative to the examined part of the system. For example if from the 1% of examined PV modules 10% have a specific failure then one has to fill in: “Failure specification for 0.1 % of the system”.

Integral data

Total system power loss [%]	Following failure specifications are based on investigated percentage of: Inverter [%]	Cable and interconnector [%]	PV module [%]	Mounting [%]	Other [%]	Comment
2			100			

Failure specification for 5 **% of the system**

Failed system part	Failure 1 specification	Power loss 1 [%]	Failure 2 specification	Power loss 2 [%]	Safety failure 1	Safety failure 2
Inverter	No failure	No detectable loss	No failure	No detectable loss	No failure	No failure
Cable and interconnector	No failure	No detectable loss	No failure	No detectable loss	No failure	No failure
PV module	Potential indu	]3%-10%]	No failure	No detectable loss	No failure	No failure
Mounting	No failure	No detectable loss	No failure	No detectable loss	No failure	No failure
Other system component	No failure	No detectable loss	No failure	No detectable loss	No failure	No failure
Comment if a field is orange						

Failure specification for 3 **% of the system**

Failed system part	Failure 1 specification	Power loss 1 [%]	Failure 2 specification	Power loss 2 [%]	Safety failure 1	Safety failure 2
Inverter	No failure	No detectable loss	No failure	No detectable loss	No failure	No failure
Cable and interconnector	No failure	No detectable loss	No failure	No detectable loss	No failure	No failure
PV module	Potential indu	]10%-20%]	No failure	No detectable loss	No failure	No failure
Mounting	No failure	No detectable loss	No failure	No detectable loss	No failure	No failure
Other system component	No failure	No detectable loss	No failure	No detectable loss	No failure	No failure
Comment if a field is orange						

Failure specification for 2 **% of the system**

Failed system part	Failure 1 specification	Power loss 1 [%]	Failure 2 specification	Power loss 2 [%]	Safety failure 1	Safety failure 2
Inverter	No failure	No detectable loss	No failure	No detectable loss	No failure	No failure
Cable and interconnector	No failure	No detectable loss	No failure	No detectable loss	No failure	No failure
PV module	Potential indu	]20%-30%]	No failure	No detectable loss	No failure	No failure
Mounting	No failure	No detectable loss	No failure	No detectable loss	No failure	No failure
Other system component	No failure	No detectable loss	No failure	No detectable loss	No failure	No failure
Comment if a field is orange						

Fig. 40: Splitting of a PID-s failure distribution into ranges of power loss. Additional failure can be easily added if they affect all the PID-s affected modules. If the PV-modules or the system has mixed failure modes one should focus on the most relevant failure concerning the power loss.

3.2.3 Enter only PV modules of a PV system

If someone has just information about of a large number of of PV modules installed in a PV system one can also use the survey sheet to input the data. One must fill in as much fields of the system basics as possible. However, one must at least fill in the fields System ID, Source of data, Climate zone, PV module type, Nominal system power, Date of system start, Date of failure documented here and of cause the category **PV modules** in the section Integral data and the full failure specification for the modules in the section. If one cannot give that input one should not use the data as input.

3.2.4 Input of special system characteristics

There are a lot special systems which may differ from standard systems. Some of these systems can be covered by the survey sheet and some not. Tab. 7 shows some special cases and gives suggestions on how to fill the special characteristics into the survey format.

*Tab. 7: Examples to input special system characteristics. **Field names** of the survey sheet are written in bold letters, choice options are written in italic letters.*

Speciality	**Choose in category**	**Item**
Any kind of tracked system	**Kind of system**	*Tracked system commercial* or *Tracked test system*
	Orientation	*Tracked*
Special location near the cost (10 km)	**Special stress**	*Island, coastal region (10 km)*
The system must be very anonymous	**Country**	*unknown*
Visual change, but no power loss	do not input	-
The PV system is located in climate zone E, but there is only a category *Cold and snow (D&E-climate)*	**Climate zone**	*Cold and snow (D&E-climate)* We decided not to differentiate between climate zone D and E
If I choose in a **power loss** column the item *]0%-3%]* the cell gets orange		The measurement technique is normally not that precise that one can state a power loss of 3% or less. If one wants to state a power loss of 3% or less a **comment** has to be added explaining how one assured the precision of the power loss measurement of 3% or less.

If somebody chooses in one category the item *other* he should specify the input in the **Comment** field of the correspondent section of the survey. One must fill in the name of the field where one choose *other* and add additional information in the following format:

Category: information

If one has multiple categories with the item *other* in one section one can add multiple comments into the **Comment** field by separating them by semicolon, e.g.:

Comment: Kind of system: Modules are integrated into noise protection wall; PV module type: Bifacial monocrystalline Si

However, the user is encouraged to select one of the existing categories even if they do not fit exactly. For the former example one could also choose the following:

Kind of system: *Facade/roof integrated commercial*

PV module: *type monocrystalline Si*

3.3 Findings of the PV system failure survey data base

In the following three subsections the composition of the collected data is shown, the methods for how the data is evaluated, and the results are presented.

3.3.1 Composition of the survey data

In this chapter the composition of the survey data is presented in Fig. 41 to Fig. 45. This allows to check the representativeness of the dataset relating to the most important PV system characteristics.

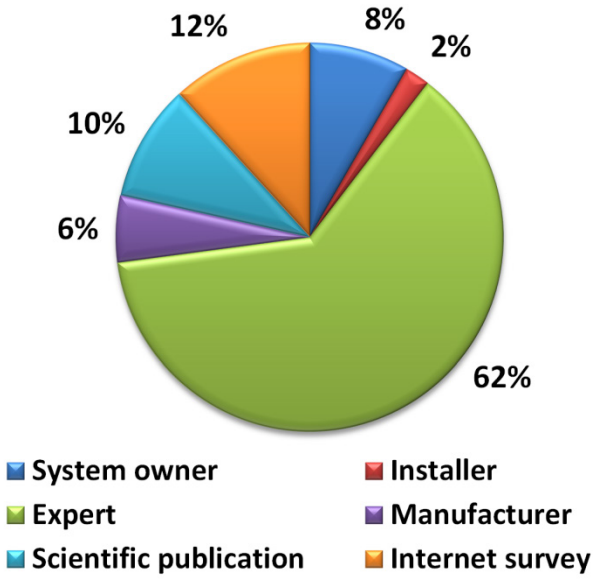

Fig. 41: Relative composition of the data sources.

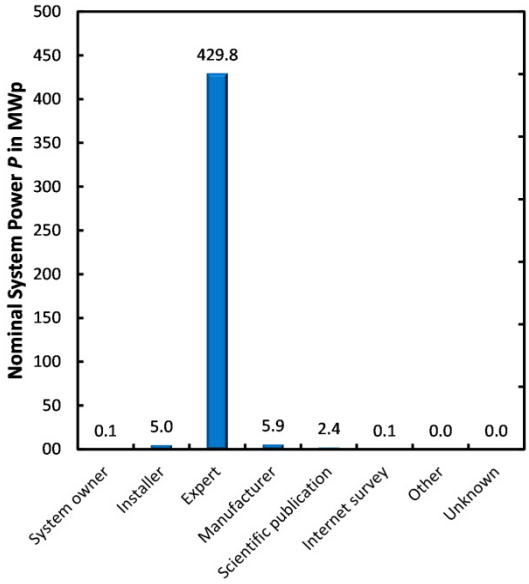

Fig. 42: Composition of the data source in summarized nominal system power.

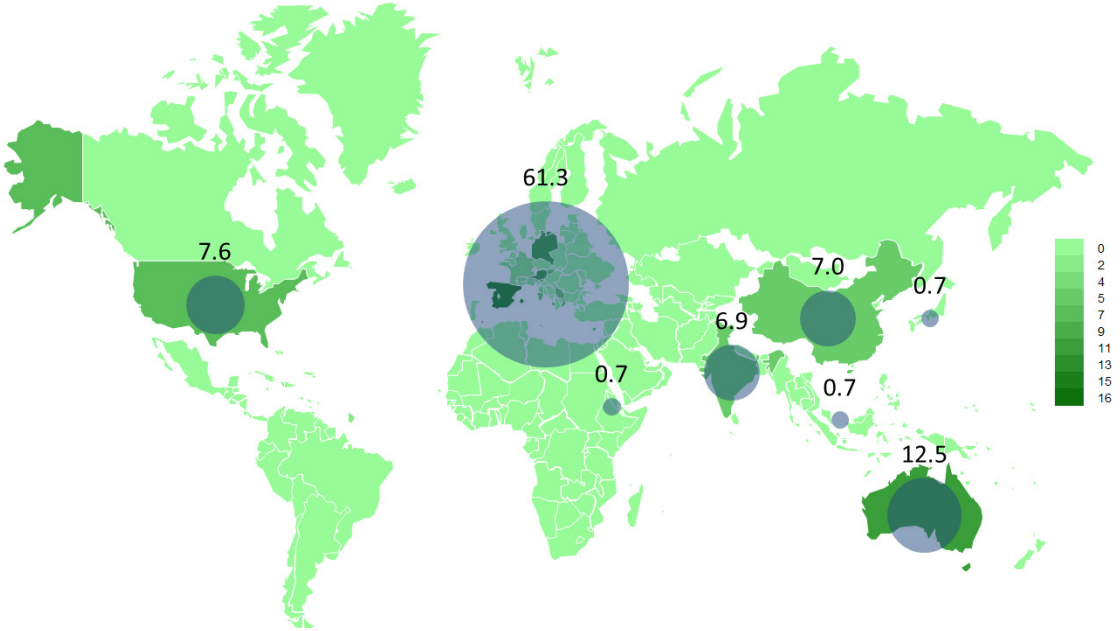

Fig. 43: Relative composition of the countries within reported data.

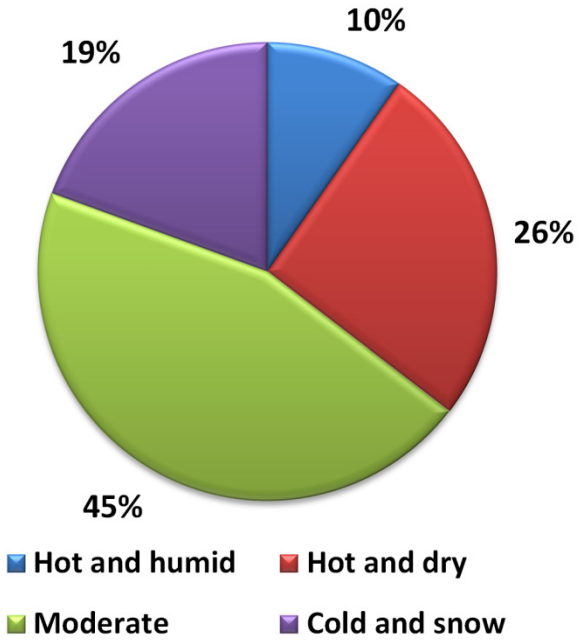

Fig. 44: Relative composition of the climate zones within reported data.

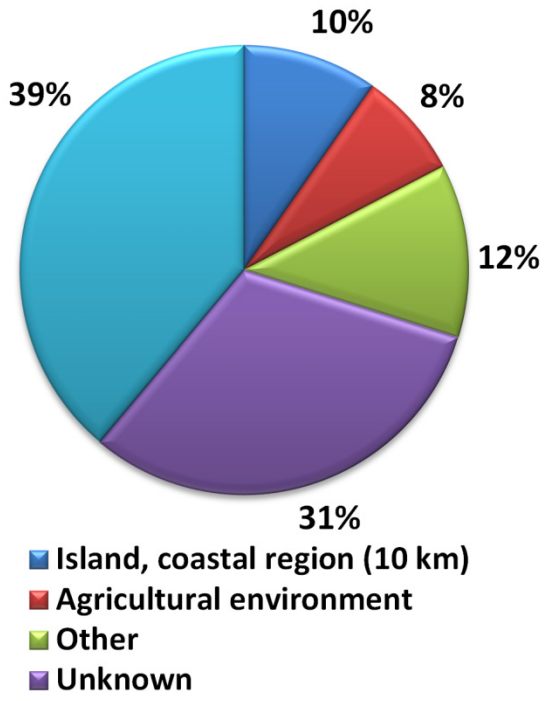

Fig. 45: Relative composition of the special stress within the reported data. The turquoise colour shows the amount of data with no comment in this section.

Especially for the stress level of the PV systems shown in Fig. 45, it is currently very difficult to define the stress levels of a site in the world. The only accessible source is the climate zone definition of Peel based on Köppen and Geiger climate zones [180]. For important stress levels like e.g. typical snow layer thickness, corrosivity of the air or dust impact no worldwide maps or definitions which could be used for the classification of a site are available.

The composition of the kind of PV systems is shown in Fig. 46. Free standing and roof top systems dominate the database. The module type distribution in the survey shown in Fig. 47 correlates well with the relative market share of the module types in the market of these technologies in years 2011-2015 with ~24% for mono, ~66% for multi, and ~10% for thin-film [201].

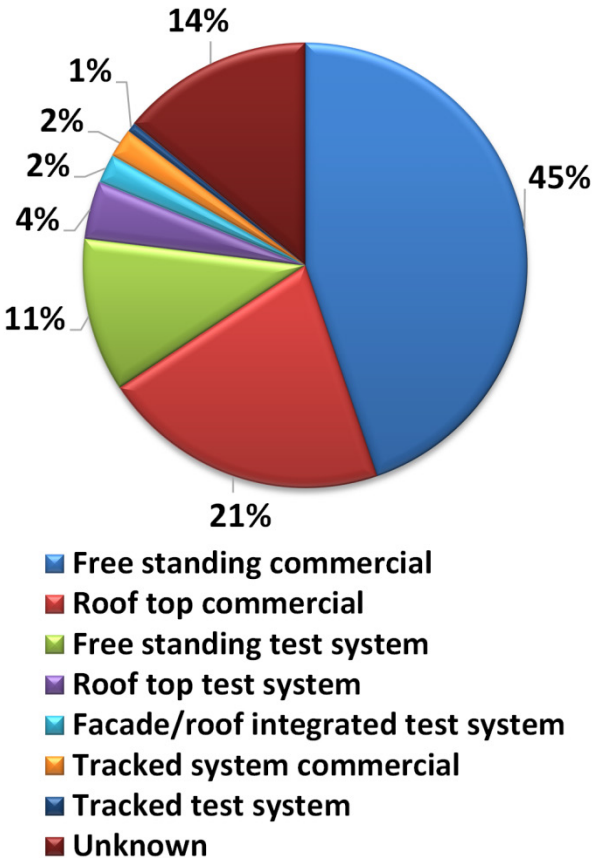

Fig. 46: Relative composition of the kind of system types within reported data.

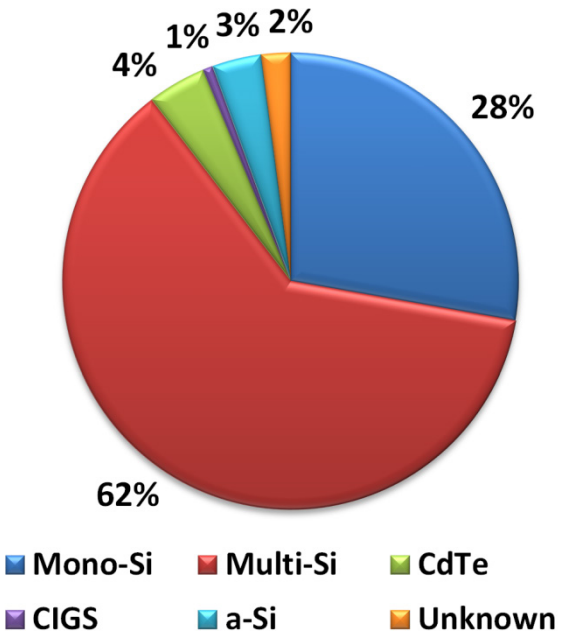

Fig. 47: Relative composition of the special stress within the reported data. The turquoise colour shows the amount of data with no comment in this section.

3.3.2 Data processing for evaluation

The power loss given by the survey participants has typically an unknown accuracy. Furthermore, it is unknown which reference value is used for the power loss calculation. In most cases one can assume that the power loss is calculated relative to the nameplate power rating because the initial value is not known or the nameplate value is the important value for the reporter.

All survey participants have reported a defect in a PV system. Non-defective systems are not reported. To make use of the manufacturer's warranty only the nameplate power rating of the modules is relevant. So the reported power losses are based on market accepted methods of determining the power loss of PV modules. In contrast to a more scientific definition of a power loss relative to the initial module power the reported power loss is a value relevant for financial negotiations.

The survey is not only restricted to PV module failures, also other system defects can be reported. However, the main part of the reported failures is PV module related. The reported system-based failures causing a power loss are not statistically significant up to now. Therefore, only module-related failures are analysed in this document.

For the time dependence of power degradation several power loss categories have been defined in the TASK13 IEA-PVPS T13-01:2014 report [1]. Two of these definitions (C,E) are applicable for statistical evaluation: Category C linear-shaped power loss degradation over time and Category E Degradation in steps over time.

If a PV system has a failure, two possible statements are drawn from the survey. Either the power loss type is of category C type then the measured power loss is converted into a degradation rate, or the power loss is of category E type and the power loss is given in power loss per installed investigated nominal power. Other categories are not able to be evaluated because of missing time dependent data. The linear degradation rate is a fairly good approximation for a small number of PV modules with no or small failures [202]. However, linear degradation often overestimates the yield loss over time because the degradation rate often increases the worse the PV modules get [Jordan2016]. Stepwise degradation (category E) over time is a good approximation for sudden catastrophic failures caused e.g. by a storm or lightning strike. Therefore, we evaluate more or less linear like degrading failure types by a degradation rate and more sudden catastrophic failures by quotient of power loss per installed investigated nominal power. Tab. 8 shows which failure category is represented by which evaluation scheme. Soiling which neither fits in one of the category is evaluated with category E, to show the possible impact.

Tab. 8: Degradation types used for the evaluation of the failures.

Cause of power loss	**Power loss category**
Delamination, Defect backsheet, Defect junction box, Junction box detached, Frame breakage/bown/defect, Discolouring of pottant, Cell cracks, Burn marks, Potential induced shunts (often named PID), Potential induced corrosion (often with thin-film modules), Disconnected cell or string interconnect ribbon, Defective bypass diode/wrong dimensioned, Corrosion/abrasion of AR coating, Isolation failure, CdTe: back contact degradation	C
Glass breakage, Hail -> glass breakage/cell breakage, Snow load -> deformed frame/glass- /cell-breakage, Storm -> deformed frame/glass-/cell-breakage, Direct lightning stroke -> defect glass/frame and defect bypass diodes, Animal -> bite/corrosion/dirt , Biofilm soiling, Dust soiling	E

Fig. 48 illustrates the definition of various partitions of a PV system being important for the definition of degradation rates of power losses. For each survey dataset i the total installed power P_i is collected in the database. For the fault analysis of a failure *x* very often only a part y_i of the total system i is investigated. Furthermore, the failure *x* affects only a part $z_{i,x}$ of the system. The partitions y_i and $z_{i,x}$ are given in percentage of the installed power. These values are the basis of the degradation rate calculations.

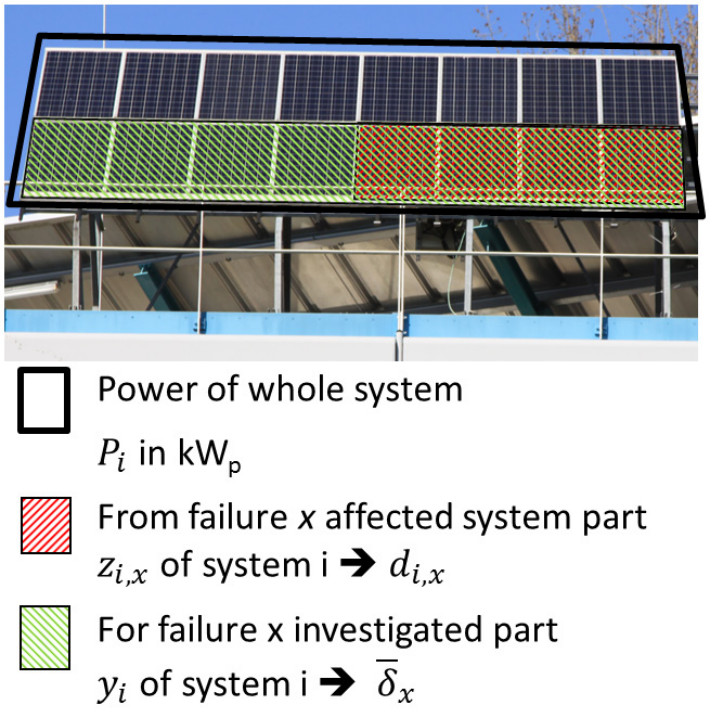

Fig. 48: Definition of various parts of a PV system with the number i. The nominal system power P_i is given in kWp. The parts $z_{i,x}$ and y_i are given in % of P_i.

The power loss $\Delta P_{i,x}$ of a specific module failure x is documented in percent of the affected nominal module power sum. The equation of the degradation rate $d_{i,x}$ of a specific module failure type x of dataset i is given by:

$$d_{i,x} = \frac{\Delta P_{i,x}}{\tau_{b,i} - \tau_{a,i}} . \qquad (28)$$

The parameter $\tau_{b,i}$ is the date of failure documentation of dataset i and $\tau_{a,i}$ is the date of system start of dataset i.

The equation for the degradation rate of the whole system is given by:

$$\delta_{i,x} = d_{i,x} \frac{z_{i,x}}{y_i} , \qquad (29)$$

where $z_{i,x}$ is the percentage of the system being affected, and y_i is the investigated system part in percent from the total nominal system power P_i. For the further evaluations it is assumed that the investigated system part is chosen large enough that the investigation result is representative for the whole system. In this case $\delta_{i,x}$ shows how much the total system is affected by the failure type x.
We define the mean degradation rates $\bar{d}_x$ for the PV modules with a failure x as:

$$\bar{d}_x = \frac{\sum d_{i,x}}{n_x} . \qquad (30)$$

The so calculated mean degradation rate is unbiased by the size of the systems in the dataset. Therefore, small systems have the same impact on the mean module degradation rate for a failure type than large systems.

The mean system degradation rate $\bar{\delta}_x$ defined in accordance to Eq. (30) again unbiased by the size of the systems in the dataset. These degradation rates allow assessing how a failure x affects the whole system power:

$$\bar{\delta}_x = \frac{\sum \delta_{i,x}}{n_x} . \qquad (31)$$

Our survey data does not allow checking if the degradation rates of the found failures are constant over time. However, the degradation rates calculated with Eq. (30)-(31) allow comparing and averaging slowly developing power loss effects.

For sudden power losses caused by a storm, a hailstorm or a lightning strike the calculation of a degradation rate makes no sense. Therefore, we evaluate what percent of the investigated system power p_x affected by any power loss after the sudden event:

$$p_{i,x} = \frac{z_{i,x}}{y_i} , \qquad (32)$$

and how much is the power loss relative to the investigated system power:

$$\pi_{i,x} = \frac{\Delta P_{i,x} z_{i,x}}{y_i} . \qquad (33)$$

3.3.3 Results

Before we evaluate the degradation rates we show the occurrence of failures over the years of operation in Fig. 49. The upper diagram shows the occurrence of all reported failures, and the lower graph shows only failures causing a power loss. Each diagram is split into the occurrence of degrading failures and sudden occurring failures. The occurrence of both failure types accumulates at the first 7 years.

When we focus on special types of failures we see that cell crack failures are mostly reported in the very early stage of PV system operation from year 1 to year 2. Systems with PID-s failure are mainly reported during year 3 and year 4. Disconnected cells or strings in the module are reported after year 4 spread over the whole operation time. Discolouring of pottant is spread over the years, but power relevant discolouring starts after year 3 with a high accumulation after 18 years of system operation. Defect bypass diodes are spread over the first 10 years of operation. The total occurrence of the other failures is too seldom for detailed discussion.

For the current status of collection of failure reports only some mean degradation rates can be analysed. Results based on less than four reports are not discussed. Therefore, in all figures presenting statistical data the basic population of PV systems is shown as number above the mean value.

Fig. 50 shows the unweighted degradation rates for the affected part of the PV systems calculated by Eq. (28). The highest impact on the performance of PV modules have defective bypass diodes in the hot and dry climate with 11%/a and in moderate climate with 25%/a. The degradation rate caused by cell cracks in the cold and snow climate is about 3%/a higher than in the moderate climate and 6%/a higher than in hot and dry climate. The PID-s effect shows a mean degradation rate of about 15% per year. In the moderate climate it is the most often found failure together with a high degradation rate. Unfortunately there are not enough PID-s events documented from other climate zones. The discolouring of encapsulant (pottant) failure is found in the hot and humid, hot, and dry and in the moderate climate as well. In the three climate zones this degradation mechanism is in the mean below 1%/a. Therefore, this effect is most often not the cause for warranty claims.

How much a failure dominates the total system power can be seen by the unweighted degradation rate of the investigated system part calculated by Eq. (29) shown in Fig. 51. For the PID-s effect in the moderate climate the degradation of the investigated system part is reduced by 3/5 compared to the degradation of the affected system part. Therefore, PID-s affects in average

about 3/5 of a system in the moderate climate zone. For cell cracks the same evaluation shows that cell cracks affect about 3/5 of the system in the moderate climate zones if they cause a power loss.

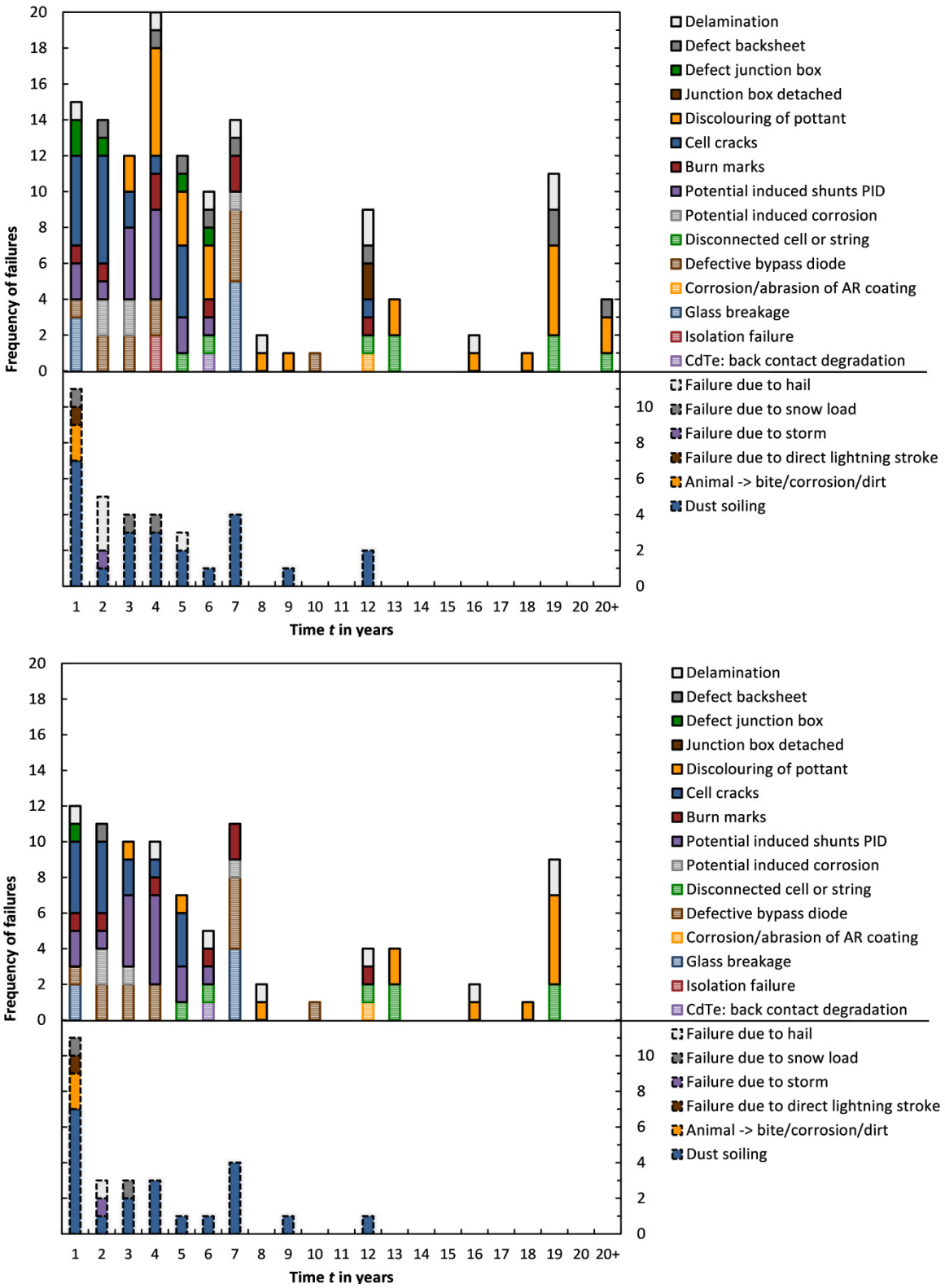

Fig. 49: Occurrence distribution of failures over the years of PV system operation. The failure occurrence is split into degrading failure and sudden occurring failures. The upper graph shows the total failures occurrence of all detected failure. The lower graph shows the occurrence of detected failure which causes a measurable power loss.

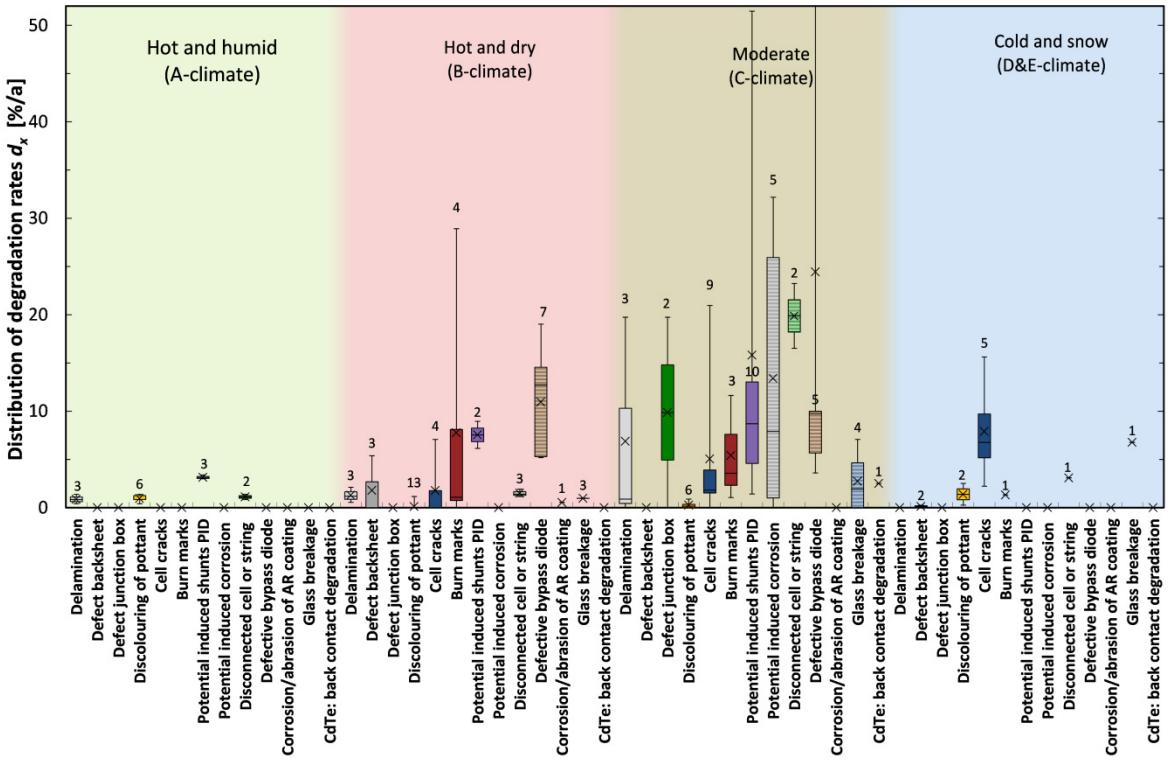

Fig. 50: Box plot of degradation rates dx of PV module affected by failures x sorted by climatic zones. The numbers show the quantity of data per failure in the database. The cross shows the mean degradation rate.

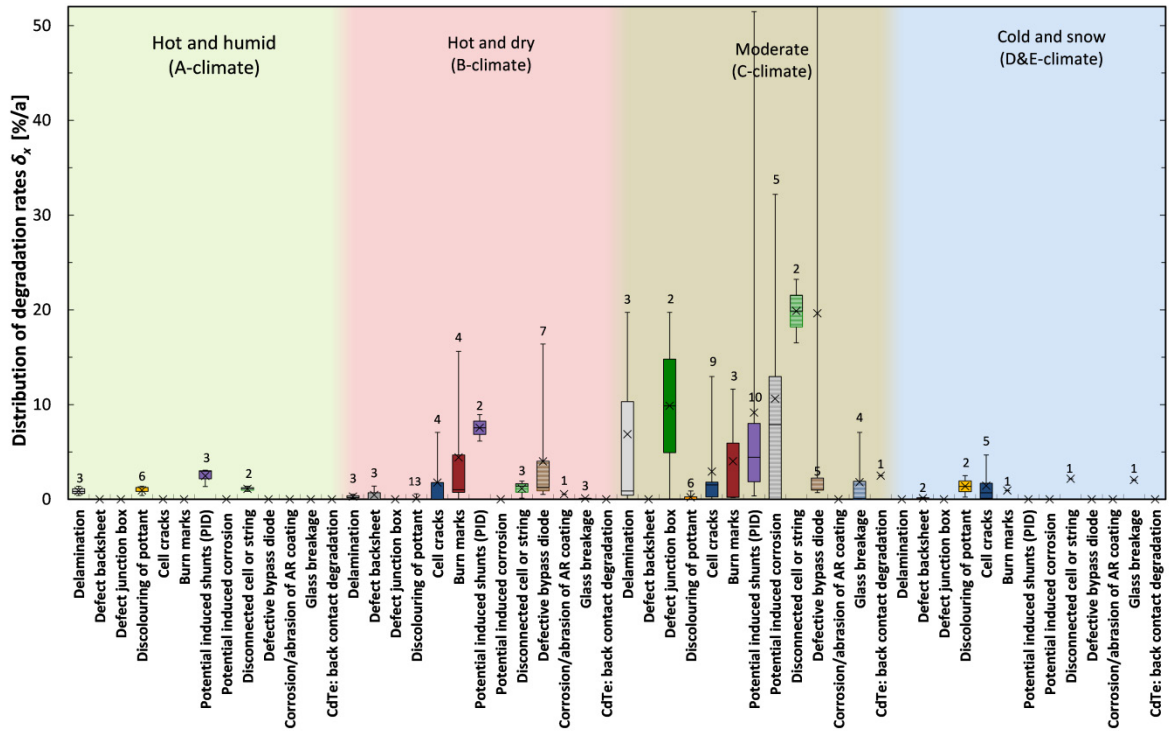

Fig. 51: Degradation rates of the investigated PV system part of PV module failure sorted by climatic zones. The numbers show the quantity of data per failure in the data-base. The cross shows the mean degradation rate.

Fig. 52 shows how much of a system is affected by a sudden event calculated by Eq. (33). As expected, soiling affects almost the whole systems in nearly all cases. There is one event of "Animal -> bite/corrosion/dirt" where animals also soil all of the modules. The events "lightning strike", "storm" and "hail" only cause a power loss on less than 10% of the modules in the system. The failure "snow load" affects about 20% of the modules in the system.

The power loss of a system caused by a sudden event is calculated by Eq. (32) and is shown in Fig. 53. Besides soiling, snow load events have the highest impact on the system power loss. The failure "snow load" affects about 20% of the modules in the system and has an impact on power output of ca. 4%. Other events, such as lightning strikes, storm, and hail only cause a power loss on less than 10% of the modules of the plant and seem to affect less than 1% of the total system power output. Except for soiling the calculations in Fig. 52 and Fig. 53 are mostly based on single to three entries in the database and are therewith only show cases.

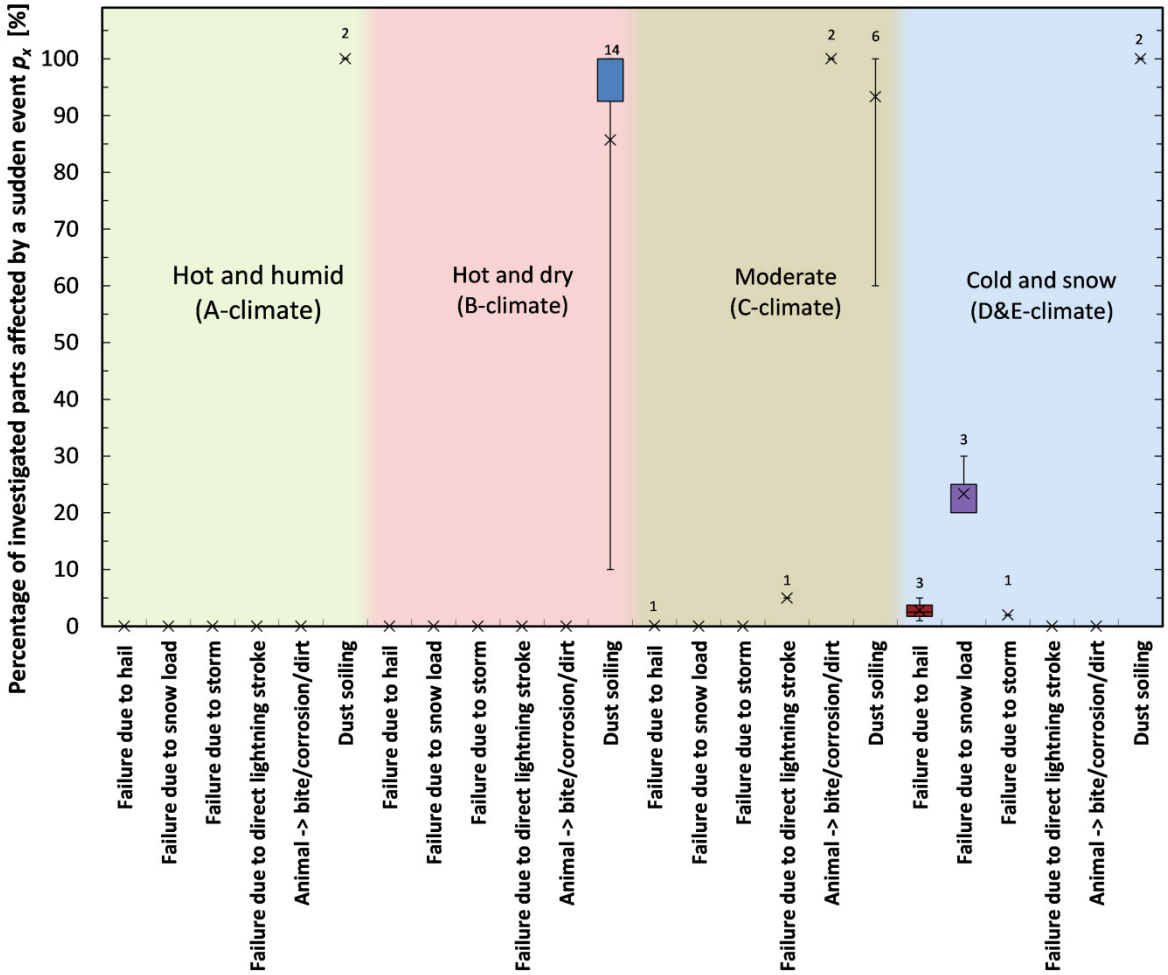

Fig. 52: Box plot of percentage of system part affected after a sudden event. The numbers show the quantity of data per failure in the database.

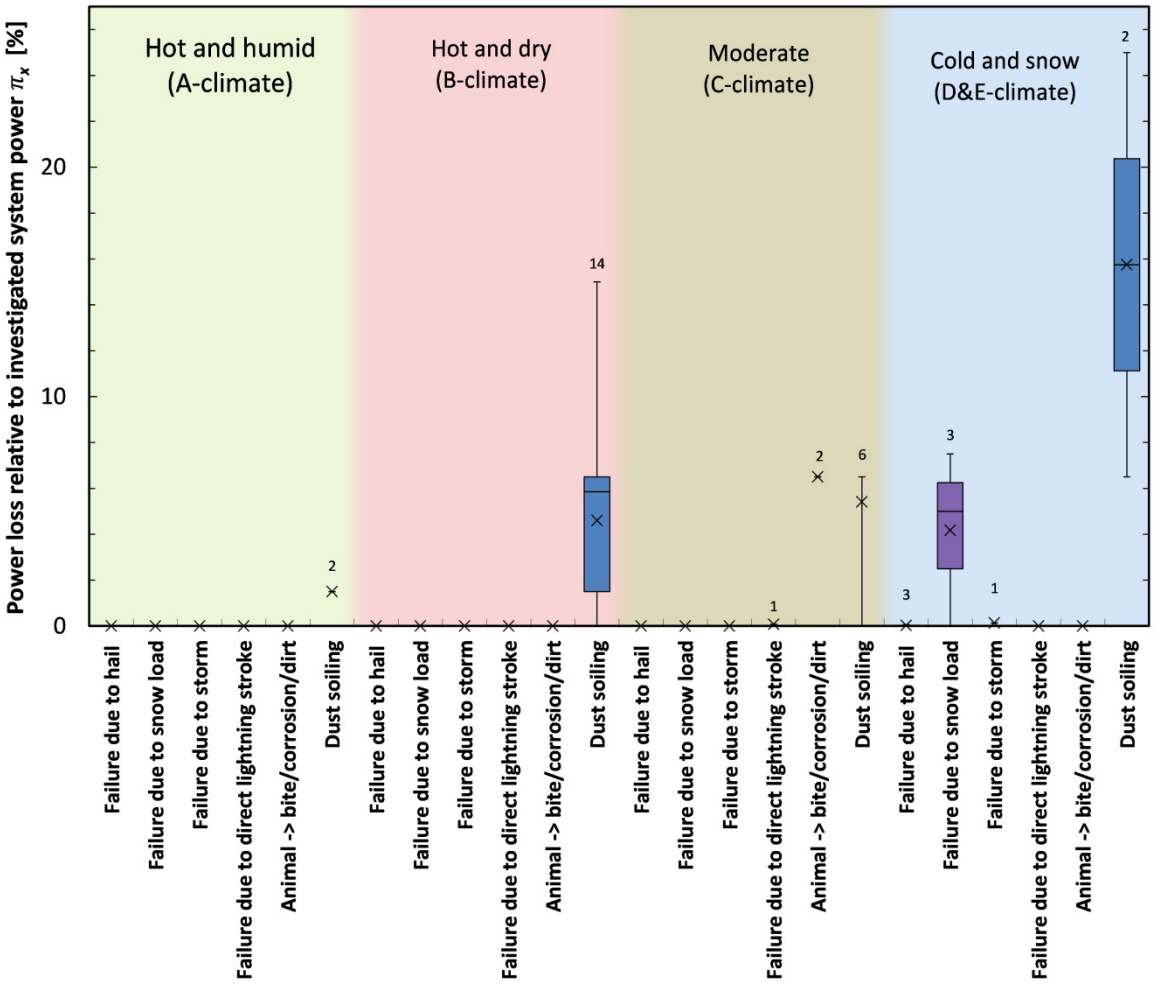

Fig. 53: Box plot of percentage of system power lost from the investigated system part after a sudden event. The numbers show the quantity of data per failure in the database.

72% of all reported failures with the special stress loads “Island, coastal region (10 km)” show a PID-s failure. From the rest data only 4.6% show PID-s. This indicates much higher PID-s risk for island and coastal regions as also found by Berghold [203]. Therefore, one would expect a much higher PID-s degradation rate for “coastal regions/island” systems. But this is not the case. The total degradation rate of the coastal regions/island systems is shown in Fig. 54 in comparison to all other systems. The mean PID-s degradation rate is much higher for other regions than for “coastal regions/island” systems. However, this is caused by some systems in other regions with an extreme high degradation rate.

The distribution of failure occurrences over the operational years of the PV system deviates from a typical bathtub curve. A reason for the difference may be that the number of installed systems changes exponentially with the year of installation. We have much more young systems in the world than old ones as shown in Fig. 55. Therefore, the failure occurrence is highly biased by a not constant annual system installation rate. This may be the reason for the high failure level at the first seven years in Fig. 49. Especially the suddenly occurring failures are highly biased by this effect.

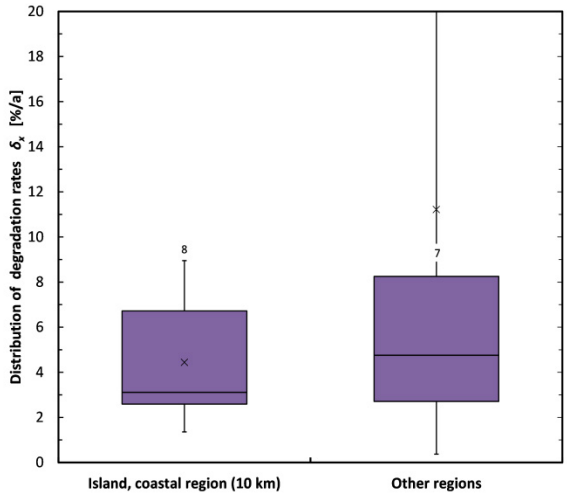

Fig. 54: Box-Whisker-Plot of degradation rate of the investigated part of the system for the PID-s effect sorted by the special stress coastal region and other. The mean value is indicated by a cross.

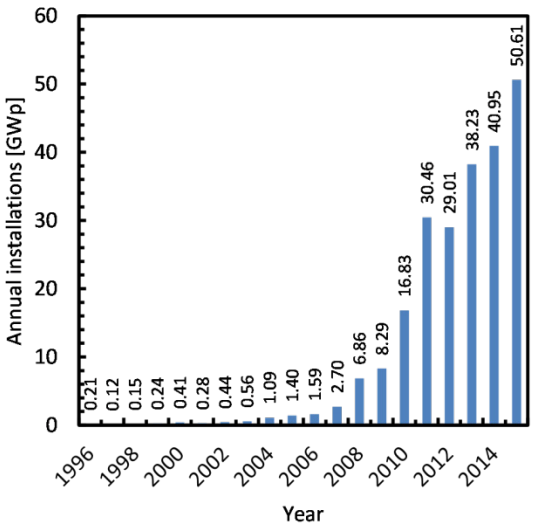

Fig. 55: Evolution of global annual PV system nameplate installations, composed from numbers in [204].

The failure type soiling does not fit into the degrading and sudden failures categories, because the power of soiled module degrades over time, but can fully be recovered. We see a dependence of dust soiling on the climate zones in Fig. 53. However, the high mean power loss due to dust in the moderate C zone (6%) does not coincide with the expectation of finding higher dust soiling losses in the the hot and dry B climate zones (4%). Probably dust soiling is strongly influenced by local conditions. Herrmann developed a model of dust soiling based on weather data and other influencing factors [205]. He showed a correlation between desert and none desert regions. To prove this correlation we would need a much more detailed climate zone resolution than performed in this study.

The anti-correlation between mean degradation rate and occurrence of PID-s in coastal regions/island systems is unexpected. Berghold presented a classification of PID-s modules into “Frame PID-s” where only the cells close to the frame are affected and “Surface PID-s” where almost all cells are affected [203]. The different affected area of the PV module serves to partition the results and influence the observed degradation rates. Berghold suggests that the “Frame PID-s” with the low degradation rate is found in hot and dry locations. But in our database only two island/coast region system are from hot and dry locations. Therefore, this “Frame PID-s” effect cannot explain the relative low degradation rate for island/coast region systems compared to other regions. But there may be some systems among the other region systems that show “Surface PID-s” leading to very high degradation rates that influence the statistic.

Maybe in coastal regions, PV systems are already affected by PID-s if the PID-s effect would not occur for the same systems in the other regions. And in the other regions we find almost heavily degrading PID-s affected systems.

The degradation rates of failure mechanism x affected modules are important for module manufacturers. It demonstrates how fast modules degrades under real-world conditions by failure mechanism x. The degradation rate of the investigated PV system part is important for the bankability of PV systems. Under the assumption that the people who analysed the failures in the system choose a representative part of the PV system for the failure analysis, the degradation rates are also representative for such systems.

The current status of the data collection of PV system failures is preliminary. For some cases inferences can be drawn from the data. The degradation rate due to cell cracks is highest in cold

and snow D/E climate zones. Cell cracks dominate the early failures in year one and two after installation. However, the system degradation rate stays below 3%/a for all climatic zones, while the degradation rates of the affected part is highest with about 8%/a in the cold and snow climate. The next dominant failure is the potential induced shunts effect in year three and four. The mean degradation rate for PID affected systems in the moderate zone is 9%/a and for the affected system parts 16%/a. The PID-s effect occurs 15 times more often in coastal/island regions than in other regions, but is less severe than in other region. Defect bypass diodes heavily affect the module and the system power. The failure occurrence is spread over the first 10 years of system operation. The discolouring of the encapsulant (pottant) is a quite commonly observed wear-out failure. But for all climate zones this is effect is in the mean well below 1%/a for the system and the affected part.

3.4 Description of the visual inspection data collection tool for PV module conditions

A visual inspection data collection tool for the comprehensive evaluation of fielded photovoltaic (PV) modules has been developed to facilitate describing the condition of PV modules with regard to their field performance and appearance [184].

This work is based on the International Energy Agency Photovoltaic Power Systems (IEA PVPS) Programme's Task 13 (Phase 1): Performance and Reliability of PV Systems, Subtask 3.2: Collecting Failures and Adapting Testing Methods to Failure Mechanism for PV Modules by providing a tool for the collection of consistent field data on module degradation and failure [206].

The proposed data collection tool consists of 14 sections, each documenting the appearance or properties of a component of a PV module [206]. Sections 1 to 3 contain information on the location, system configuration and module identification. Sections 4 to 13 focus on individual module components, starting from the rear and finishing at the front of the module. Section 14 documents locations of electronic records (I-V curves, infrared images, etc.). If a new type of defect is found that cannot be adequately described by the options available in the tool, a section entitled "Other" is available for recording anomalous observations at the end of the collection tool (section 15). For data collection requiring numerical input (e.g. altitude, length), metric units are assumed throughout the collection tool.

In order to complete the inspection, the following tools are required: a tape measure with centimeter and millimeter gradations and a pen or other recording implement. It can be useful to directly record the data from the field into the spreadsheet program using a laptop computer or a tablet computer with the collection tool in Microsoft Excel which can also be used in Google Documents Sheets for easier handling in the field. A digital camera is recommended. In the data collection tool's current form, it takes a pair of two experienced inspectors ca. 10 minutes to conduct a full visual evaluation of a single module. A set of modules with exactly the same models could be visually evaluated by two experienced individuals in a period of 5 minutes per module.

In the following, we explain the required input for the PV module condition data acquisition. The module condition data sheet itself is accessible from the PVPS home page [206].

0. Site information: The *Latitude* and *Longitude* fields should be recorded to the nearest hundredth of a degree and should indicate the direction from the equator (+ for North, - for South) or from the Prime Meridian (+ for East, - for West).

1. System Data: The relevant data for the design of the PV system: multiple module system, system bias, system grounding. It should be noted that this section does not refer to the module frame grounding, which is handled in Section 7.

2. Module Data: Besides the module technology type, which should be selected, the certifications section also should be checked and filled out. The estimated deployment date should be recorded as the nearest known date or date range in which installation occurred. The data/information on electrical performance characteristics can be found at module's nameplate.

3. Rear-side Glass: The condition of the glass on the rear side should be evaluated and the damage categorized. The number of cracks/chips and their locations should be catalogued.

4. Backsheet: The appearance of the backsheet should be categorized as "like new", "minor discolouration", or "major discolouration". Discolouration that is considered as minor and major are based on the degree of discolouration. "Wavy (delaminated)" is one of the defects in the texture of the backsheet, which means bumps, bubbles, or ripples in the backsheet have an air gap between the backsheet and the rest of the module or between layers of a multi-layered backsheet. The material quality section is evaluated by passing a finger across the backsheet. Based on the amount of white powder transfer to the finger, a chalking quality should be categorized as either "slight" or "substantial". Evaluating damage to the backsheet is to indicate the types of damage present and provide additional details. The fraction of area exhibiting a particular damage type should be estimated by eye to the closest available option among <5%, 5-25%, 50%, or 75-100% (consistent overall).

5. Wires/Connectors: All types of damage present should be marked and the condition of the connectors should also be cataloged, as well as connector type and any observed damage.

6. Junction Box: The damage to the junction box (JB) should be further classified by selecting all applicable damage types among the following options: weathered, cracked, burnt, and/or warped. "Weathered" refers to damage due to environmental exposure such as UV damage, abrasion, or leaching and is manifested as a colour or texture change. For modules with attached wires, how well the wires are attached to the junction box should be evaluated, as well as the quality of the seal between the wires and the junction box and the evidence of prior arcing.

7. Frame Grounding: The presence and condition of frame grounding should be evaluated. For module designs that lack a proper frame grounding clip or connection and/or for modules that have such a fixture, but has not been connected, the inspector should mark the original state as "no ground."

8. Frame: The appearance of the frame should be evaluated and the damage including discolouration or corrosion should be recorded.

9. Frameless Edge Seal: The inspector should evaluate the appearance of the edge seal, giving further information about the fraction of area affected if the material is discoloured. All applicable damage types should be selected, with the fraction of area affected indicated if delamination has occurred.

10. Glass/Polymer (front): The material, features of the front panel should be evaluated and noted. Furthermore, the data for degree of soiling, e.g. composition, should be collected. The damage should be categorized and the number of cracks/chips and their locations should be cataloged.

11. Metallization: For metallization that can be visually inspected, the inspector should evaluate its appearance and any damage:

Light discolouration: mean an apparent luster loss or yellowing of the metallization.

Dark discolouration: is for metallization that is brown or black in colour.

Corrosion: is marked by the presence of galvanic products that may appear powdery, white, light gray, and/or have a yellow, blue, or green tinge.

Burn marks: are indicated by the presence of brown or black colouration, bubbling or melting of the polymeric encapsulant, and/or glass breakage or local loss of backsheet material.

12. Silicon (mono or multi) module: This section is referred to single and polycrystalline silicon modules only. Besides the inspection of layout, discolouration should be evaluated. The predominant discolouration should be classified, pertinent details about the number of discoloured cells, degree of discolouration, and all locations where discolouration is present should be recorded as well.

13. Thin-film module: Section 13 pertains to thin-film modules including amorphous silicon, CdTe, CIGS/CIS and emerging technologies that are more similar to these than crystalline silicon wafer technologies. Similar to section 12, the module layout, appearance, and damage should be evaluated and recorded. The extent of delamination should be categorized. Any locations where delamination has occurred should be noted, as well as the predominant delamination type. Absorber delamination is marked by a silver or sparkling appearance that often begins from module edges and follows along the edges of scribe lines to create a characteristic appearance referred to as 'bar-graph'-type delamination, whereas AR coating delamination has the appearance of bubbles or buckling.

14. Electronic Records: Section 14 provides a space to record various electronic records: digital photo files, I-V curve(s) and electroluminescence (EL) and infrared (IR) images. If the *I-V* response of PV module is measured, the connector function should be evaluated as one of the provided options: functions, no longer fits, or exposed (connector does not properly seal the electrical connection). If a test of the bypass diodes is performed, the total number of diodes should be recorded, along with the number of diodes that are found to be shorted or in open circuit condition and any evidence of damage or overheating of diodes.

Cataloguing visually observable defects and correlating this data with climate zones and exposure time period will provide statistics that determine whether a particular visual defect is relevant for specific locations and will give information on the degree of degradation over time. In this section we use the same climate groups as in chapters 3.2 and 3.3 with the following structure: Hot and humid (A-climate); Hot and dry (B-climate); Moderate (C-climate); Cold and snow (D&E-climate). However, in this case the location data of the PV module condition sheet is used to assign the climate zone according to the Köppen-Geiger climate classification system updated by Kottek et al. [207]. In order to better understand the described failures that are detectable by visual inspection, photos of these failures for each section/component are provided in Tab. 9.

Tab. 9: Overview of PV module failures detectable by visual inspection in the field.

#	Section	Option 1	Option 2	Option 3	Option 4	Option 5
4	**Backsheet**	Burn marks	Bubbles	Delamination	Cracks/ scratches	Abrasion
		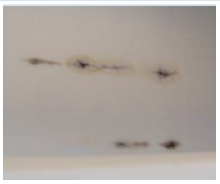			 [182]	
5	**Wires**	Cracked/ disintegrated insulation	Burnt	Corroded	Animal bites/marks	
					 [208]	
5	**Connectors**	Weathered	Cracked	Burnt	Corroded	

#	Section	Option 1	Option 2	Option 3	Option 4	Option 5
					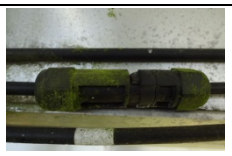	
6	**JB Lid**	Loose	Fell off	Cracked		
						
6	**JB adhesive (attachment)**	Loose/brittle	Fell off			
			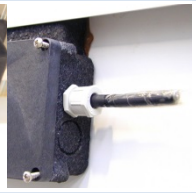			
6	**JB wire attachments**	Loose	Fell off	**Section: Seal leak**	Arced/starts a fire	
		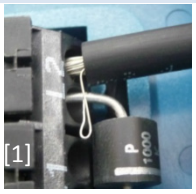 [1]			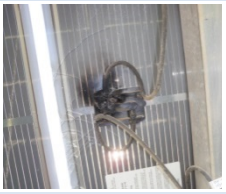	
7	**Frame Grounding**	Some corrosion	Major corrosion			
			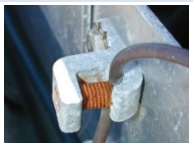 [209]			
8	**Frame**	Minor corrosion	Major corrosion	Frame joint separation	Bent frame	discolouration
		 [182]		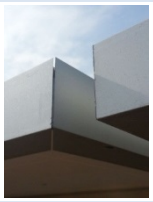		
8	**Frame Adhesive/ adhesive tape**	Adhesive oozed out	Adhesive missing in areas	Delamination of tape	Adhesive tape missing in areas	
						
9	**Frameless edge seal**	Visibly degraded	Squeezed/ pinched out	Shows signs of moisture	Fraction delaminated	

#	Section	Option 1	Option 2	Option 3	Option 4	Option 5
			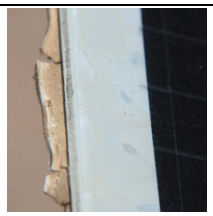			
10	**Glass/polymer (front)**	Shattered (tempered)	Cracked	Chipped	Milky discolouration	
		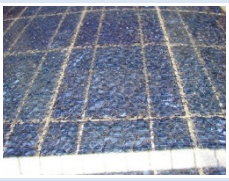			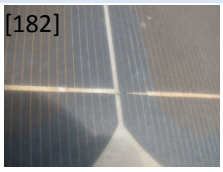 [182]	
11	**Busbars**	Obvious corrosion	Diffuse burnmarks			
		 [210]				
11	**Cell interconnect ribbon**	Obvious corrosion	Burn marks	Breaks		
		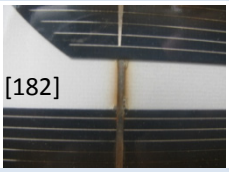 [182]				
11	**String interconnect**	Obvious corrosion	Burn marks	Breaks	Arc tracks	
		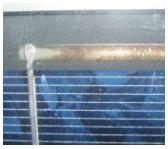			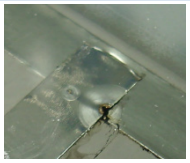	
12	**Silicon module**	Burn marks	Cracking	Moisture	Worm marks/snail tracks	delamination
			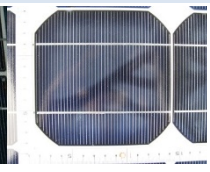		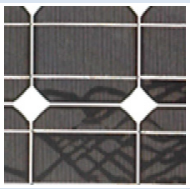	 [1]
13	**Thin film module**	Burn marks	Cracking	Possible moisture	Foreign particle embedded	Delamination
			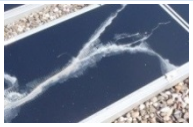			

3.5 Findings of the PV module condition data base

In the following three subsections the composition of the collected data is shown, the methods how the data is analysed and the results are presented.

3.5.1 Composition of the PV module condition data

In this subsection the composition of the PV module data is presented. This allows the evaluation of how representative are the datasets in relation to the most important PV module characteristics and climate zones.

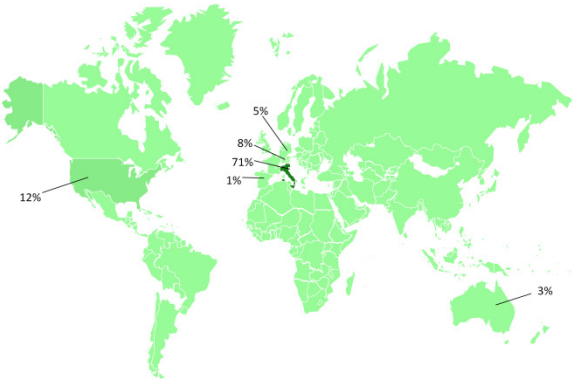

Fig. 56: Collected data distribution over the countries colour coded in percentage of the total number of contributions. Contributions from European countries are summarized to one bubble.

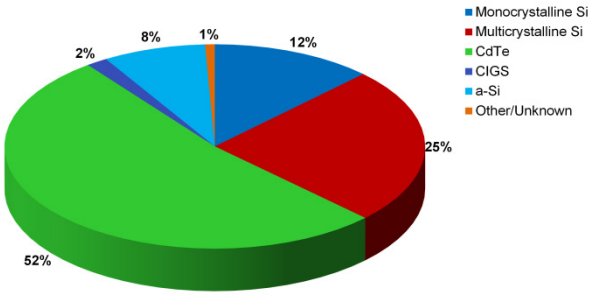

Fig. 57: Relative composition of the PV module technologies used in the reported PV module data.

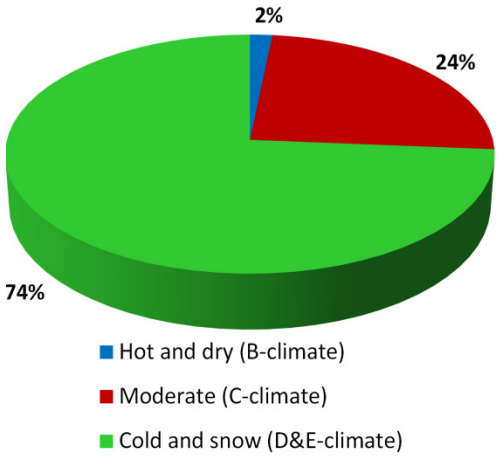

Fig. 58: Relative composition of the climate zones within reported data according to Köppen-Geiger climate classification system [207].

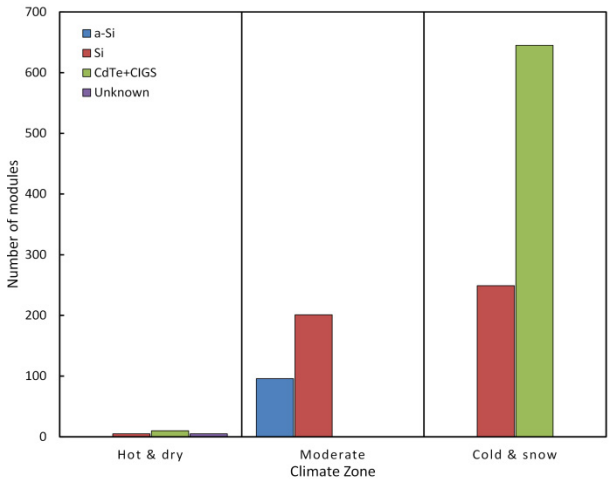

Fig. 59: Absolute number PV module technologies classified to Köppen-Geiger climate classification system [207].

A total of 1211 PV module condition datasets from seven countries have been collected and analysed. Most of the PV modules are installed in Europe, a majority of it in Northern Italy (see Fig. 56). The cold & snow climate dominates the database with 74% of the datasets, followed by 24% datasets of moderate climate (Fig. 58). Unfortunately, we have only 2 % PV module condition data in hot & dry climate and no data available in hot & humid climate.

The distribution of PV module technologies is not representative of the total installed capacities in those countries. We have more than half of the collected datasets of module technology CdTe (52%), multi-Si modules (25%), mono-Si modules (12%), and a-Si (8%) as shown in Fig. 57.

The visual inspection of the fielded PV modules took place after a variable number of years after PV installation. The time of inspection relative to the first exposure or installation varies between 1 year and more than 20 years. The majority of PV module condition inspections took place in year 5 to 7 after installation date (60%), followed by year 1 to 3 (26%) and more than 20 years after installation (8%). Therefore, the recorded failures are also grouped in these three time intervals (subsection 3.5.3).

3.5.2 Data processing for evaluation

The database "PV module failure analysis" from TÜV Rheinland Energy GmbH is used to collect the visual inspection data and to analyse the fielded PV module conditions. According to the categories in the module condition sheet, the database is divided into a main- and a sub categories and the value of the category. Each main- and sub-category is related to each other in the source code.

To evaluate the failure rates for different PV module technologies and different climates, we classified failures related to the documentation of PV module condition as described in Section 3.4. In Tab. 10, the specific failure classification is given, if one of the listed failures occurs, e.g. the failure "defect backsheet" is identified, if one of the four damage types in section "4 Backsheet" was recorded: Bubbles >5 mm, delamination, cracks/scratches or abrasion of backsheet.

Tab. 10: Definition of failures based on the documentation of PV module conditions in the field used for result figures in subsection 3.5.3.

Failure Definition	**Definition: one of the following options is chosen in the documentation of PV module condition**
Defect backsheet	4. Bubbles with dimension >5 mm 4. Delamination 4. Cracks/scratches 4. Abrasion
Defect junction box	6. Cracked (box) 6. Burnt (box) 6. Loose (lid) 6. Fell off (lid) 6. Cracked (lid) 6. Loose/brittle (adhesive) 6. Fell off (adhesive) 6. Loose & fell off (wire attachments) 6. Seal will leak 6. Arced/started a fire
Defect frame (only Si)	7. Major corrosion (frame grounding) 8. Frame joint separation 8. Frame cracking 8. Bent frame 8. Adhesive oozed out 8. Adhesive missing in areas 8. Delamination of tape

Failure Definition	Definition: one of the following options is chosen in the documentation of PV module condition
	8. Adhesive tape missing in areas
Defect frame seal	9. Visibly degraded 9. Squeezed/pinched out (material) 9. Shows signs of moisture penetration (material) 9. Fraction delaminated
Glass breakage	10. Shattered 10. Cracked 10. Chipped
Cell cracks	12. Cracking (only in Si & a-Si figures) 13. Cracking (only in CdTe & CIGS figures)
Delamination of module	12. Delamination over cells (only in Si & a-Si figures) 13. Delamination small localized and extensive (only in CdTe & CIGS figures)
Moisture ingress	12. Moisture (only Si)
Snail tracks	12. Worm Marks/Snail Tracks (only in Si and a-Si figures)
Discolouration of encapsulant	12. Major/Dark discolouration (only in Si and a-Si figures) 13. Light and dark discolouration (only in CdTe & CIGS figures)
Burn marks	4. Backsheet 11. Busbars: diffuse burn marks 11. Cell interconnect ribbon 11. String interconnect 12. Silicon module(only in Si and a-Si figures) 13. Thin film module (only in CdTe & CIGS figures)

3.5.3 Results

The distribution of the occurrence of PV module failures over the climate zones are grouped for the 3 different PV module technologies: Si PV modules (455), CdTe and CIGS modules (655) and a-Si PV modules (96). For the first group, failures are detected in moderate C and cold & snow D/E climates, but not in hot & dry climates A due to the low number of inspected Si modules (5). When we focus on the specific types of failures of Si modules, we find that moisture ingress (19%), defect frame (17%), snail tracks (12%), and defect backsheet (9%) are the most frequent failures for this technology (see Fig. 60). The percentage given is the observed occurrence per failure type compared to the total number of inspected modules of this technology and in this climate zone. Thus, we find that moisture ingress and snail tracks are the prominent failure types for moderate climate, while defect frame are dominant for Si modules in cold & snow climates.

The distribution of failures CdTe and CIGS modules (see Fig. 61) is only relevant for the cold & snow climate (645) due to the low number of those modules in hot & dry climate (10). The dominant failure type for this group is delamination – small, localized - with 13%, followed by defect frame seal with 4%.

For the a-Si modules (96) in the same location at moderate climate, we find defect frame (100%) and delamination over cell (24%) as dominant failures as shown in Fig. 62. The high value of both failures types is due to the very long period between installation date and inspection date of over 30 years.

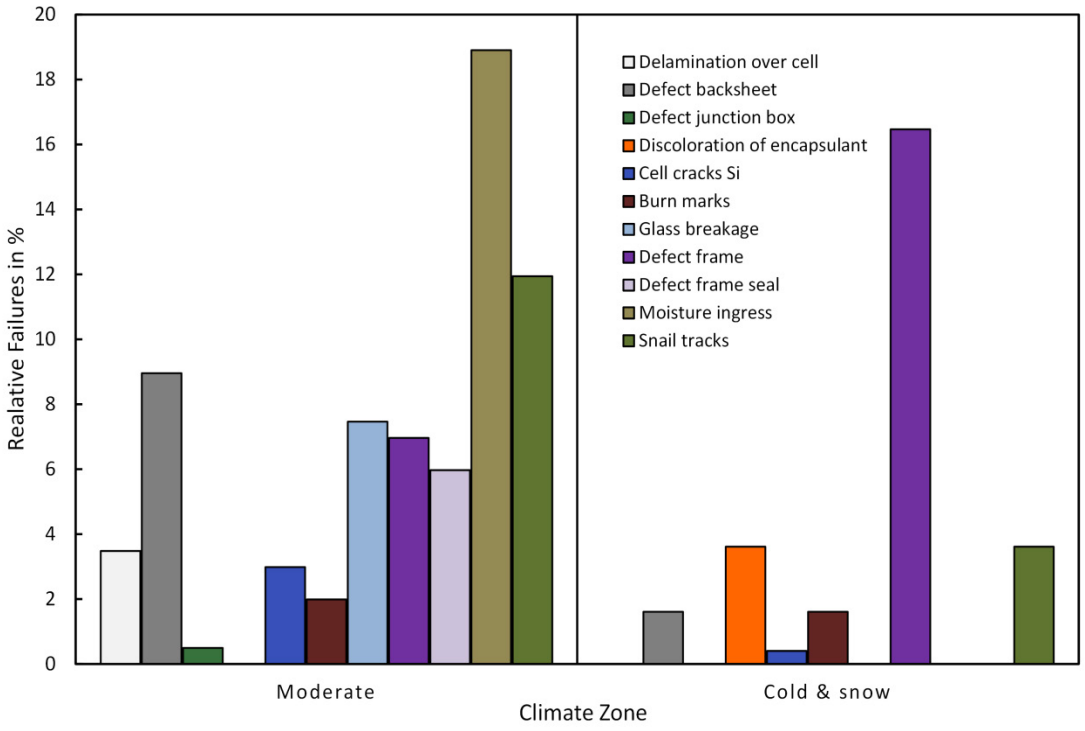

Fig. 60: Distribution of silicon PV module failures in the field classified in different climate zones according to Köppen-Geiger climate classification system [207].

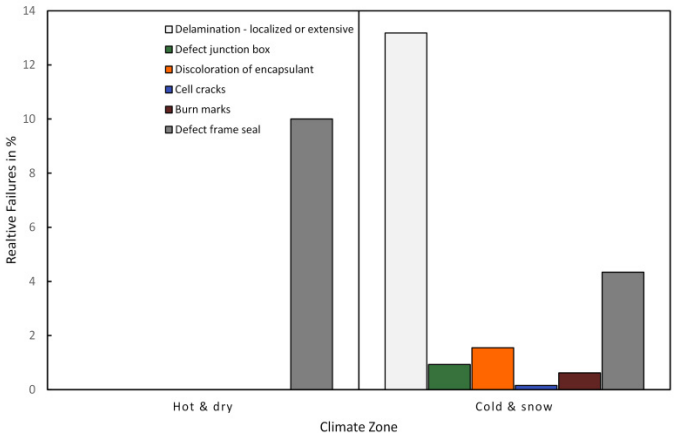

Fig. 61: Distribution of CdTe and CIGS module failures in the field classified in different climate zones according to Köppen-Geiger climate classification system [207].

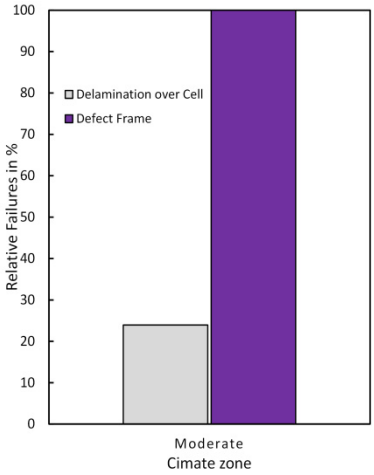

Fig. 62: Distribution of amorphous silicon module failures in the field classified in different climate zones according to Köppen-Geiger climate classification system [207]. *The amorphous silicon modules were installed more than 30 years prior to inspection.*

The cumulative distribution of the failure types over the period between inspection and installation for Si PV modules is shown in Fig. 63 grouped in two time periods, 0 to 3 years (170 modules) and 0 to 7 years (395 modules). For the first three year period, snail tracks (14%) and delamination over cell (11%) are the dominant failure types. For the cumulative failures during the period 0 to 7 years, the relevant failures types are defect frame (11%) and snail tracks (8%). Thus snail tracks seem to primarily appear during the first 3 years after installation, while the defect frame requires a longer module exposure time than 3 years in the field. This confirms the experience that snail tracks show up during the first half year after installation [1].

The observation of a significant increase of failures of the defect frame type (1% vs 11%) and the moisture ingress type (1% vs 7%) from time period 0 to 3 years to time period 0 to 7 years can demonstrate a possible correlation between these two failures. Furthermore, according to the nature of the failure moisture ingress, it is more likely to happen when failures such as glass breakage and defect frame have already occurred. Another important factor to be considered is the aging of the PV modules which is different for the two exposure periods. In the time period from 0 to 3 years, at least failure was detected for 35% of the inspected modules. On the other hand, during time period 0 to 7 years, at least one failure was detected for 40% of the inspected modules. This deviation of more than 12% in detected failures between the two time periods can be due to the aging factor.

The cumulative distribution of the failure types for fielded CdTe and CIGS modules is shown in Fig. 64 grouped in the same time periods, 0 to 3 years (150 modules) and 0 to 7 years (505 modules). For the first period, delamination - small localized (5%) - is the only and dominant failure type. In the cumulative distribution during 0 to 7 year-period, this failure type increases to 17%, followed by defect frame seal with 6%. We can therefore conclude that delamination of CdTe modules seem to increase by a factor of 3, based on one module type and on inspection at the same location.

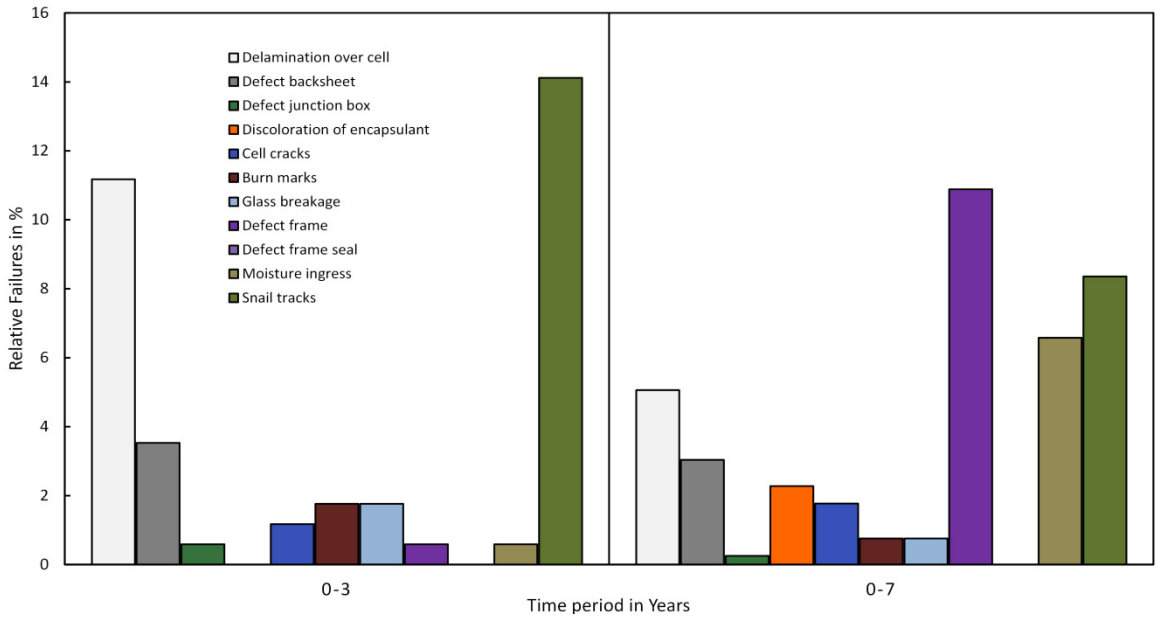

Fig. 63: Cumulative distribution of normalized failures over time periods between installation and inspection dates for fielded silicon PV modules. Soiling is not included in this graph.

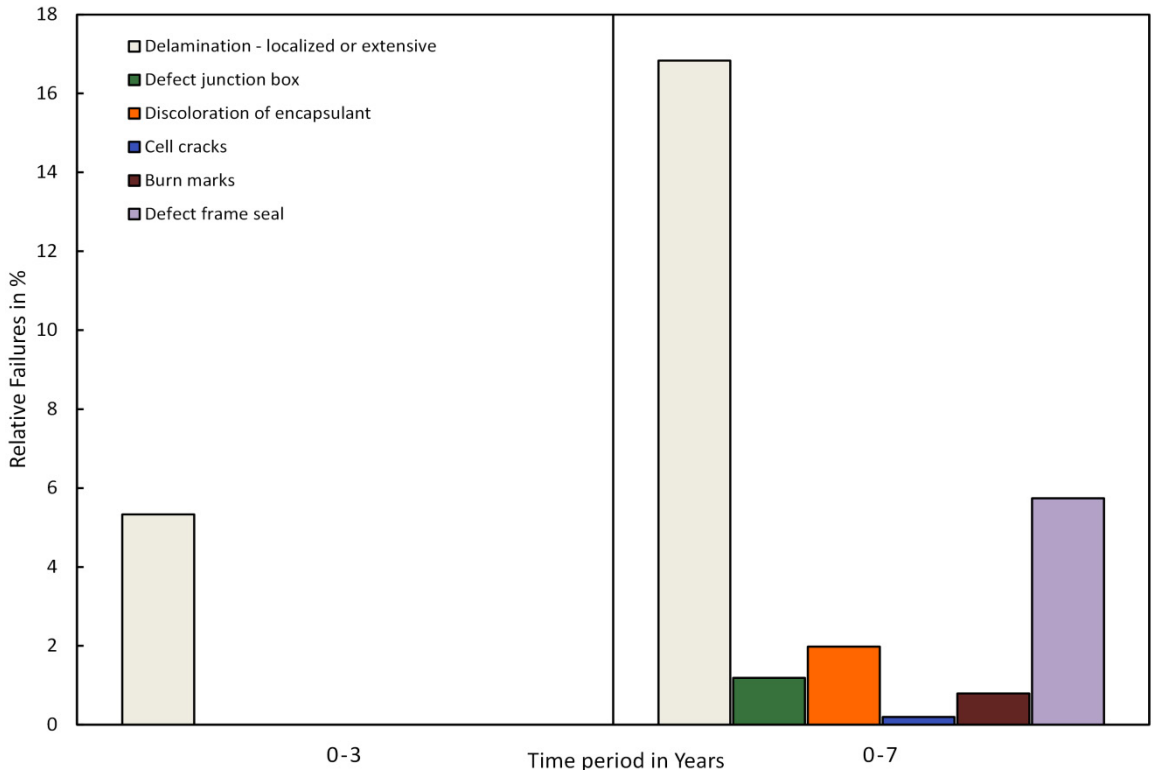

Fig. 64: Cumulative distribution of normalized failures over time periods between installation and inspection dates for fielded CdTe and CIGS modules. Soiling is not included in this graph.

4 Local and Operational Stressors for PV Modules

Based on the results to date, here we attempt to give recommendations for the rank order of the most important test methods depending on climatic zones to allow customers to identify the most important test for their application and location. Comparisons and measurement uncertainties

4.1 Implications of data base evaluation on local climatic stressors

The failure relevance and degradation rates resulting from the data show no strong correlation with Köppen and Geiger climatic zones. The climatic zones of Köppen and Geiger are designed to categorize zones with similar plant growth conditions, and the plants compatible with different climatic zones are responding to the temperature, temperature ranges and humidity in the KG climatic zone. Jordan also reported that he not find a clear correlation between degradation rates and climatic zones [202]. In 2017 Hu has published power degradation rate analysis applied to 5 minute interval time-series data on over 1000 PV power plant inverters in 9 KG climatic zones [211], [212]. In a statistical analysis of 655 PV inverters across these KG-CZs, he finds the most significant rank-ordered contributor to the power charge rate is the KG-CZ, followed by the PV module brand/model. This study is distinguished by the sample set size and the data quality, coming from large PV power plant owners. This suggests that KG climatic zones may, with sufficient data volume and quality, be a relevant classification for the relevant exposure conditions of PV plants.

The categorization of locations into the KG-CZ have threes essential problems. There are plenty maps for the KG-CZ developed by different authors e.g. [180], [213]–[215] which update the maps from time to time. One reason for the updates is the climate change which also changes the local climates [214]. However, this problem has to be handled by every categorization system. So there must be a clear rule how to categorize e.g. a 1 year old and a 20 year old PV system into the KG-CZ which change with the time. The current studies do not consider this change in local stresses. The KG-CZs are well defined. But they are evaluated on different base data and/or evaluation procedures. So, different base data or evaluation procedures lead to different maps. E.g. East Germany is in the map of Kottek [213] a Cfb climate, but in a map of Peel [180] a Dfb climate. In Germany many PV systems are installed. Therefore, this example shows that depending of the KG-CZ map in use many PV systems are categorized in a different way. Even the climate zone groups used in various studies are defined in different ways [98], [202], [212]. E.g. Jordan uses the categories Hot & Humid (Af, Am, As, Aw, Cwa, Cfa), Desert (BWh, BWk), Moderate (Cfb, Csa, Csb, BSh, BSk), Snow (Dfa, Dfb, Dfc, ET), Hu uses Tropical (Am), Arid (BSh, BSk, BWh), Temperate (Cfa, Csa, Csb), and Could (Dfa, Dfb), and Köntges uses Hot and Humid (A), Hot and Dry (B), Moderate (C), and Cold and snow (D&E). In the future we have to agree on one categorization system for climatic zones being comparable in between the studies. Furthermore, the categorization with the Köppen and Geiger climate zone does not account for stressors besides temperature and humidity. Therefore, it is helpful to use additional categorization factors that account for more specific stress factors of solar modules.

Independent of climatic zones some crystalline silicon PV module failure stand out with a high power loss if a PV system is affected by the failure or they occur very often. These are in the order of impact potential induced degradation, failure of bypass diodes, cell cracks, and discolouration of the pottant material.

This outstanding failures may be a result of the fact that for potential induced degradation, bypass diodes, and discolouration of the pottant material no appropriate test exist in the standard IEC

61215 design qualification and type approval test. Currently for most of these failure types tests are in development, but they are not included in the current revision of the IEC 61215.

Therefore, we recommend PV plant designer not only to check for an approved IEC61215 test for the used PV modules, but also for additional tests for PID (IEC/TS 62804), bypass diode test (IEC 62979, IEC/TS 62916) and extended UV-degradation in the new IEC 61215:2016. The results of the UV degradation test in the new IEC 61215:2016 is no pass fail criteria, so one must access the test report itself to check the remarks on the UV-tests.

Besides PV module failure the PV failure with the highest impact on the PV performance is the soiling of crystalline silicon and thin-film PV modules in special regions. The occurrence, but not the soiling impact on the modules power correlates with the climate zones of Köppen and Geiger. However, the Köppen and Geiger system is not able to differentiate effectively between different soiling affected locations. How stress zones could be defined for soiling is shown exemplary in chapter 4.2.

4.2 Climatic stress classification for PV modules with the help of Geographical Information Systems

For investors of PV systems at a specific location the question occurs if the chosen location will add additional risks for the reliability of the PV system. Therefore, it would be helpful to have a categorization system which allows assessing the local stresses for PV systems, to give an investor a basis for the investment decision. In the following chapters the applicability of categorization systems for local stresses are discussed.

4.2.1 Categorization of local loads with Köppen-Geiger climate zone or new categorization systems

Using climate classification is one way to evaluate the stress factor conditions for PV modules at different locations. The Köppen-Geiger system [215], in use since 1884 illustrates well the general approach of the stress classification for PV modules, but it has not been extensively studied for use in PV stress classification, and to date there are contradictory findings as per its applicability (Fig. 65).

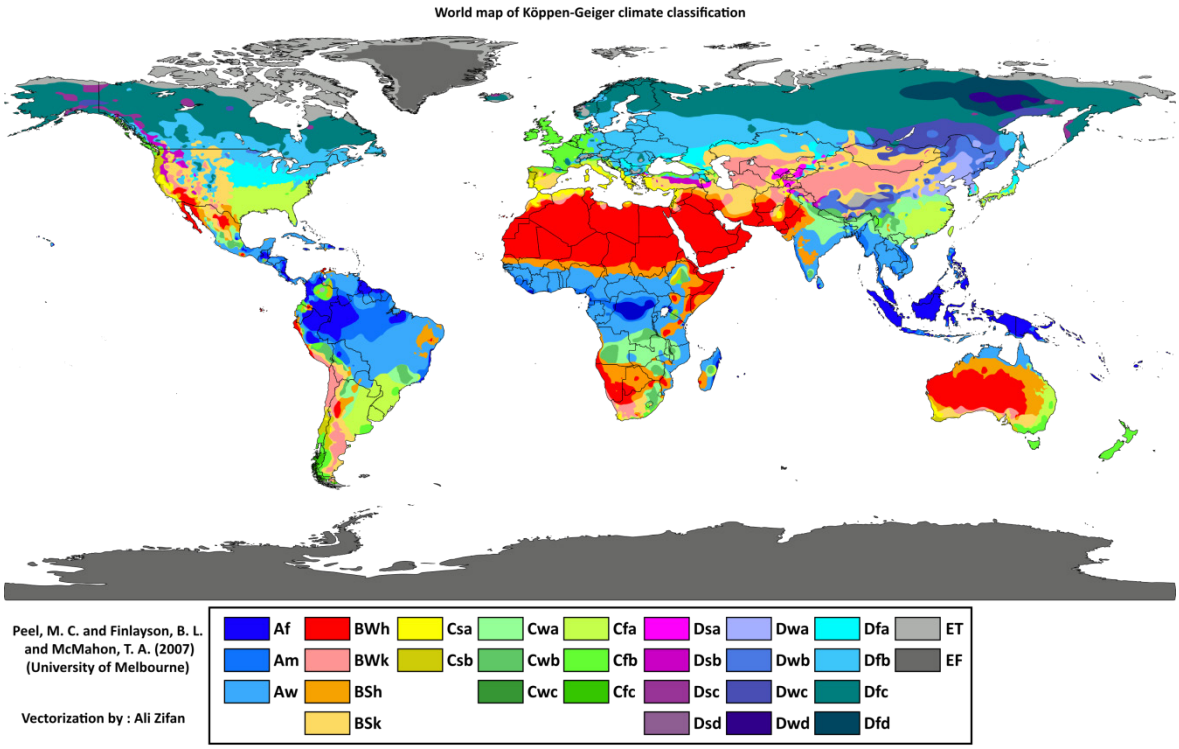

Fig. 65: Köppen-Geiger climate classification system.

The climatic conditions covered with Köppen-Geiger groups are covering temperature and humidity stress (see Fig. 66) which does not cover all important stress factors for the application in PV degradation studies. Many other environmental stress factors are relevant for PV module degradation like UV irradiance, soiling, temperature cycling or humidity and therefore should be involved in a classification for PV. Moreover by Köppen-Geiger classification the temporal resolution of the data (annual and monthly averages) is low. Therefore, classifying the environment-related stress for PV modules by determining the max., min. values and the fluctuation frequency between these values might be necessary.

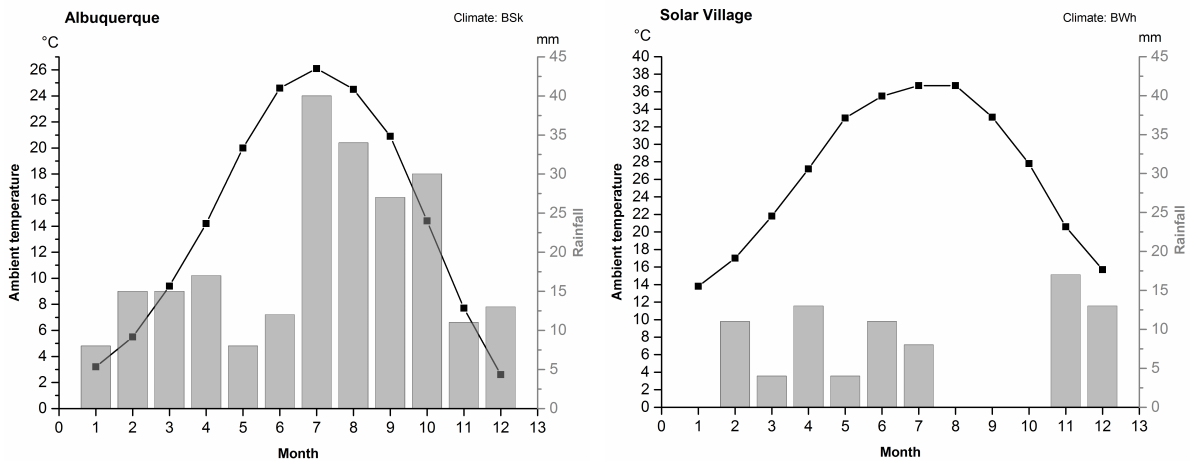

Fig. 66: Climate diagrams based on Meteonorm datasets [216] *for two locations showing the variance between the climate conditions within one climatic group according to the Köppen-Geiger climate characteristic.*

Experience shows that the stress for solar components varies in different climate zones, but until today no globally available geographically explicit stress classification system for PV technologies

exists beyond first order approaches like Köppen-Geiger which come from other applications. Following the strategy to reduce investment risks and operating and maintenance costs, it is necessary to adapt the materials and components of solar energy systems specifically to regional environmental conditions. The aim of stress classification systems is to assist in the identification of the individual stress conditions for every location on the earth's surface. By integrated geographical analysis, the site-specific information from outdoor testing facilities can be extrapolated at the global level to obtain sets of environmental-related risk factors. Because of the high spatial and temporal diversity of the influencing parameters, the use of e.g. Geographic Information Systems (GIS) is suitable as a base instrument for the modelling. Slamova and Herrmann et al. have started to analyse the corrosivity in the coastal regions, mapping of soiling potential for glazing materials in the Middle East and North Africa (MENA) regions and validation work by comparing satellite UV irradiation data with ground based measurements [205], [217], [218].

The stress classification system shall serve as a decision support tool for the industry (manufacturers, investors, lenders, and project developers) and help to improve knowledge and services that can provide higher confidence to solar power systems. Global classification can be provided separately for each factor with regard to reducing performance of PV systems and material degradation. The digital data layers are representing quantitative descriptions and qualitative categorizations of individual stress factors.

4.2.2 Stress factor mapping applied to soiling in MENA region

In the following the concept of stress factor mapping is illustrated with the example of a classification of soiling risks in the MENA region.

Soiling, induced by accumulation of airborne dust and other inorganic and organic particles on the surface of PV panels triggers optical losses and reduced transmittance of the glazing and therefore causes a reduced yield of affected solar systems.

Several empirical case studies investigated this phenomenon by correlating the time of exposure or the amount of dust on glazing materials with the measured performance of PV panels and solar collectors, see e g [219] or [220] . All studies report a reduction in efficiency (losses up to 30% or more) with increasing soiling rates. In addition, exposure to frequent dust storms degrades the surface of PV panels by mechanical abrasion. The natural soiling potential is closely connected to dust emission, transport, and deposition processes. Depending on individual environmental and meteorological conditions a high spatial and seasonal variability on the global scale is expected. The GIS based modelling of global soiling risk was performed by integrating the techniques for acquisition and processing of the spatially distributed data taking into account the influence of the main soiling factors [205]. The stress classification map of qualitative information of soiling risk in the MENA region (Fig. 67) reveals a clear difference between the desert and none desert areas at the borders of the investigated area with steppe and moderate climate. But there is also a significant variation within the desert regions. High soiling risks are implied for the southwest Sahara, the region of Nile, the south of the Arabian Peninsula, and parts of Iran. In contrast, the regions east of the Nile on the African continent as well as the Asir Mountains on the western Arabian Peninsula and the high altitude areas of Iran show significantly lower soiling risks. In the presented case, the soiling risk is related to the airborne dust loads which have been calculated using climatic and ambient conditions. Different surface properties or specific properties of PV modules have not been included, and therefore it has to be seen as a qualitative value.

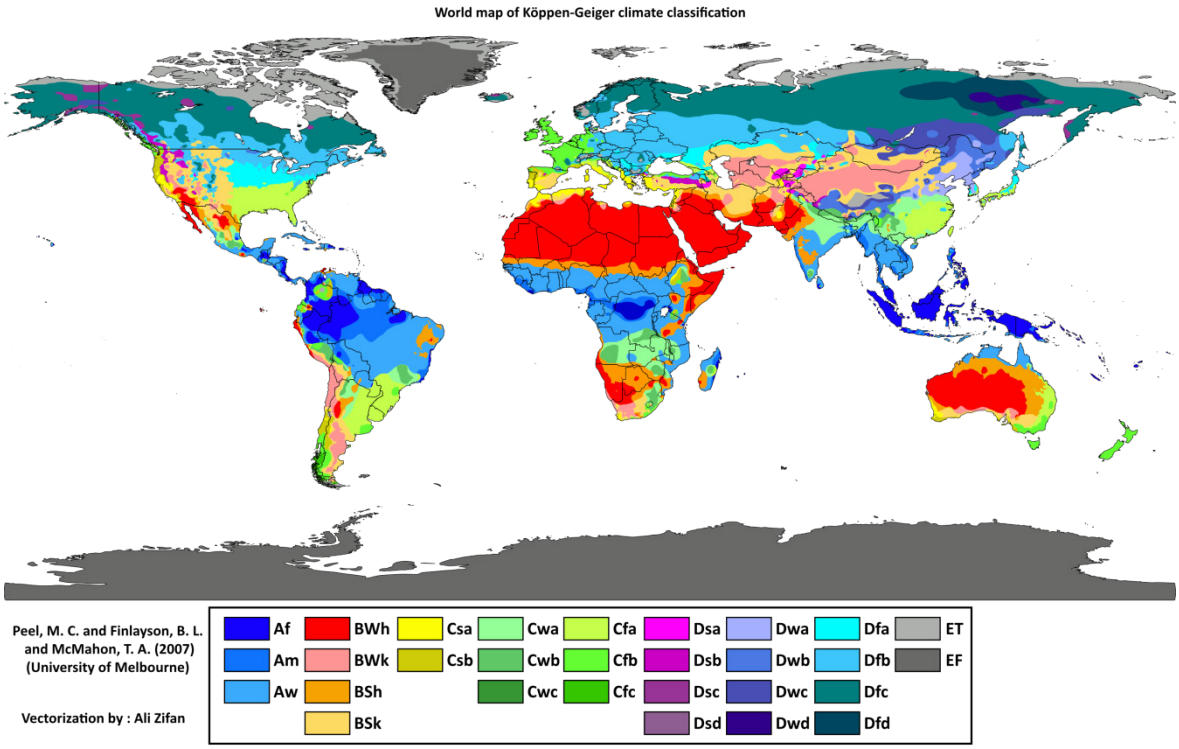

Fig. 67: GIS-based map of the qualitative soiling risk in the Middle East and North Africa (MENA region) on the basis of satellite data and historical ground-based meteorological measurements [221].

4.3 Interpretation of test methods according to local loads

PV modules have to withstand a multitude of very different kinds of environmental and electrical stressors and loads, from UV irradiance and thermal loads which can cause chemical degradation of materials to mechanical loads due to external loads like wind and snow or due to temperature cycles and gradients. This subsection describe the main influences and the most important topics which have to be taken into account when test methods appropriate to local loads and conditions are to be designed. This subsection also shows potential general approaches to define test sequences and study protocols and shows examples of adapted tests. However, it cannot give a complete description of such tests or even defined test sequences for different climates.

4.3.1 General requirements of test methods for reliability testing

Several test methods are available which aim at simulating loads in the lab to investigate the durability of the modules under defined loads. These tests often use a level of loads, e.g. 85°C and 85% RH. used in the well-known IEC 61215 damp heat test, to produce comparable results for different modules, but they do not have a direct correlation with degradation modes, mechanisms or effects observed under real operational conditions or real environmental stressors. Furthermore, these tests do not give information with regard to the actual service lifetime of a module under real world conditions. This is usually not possible with such standardized tests since the their exposure conditions have differing effects on the various materials used from one module type to another, and so different degradation processes (mechanisms and pathways) with different reaction kinetics are activated leading to a different effect of the external stressors on the PV modules [153].

The actual stresses and loads for a PV module also depend very much on the local conditions, influenced by the type of system and installation and also by the local climatic conditions which

can be very different as described in chapter 4.2. Therefore, test methods which address the local load conditions are important and crucial to determine meaningful results of tests.

To design realistic and quick accelerated aging tests, the comparison and cross-correlation of the observed responses to specific degradation mechanisms induced by outdoor exposure and by accelerated aging test conditions is indispensable [222]. A comprehensive degradation analysis has to be performed, i.e. by means of power measurements, electroluminescence imaging and Raman spectroscopy to analyse the correlation of real weathering and accelerated testing.

When test methods (including both exposure conditions and evaluation procedures) and / or test sequences shall be developed according to local conditions, it is important to initially decide which stressors and loads shall be included or are seen as most important. This focusing is important since usually the combination of all occurring loads leads to numerous interactions among degradation mechanisms which cannot be explained or correlated with specific loads and so lead to very complicated conditions with respective high requirements for the test equipment. Also the possible acceleration of lab tests in comparison to outdoor conditions is limited if the kinetics of specific effects and cross-correlations between indoor and outdoor stressors and stress levels are not known. Procedures to develop service life tests are described in literature, e.g. by Saunders [223] or for specific examples of materials in solar thermal applications [224].

One possibility to reduce complexity of testing is to separate the testing of functionality and reliability. To test e.g. surfaces or coatings to reduce soiling effects, the functionality can be tested in a set of soiling tests, like e.g. described by Klimm et al. [164]. Standard weathering test exposures like UV-testing or damp-heat testing combined with easy to use analytical evaluation methods, for surface properties e.g. contact angle measurement or optical measurements can be named, can be used to analyse the sensitivity of the surfaces to different loads to learn about the reliability.

4.3.2 Potential induced loads

Extrapolation of module lifetime using the ratio of the rate of charge transfer from an accelerated lifetime test in an environmental exposure chamber to outdoor conditions has been performed by a number of researchers [225]–[227]. Extending this, modelling and prediction of the magnitude of the coulomb transfer for various climates, to give relative metrics for the stress the climates impart and insight on how to test photovoltaic (PV) modules for durability to PID in differing climatic zones.

Coulombs transferred (or leakage current I_{leak}) from module to ground is frequently monitored in PID studies and used as an indicator of the effect of the environment on conductivity of the surface, glass, encapsulant and mounting. Presently, the consensus is that leakage current is not a universal indicator of degradation because some current transfer pathways into the module may be more deleterious than others [228]–[230]. Further, PID recovery processes seen in some PV modules mean that coulomb transfer causing degradation may proceed, only to have module power recover when the modules are warm and dry and the PID stress is reduced [231]. On the other hand, coulombs transferred is considered a direct factor in electrochemical degradation processes such as transparent conductive oxide corrosion that occurs when there is humidity ingress in thin-film modules [32], [232] and is believed to be a factor in some delamination mechanisms of crystalline silicon modules [33]. Electrochemical corrosion processes associated with current transfer are not considered to be recoverable.

Unlike conventional crystalline silicon module technology, coulombic correlations have sometimes been successfully made between the extent of power degradation in accelerated testing of thin-film modules and those modules that are field-mounted [225]. It may therefore be possible to project the acceleration in leakage current in various outdoor environments based on coulombs transferred as a function of weather conditions; such a method has been proposed to estimate PID in the field [233]. However, there are multiple degradation mechanisms that may occur

because of system voltage stress in thin-film modules. The ability to universally use coulombs transferred from the module cell circuit to ground and relate it with the module power degradation due to system voltage stress may therefore have limits—it may be possible for some mechanisms and not for others.

The coulombs transferred method is to determine (A) coulombs transferred for a given failure criterion indoors in-chamber and measure (or if possible, predict based on weather data (B), the coulombs per unit time the module type leaks in an outdoor environment, then divide A/B to determine the expected time to failure in the outdoor environment. This method assumes that a coulomb transferred in-chamber will cause the same net impairment to the module power as a coulomb transferred in the natural environment. Application of the method has for some module types shown correlation between power loss and coulombs transferred comparing chamber and field-mounted modules [225]. However, in other cases, this method has been found to overestimate the rate of degradation for one module type, possibly due to recovery of the PID by shunting that can occur in the field (due to the temporal variation of the exposure conditions outdoors). Additionally, PID rate can vary depending on whether there has been moisture ingress into the module. Comparing coulombs transferred in chamber and in the field for four module types, it was found the method correctly identified the module type that failed first in the field [226].

Current transfer can increase greatly if the module is wet from dew or rain. Algorithms to distinguish between when the module is wet vs. dry are required. With the aid of this distinction, regression analyses may then be applied for each of the module states to obtain predictive models of current transfer between modules and ground as a function of module temperature and meteorological conditions. Further, chamber testing (considering both the condensed or uncondensed state of moisture on the module) may be used to obtain current transfer rate equations for the module type in question [234].

A number of methods may be used as indicators to understand if a module is wet in a given environment, which will determine the nature of the current transfer: (1) a wetness sensor (ohms) indicates the electrical resistance reading of the interdigitated surface resistor is lower, thus wetter; (2) module surface RH (SRH), whereby ambient RH and temperature are used to compute the dew point, which is transferred to the module temperature; (3) the derivative of module SRH with respect to time, which shows an inflection when the module dries and heats up; (4) the difference in the module temperature from dew point temperature, an indicator of the likelihood residual condensed water exists on the module after rain and dew condensation; and (5), tipping bucket rain gauge data. Using such metrics together to judge the condensed and uncondensed humidity states on the module allows us to model the states separately and with better accuracy.

Current transferred from the active cell circuit to ground in thin-film modules under system voltage stress in Florida can be seen with respect to meteorological data in Fig. 68. For reference, superimposed are current transfer curves obtained in chamber tests at 10% relative humidity and in a water bath (wet leakage current testing conditions). With this, functions predicting the mode and rate of coulomb transfer can be developed for use in estimating the relative PID stress associated with temperature, moisture, and system voltage and then applied to other climates.

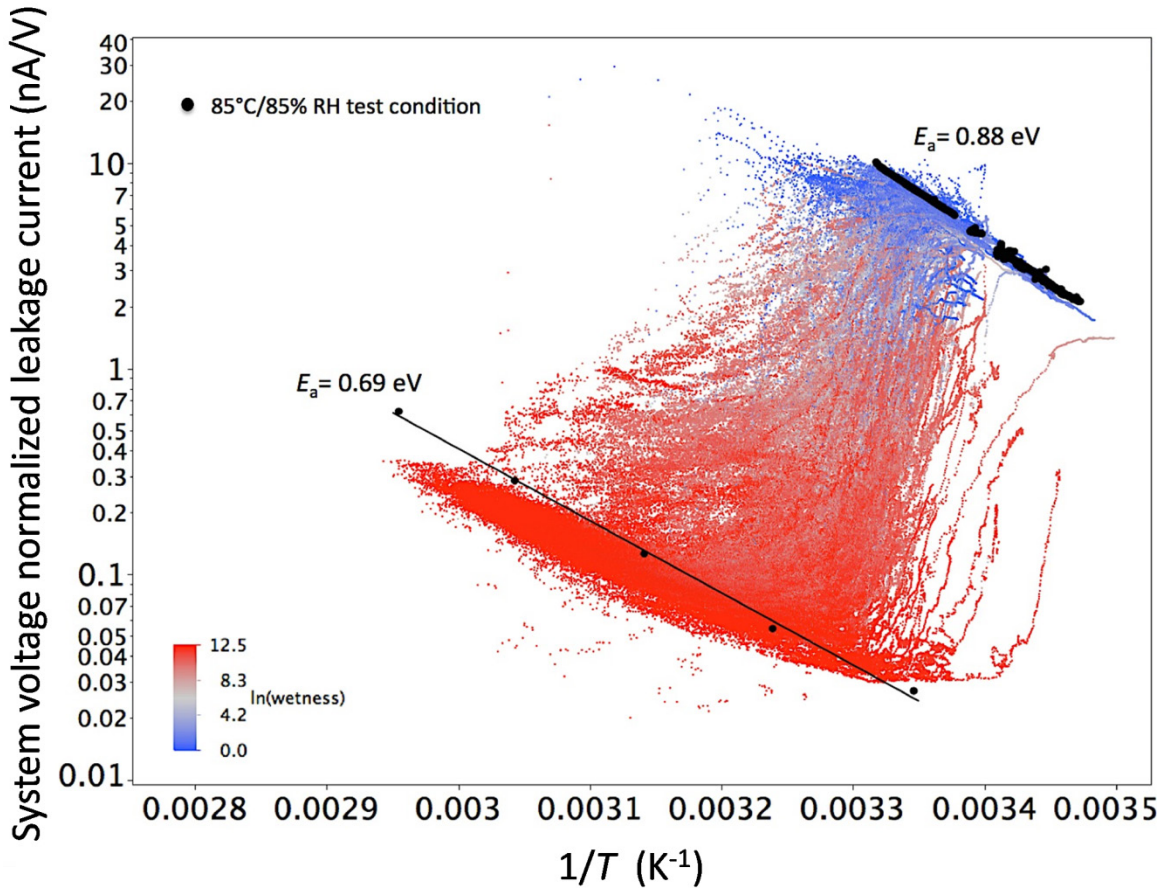

Fig. 68: System voltage-normalized current over a period of about six months for a module held by edge clips in Florida, USA (red-blue data, where blue is wet and red is dry according to the wetness sensor). Results in a dry chamber (10% RH, five lower points), wet leakage current tests (upper data) and for the 85°C 85% RH chamber test condition performed on a sister module are superimposed in black.

Linear regression models fitted to data obtained for the thin-film modules shown in Fig. 68 are performed. Considering the exponential function of current on module temperature *T* and relative humidity RH [235][236], the resulting model equations for current transfer give approximately order of magnitude accuracies for I_{leak}/V. These predictive model functions for the system voltage normalized leakage current determined for the thin-film module based on Florida data are as follows:

$$\frac{I_{leak}}{V_{Morning\ dew,rain}} = 6.43 \cdot 10^{15}\ \mathrm{nA/V}\ e^{\frac{-1.41\cdot10^{-19}\mathrm{J}}{kT}}, \qquad (34)$$

$$\frac{I_{leak}}{V_{Morning\ no\ dew}} = 3.59 \cdot 10^{8}\ \mathrm{nA/V}\ e^{\frac{-1.41\cdot10^{-19}\mathrm{J}}{kT}} e^{\frac{0.08\cdot SRH}{\%}}, \qquad (35)$$

$$\frac{I_{leak}}{V_{Afternoon}} = 1.19 \cdot 10^{9}\ \mathrm{nA/V}\ e^{G\cdot 0.0012\ \mathrm{m^2/W}}\ e^{\frac{-1.138\cdot10^{-19}\mathrm{J}}{kT}} e^{\frac{0.089\cdot SRH}{\%}}, \qquad (36)$$

where *G* is global horizontal irradiance in units of W/m², *SRH* is the module surface relative humidity in %. Other variables have their usual meaning.

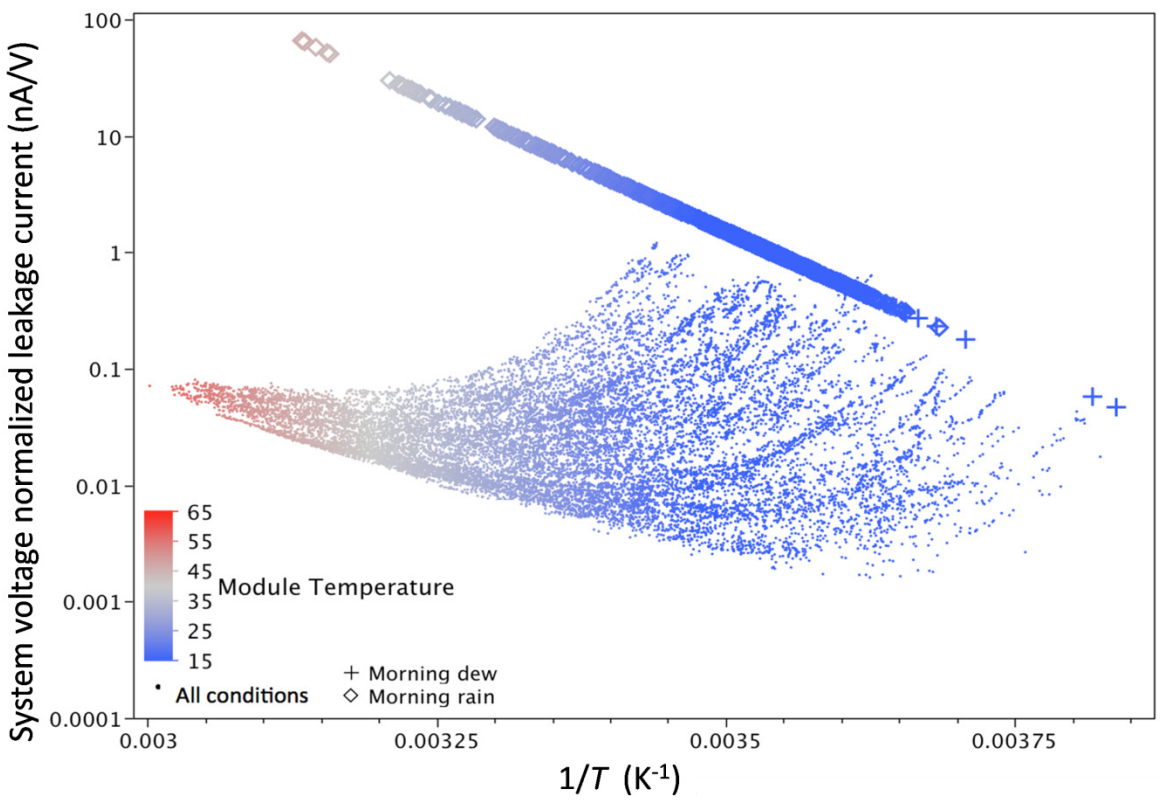

Fig. 69: Calculated current transfer from a module in Colorado, showing current transfer with Arrhenius relationship when the module is wet and the result of the regression function derived from Florida data when humidity is uncondensed.

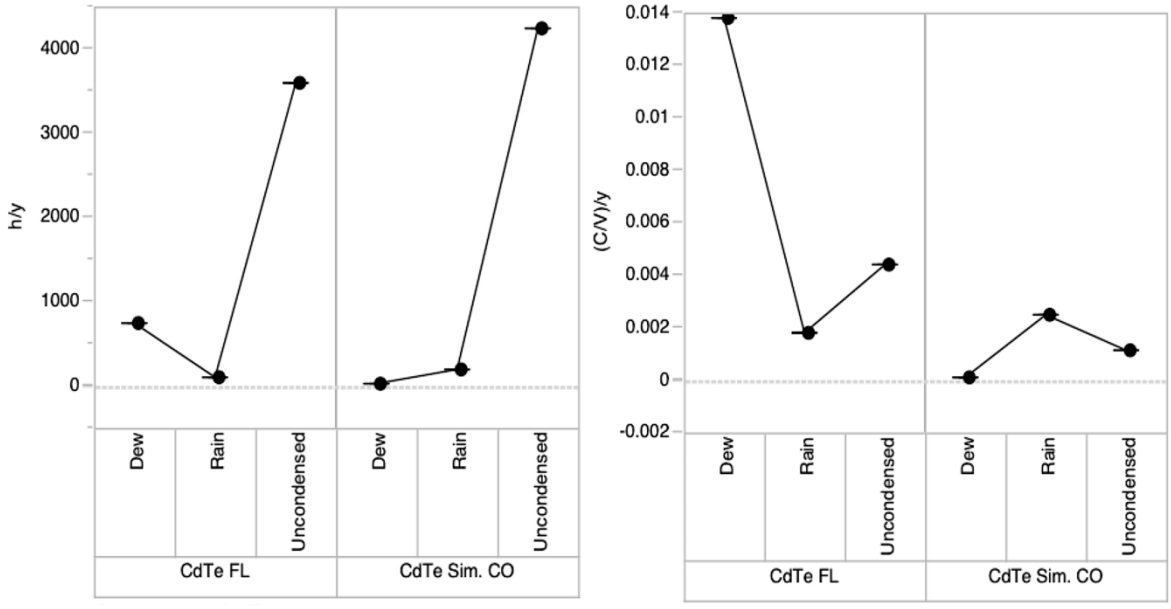

Fig. 70: (a) Time at each surface state, and (b), charge transferred for a CdTe module measured in Florida (FL) and simulated in Colorado (CO).

The determined relationships between current transfer and module conditions in Florida for regimes are for Eq. (34) morning dew or rain, where a simple Arrhenius function when the module is wet can be used; Eq. (35), the morning, after the condensation has dried; and Eq. (36), the afternoon.

These equations are projected onto a module temperature and field meteorological data in Colorado, USA, to predict the coulombs transferred for a year in Colorado in Fig. 69. Summing up the current transfer data for Florida (Fig. 68) and Colorado (Fig. 69), total coulombs transferred in Colorado are found to be lower, calculated to be overall 19% of that of Florida, primarily associated with minimal morning dew and lower humidity as seen in Fig. 70.

Some variables that remain to be examined include the effect of module mounting tilt. A horizontal mounting, as was the case for the modules mounted in Florida, can lead to longer water retention on the surface. Soiling can also affect surface conductivity, which can vary as an additional independent parameter as a function of time [237]. Additional testing, validation and development of the modelling method are anticipated to lead to more refined predictions.

4.4 Climate and load adapted testing

PV modules have to withstand a large variety of different environmental and electrical stressors and loads which can be related to the local and operational conditions. As this chapter shows by some examples, these loads depend highly on the specific local conditions of the specific system. Of special importance in this topic is the specific combination of stressors for the degradation of materials and so also of the PV modules themselves.

The specific load conditions can be transferred to accelerated tests and simulated in the lab, but since the effects of the loads on the modules depend very much on the specific materials used in the module construction, the time transfer function between real operational exposure conditions and the accelerated test exposure conditions also depends on the specific module design. This very much limits the possibility to develop standardized accelerated lifetime tests for PV modules since even module types which look quite similar, like e.g. the large number of c-Si modules with glass-backsheet setup, show a large variety of materials. If a comparison between different technologies or module designs is required, the comparability is even more limited.

It is important to say that the established tests (exposure conditions and evaluation procedures) deliver very valuable results which indicate weaknesses of the module types or sensitivities towards different loads or stressor combinations, but they cannot deliver answers regarding defined lifetimes.

Several tests have been developed to identify and - if possible - quantify the sensitivity of modules towards single additional loads like potential loads causing the so called potential induced degradation (PID) effect or reduction of performance due to soiling loads. These tests indicate the sensitivity of the module type, but one has to be very careful if the results are to be used to predict the real behavior of a module type at a certain site. This is due to the fact that e.g. soiling effects depend on the local soil type, the climatic conditions and the module design, especially the surface properties of the module type, and therefore vary from site to site and from one module type to another type of module.

Conclusion

Photovoltaic modules with c-Si technologies show median degradation rates in the 0.5–0.6%/a range with the mean in the 0.8–0.9%/a range [202]. Other technologies like Hetero-interface technology and microcrystalline silicon technologies, exhibit degradation around 1%/a and thin-film products are similar to c-Si, but with a high variation of the degradation rate in different products and various reported studies. However, reports on degradation rates tend to focus on not so well working systems, so the majority of real PV systems are expected to show lower degradation rates. In this document we focus on distinct failures causing a degradation of PV modules.

The literature review showed that in most cases interactions between materials in the PV module are the main root cause for PV module degradation. Generally the PV module failure modes are described very well in the literature, including their main driving forces and critical factors. In addition the right combination of an encapsulant and a backsheet film can be beneficial, as most of the described degradation modes depend on the availability of oxygen, water vapour, and acetic acid, a degradation by-product of EVA. Hence, the permeation properties of the particular encapsulation and backsheet films used are of prime importance for the reliability of PV modules. For example, in order to avoid or reduce potential induced degradation it is desirable to combine an encapsulant film with reduced water vapour transmission rate and higher volume resistivity with a backsheet films that shows selective permeability, i.e. high resistance to water vapour transmission and low resistance to acetic acid transmission.

Next to the critical role of the correct choice of materials and components for the PV module, also the PV module lamination process can have an influence on long-term reliability. Here poorly crosslinked EVA encapsulant, but also too long lamination times are mentionable, which can lead to accelerated degradation or increased delamination.

Forecasting or predicting the degradation of a specific PV module failure is still a challenging task. For some failure types, such as potential induced degradation or silver finger corrosion, predictive models are in development which have a highly predictive accuracy on a heuristic level. That means if one has a final material composition for a particular PV module one can do tests on the module and predict the power degradation rate for a specific module from test data. From the modelling we learn that power degradation due to PID is super linear with the applied voltage. Therefore, PV systems with high system voltages of up to 1500 V have to take special care of this failure mode. For the cell cracking failure type some assessment can be done to estimate the maximum power loss due to this failure, but no model is yet available which calculates the power loss considering its dependence on local loads. Cell cracking is less harmful for modules with more busbars, but more harmful for modules with higher fill factor. For other failure types (like EVA browning and delamination) the basic mechanisms of the failure are understood, but no models are currently available. Dust and biological soiling are not in fact a module failure, but they still causes serious power degradation and yield loss in the field. It is one very important cause of power loss of PV systems all over in the world. For these failure types we give some background and measurement methods on how to quantify the impact of the soiling for one location.

To identify the relevance of the different failure types, we conduct a survey of PV module failures and a survey on visual PV module conditions in the field. Potential induced degradation is the most often found module failure in the field and results in a high mean degradation rate of ca. 15%/a for the affected modules. The PV community should take additional efforts to include a PID test procedure into the IEC 61215 standard so as to avoid further module failures in the field. Cell cracks are also found to be a common problem, but this type of failure does not harm the module power too much (below 3%/a). However, in cold and snow climate zones (D&E in Köppen and Geiger classification) cell cracks seem to have a more pronounced impact. Here relatively high

mean degradation rates of ca. 7%/a can be found. Therefore, in regions with high snow loads and long periods below 0°C PV modules that are more resistant to cell cracking should be chosen. A relative high impact on the performance of the modules has a failure caused by defective bypass diodes. For the most common modules with 3 bypass diodes already one shunted bypass diode reduce the module's output power by ⅓. This failure type is quite common. This failure may be caused by wrong specification and choice of the bypass diodes or by a high voltage event. A bypass diode which changes into open-circuit failure mode causes yield loss during shading of the module and may also cause hot spots and a fire risk arise. But without shading these modules show no power loss. Therefore, a wide range of power loss levels are found for this failure in our survey. For bypass diode failures also more appropriate tests should be added to the IEC 61215.

One of the most important wear-out failures is the browning of the encapsulant material and module delamination especially for thin-film solar modules. Encapsulant browning becomes relevant in the wear-out phase of the module, because its degradation rate is typically about 1%/a for affected modules. This determines how much energy the module will produce over the nominal service life. This failure cannot be prevented by the design qualification and type approval test, because it is a wear-out failure. But it is recommended that a test is performed to assess encapsulant browning. The test IEC 61345 describes an UV test procedure for UV exposure. However, this standard is already old and will be withdrawn in the near future. There is no replacement test in sight. The UV degradation procedure used in the current IEC 61215 is slightly intensified compared to the previous standard. However, a pass/fail criterion is still missing. But a remark in the test report about browning of the laminate may be a first hint on fast browning of the tested module. There are new procedures defined for material testing in IEC 62788, but this does not help to assess the browning resistance of modules. Therefore, some new efforts must be taken to allow the assessment of the most important wear-out failure browning of encapsulation materials.

We found no clear picture for failure occurrence or degradation in different climate zones. Even no clear correlation of soiling and climate zones is found. Therefore, we need an additional new classification on local stressors (dust, UV radiation, irradiance, wind, etc.) and stress levels. The Köppen-Geiger classification, since it is developed for agriculture and plant growth in different regions, may not consider all particular factors that play an important role for PV systems. As more PV systems are operating in diverse climatic zones, stronger correlations between KG climatic zones and failure modes may arise. New efforts to establish cross-correlations between lab-based testing and outdoor real-world PV module performance and failures, coupled with studies of systems in diverse climatic zones will help identify new stressors that play critical roles in PV module degradation and failures.

References

[1] M. Köntges, S. Kurtz, C. Packard, U. Jahn, K. A. Berger, K. Kato, T. Friesen, H. Liu, M. Van Iseghem, J. Wohlgemuth, D. Miller, M. Kempe, P. Hacke, F. Reil, N. Bogdanski, W. Herrmann, C. Buerhop-Lutz, G. Razongles, and G. Friesen, *Review of Failures of Photovoltaic Modules*. IEA, 2014.

[2] A. W. Czanderna and F. J. Pern, "Encapsulation of PV modules using ethylene vinyl acetate copolymer as a pottant: A critical review," *Sol. Energy Mater. Sol. Cells*, vol. 43, no. 2, pp. 101–181, Sep. 1996.

[3] A. Schneider, J. I. Fidalgo, R. M. Martínez, A. Halm, J. Rabanal-Arabach, and R. Harney, "Material Developments Allowing for New Applications, Increased Long Term Stability and Minimized Cell to Module Power Losses," in *Proc. 31st EUPVSEC*, 2015, pp. 153–156.

[4] I. Fidalgo, R. Merino, and B. Pérez, "Lamination Cycle Time Optimization Using New POE Encapsulants," in *Proc. 32th EUPVSEC*, 2016, pp. 183–186.

[5] F. Pern, "Factors that affect the EVA encapsulant discoloration rate upon accelerated exposure," *Sol. Energy Mater. Sol. Cells*, vol. 41–42, pp. 587–615, Jun. 1996.

[6] F. J. Pern, "Ethylene-vinyl acetate (EVA) encapsulants for photovoltaic modules: degradation and discoloration mechanisms and formulation modifications for improved photostability," *Angew. Makromol. Chemie*, vol. 252, no. 1, pp. 195–216, Dec. 1997.

[7] A. Morlier, S. Klotz, S. Sczuka, I. Kunze, I. Schaumann, S. Blankemeyer, M. Siegert, T. Döring, T. Alshuth, U. Giese, M. Denz, and M. Köntges, "Influence of the curing state of ethylene-vinyl acetate on photovoltaic modules aging," in *Proc. 28th EUPVSEC*, 2013, pp. 2832–2837.

[8] C. Peike, L. Purschke, K.-A. Weiss, M. Kohl, and M. Kempe, "Towards the origin of photochemical EVA discoloration," in *Proc. IEEE 39th Photovoltaic Specialists Conference*, 2013, pp. 1579–1584.

[9] I. Hintersteiner, L. Sternbauer, S. Beissmann, W. Buchberger, and G. Wallner, "Determination of stabilizers in polymeric materials used as encapsulants in photovoltaic modules," *Polym. Test.*, vol. 33, pp. 172–178, 2014.

[10] N. S. Allen, M. Edge, M. Rodriguez, C. M. Liauw, and E. Fontan, "Aspects of the thermal oxidation, yellowing and stabilisation of ethylene vinyl acetate copolymer," *Polym. Degrad. Stab.*, vol. 71, no. 1, pp. 1–14, Jan. 2000.

[11] B.-Å. Sultan and E. Sörvik, "Thermal degradation of EVA and EBA—A comparison. I. Volatile decomposition products," *J. Appl. Polym. Sci.*, vol. 43, no. 9, pp. 1737–1745, Nov. 1991.

[12] P. Klemchuk, M. Ezrin, G. Lavigne, W. Holley, J. Galica, and S. Agro, "Investigation of the degradation and stabilization of EVA-based encapsulant in field-aged solar energy modules," *Polym. Degrad. Stab.*, vol. 55, no. 3, pp. 347–365, Mar. 1997.

[13] N. S. Allen, M. Edge, M. Rodriguez, C. M. Liauw, and E. Fontan, "Aspects of the thermal oxidation of ethylene vinyl acetate copolymer," *Polym. Degrad. Stab.*, vol. 68, no. 3, pp. 363–371, May 2000.

[14] M. Rodríguez-Vázquez, C. M. Liauw, N. S. Allen, M. Edge, and E. Fontan, "Degradation and stabilisation of poly(ethylene-stat-vinyl acetate): 1 – Spectroscopic and rheological examination of thermal and thermo-oxidative degradation mechanisms," *Polym. Degrad.*

Stab., vol. 91, no. 1, pp. 154–164, Jan. 2006.

[15] M. D. Kempe, G. J. Jorgensen, K. M. Terwilliger, T. J. McMahon, C. E. Kennedy, and T. T. Borek, "Acetic acid production and glass transition concerns with ethylene-vinyl acetate used in photovoltaic devices," *Sol. Energy Mater. Sol. Cells*, vol. 91, no. 4, pp. 315–329, Feb. 2007.

[16] C. Peike, P. Hülsmann, M. Blüml, P. Schmid, K.-A. Weiß, and M. Köhl, "Impact of Permeation Properties and Backsheet-Encapsulant Interactions on the Reliability of PV Modules," *ISRN Renew. Energy*, vol. 2012, pp. 1–5, 2012.

[17] U. Weber, R. Eiden, C. Strubel, T. Soegding, M. Heiss, P. Zachmann, K. Nattermann, H. Engelmann, A. Dethlefsen, and N. Lenck, "Acetic acid production, migration and corrosion effects in ethylene-vinyl-acetate-(EVA) based PV modules.," in *Proc. 27th EUPVSEC*, 2012, pp. 2992–2995.

[18] J. Kapur, A. Bennett, J. Norwood, B. Hamzavytehrany, and I. Kueppenbender, "Tailoring Ionomer Encapsulants as a low cost solution to potential induced degradation," in *Proc. 28th EUPVSEC*, 2013, pp. 476–479.

[19] S. C. Pop, R. Schulze, X. Wang, B. Yuan, J. Kapur, K. Stika, C. Westphal, H. Antoniadis, and A. Meisel, "Ionomer-based PID-resistant encapsulant for PV modules," in *Proc. 29th EUPVSEC*, 2014, pp. 152–157.

[20] A.-J. Steiner, W. Krumlacher, H. Muckenhuber, M. Plank, K. Sundl, and E. Ziegler, "New Thermoplastic, Non-Curing Encapsulation Material for PV Module Applications," in *Proc. 28th EUPVSEC*, 2013, pp. 2816–2819.

[21] F. Rummens, "Long Term Accelerated Weathering Tests on 'Coupons' to Develop New Classes of Backsheets," in *Proc. 31st EUPVSEC*, 2015, pp. 2478–2481.

[22] G. Stollwerck, W. Schoeppel, A. Graichen, and C. Jaeger, "Polyolefin Backsheet and New Encapsulant Supress Cell Degradation in the Module," in *Proc. 28th EUPVSEC*, 2013, pp. 3318–3320.

[23] D. C. Jordan and S. R. Kurtz, "Photovoltaic Degradation Rates-an Analytical Review," *Prog. Photovoltaics Res. Appl.*, vol. 21, no. 1, pp. 12–29, Jan. 2013.

[24] J. F. Rabek, *Photodegradation of Polymers*. Berlin, Heidelberg: Springer Berlin Heidelberg, 1996.

[25] K. Thaworn, P. Buahom, and S. Areerat, "Effects of Organic Peroxides on the Curing Behavior of EVA Encapsulant Resin," *Open J. Polym. Chem.*, vol. 2, no. 2, pp. 77–85, 2012.

[26] J. Kovářová, J. Rotschová, O. Brede, and M. Burgers, "The effect of transformation products of the antioxidant BHT on the initial stages of thermo- and photo-oxidation of LDPE," *Can. J. Chem.*, vol. 73, no. 11, pp. 1862–1868, Nov. 1995.

[27] J. L. Hodgson and M. L. Coote, "Clarifying the Mechanism of the Denisov Cycle: How do Hindered Amine Light Stabilizers Protect Polymer Coatings from Photo-oxidative Degradation?," *Macromolecules*, vol. 43, no. 10, pp. 4573–4583, May 2010.

[28] P. Bortolus, N. Camaioni, L. Flamigni, F. Minto, S. Monti, and A. Faucitano, "Photostabilization mechanisms of hindered amine light stabilizers: interaction of singlet and triplet anthracene with piperidine model compounds," *J. Photochem. Photobiol. A Chem.*, vol. 68, no. 2, pp. 239–246, Sep. 1992.

[29] M. P. Murray, L. S. Bruckman, and R. H. French, "Photodegradation in a stress and

response framework: poly(methyl methacrylate) for solar mirrors and lens," *J. Photonics Energy*, vol. 2, no. 1, p. 22004, Nov. 2012.

[30] R. H. French, R. Podgornik, T. J. Peshek, L. S. Bruckman, Y. Xu, N. R. Wheeler, A. Gok, Y. Hu, M. A. Hossain, D. A. Gordon, P. Zhao, J. Sun, and G.-Q. Zhang, "Degradation science: Mesoscopic evolution and temporal analytics of photovoltaic energy materials," *Curr. Opin. Solid State Mater. Sci.*, vol. 19, no. 4, pp. 212–226, Aug. 2015.

[31] L. S. Bruckman, N. R. Wheeler, J. Ma, E. Wang, C. K. Wang, I. Chou, Jiayang Sun, and R. H. French, "Statistical and Domain Analytics Applied to PV Module Lifetime and Degradation Science," *IEEE Access*, vol. 1, pp. 384–403, 2013.

[32] G. R. Mon, L. Wen, R. G. J. Ross, and D. Adent, "Effects of Temperature and Moisture on Module Leakage Current," in *Proc. 18th IEEE Photovoltaic Spec. Conf.*, 1985, pp. 1179–1185.

[33] J. H. Wohlgemuth, P. Hacke, N. Bosco, D. C. Miller, M. D. Kempe, and S. R. Kurtz, "Assessing the causes of encapsulant delamination in PV modules," in *Proc. IEEE 43rd Photovoltaic Specialists Conference (PVSC)*, 2016, pp. 0248–0254.

[34] M. Kempe, "Modeling of rates of moisture ingress into photovoltaic modules," *Sol. Energy Mater. Sol. Cells*, vol. 90, no. 16, pp. 2720–2738, Oct. 2006.

[35] J. Wohlgemuth, T. Silverman, D. C. Miller, P. McNutt, M. Kempe, and M. Deceglie, "Evaluation of PV module field performance," in *Proc. IEEE 42nd Photovoltaic Specialist Conference (PVSC)*, 2015, pp. 1–7.

[36] Schulze, S.-H. Pander, M. Dietrich, and M. S. Ebert, "Encapsulation polymers – a key issue in module reliabilty," *Photovoltaics Int.*, vol. 11, pp. 118–126, 2011.

[37] L. Felton, "Low-Cost Manufacturing of High-Efficiency, High-Reliability String Ribbon Si PV Modules, NREL/SR-520-45902," 2009. [Online]. Available: http://www.nrel.gov/docs/fy09osti/45902.pdf. [Accessed: 24-Mar-2017].

[38] L. Heng-Yu, R. Théron, G. Röder, T. Turlings, Y. Luo, R. Lange, F.M., C. Ballif, and L.-E. Perret-Aebi, "Insights into the encapsulation process of photovoltaic modules: GC-MS analysis on the curing step of Poly (ethylene-co-vinyl acetate) (EVA) encapsulant," *Polym. Polym. Compos.*, vol. 20, no. 8, pp. 665–672, 2012.

[39] H. Li, L. Yun, C. Ballif, and L.-E. Perret-Aebi, "Modeling of voids evolution in the encapsulation process of photovoltaic modules," *Polym. Polym. Compos.*, vol. 23, no. 6, pp. 375–388, 2015.

[40] C. R. Cording, "Optimizing photovoltaic module glass reliability," in *Proc. SPIE 7048, Reliability of Photovoltaic Cells, Modules, Components, and Systems*, 2008, p. 70480J.

[41] H.-Y. Li, L.-E. Perret-Aebi, R. Théron, C. Ballif, Y. Luo, and R. F. M. Lange, "Optical transmission as a fast and non-destructive tool for determination of ethylene-co-vinyl acetate curing state in photovoltaic modules," *Prog. Photovoltaics Res. Appl.*, vol. 21, no. 2, pp. 187–194, Mar. 2013.

[42] U. Eitner, M. Pander, S. Kajari-Schröder, M. Köntges, and H. Altenbach, "Thermomechanics of PV modules including the viscoelasticity of EVA," in *Proc.26th EUPVSEC*, 2011, pp. 3267–3269.

[43] H.-Y. Li, L.-E. Perret-Aebi, V. Chapuis, C. Ballif, and Y. Luo, "The effect of cooling press on the encapsulation properties of crystalline photovoltaic modules: residual stress and

adhesion," *Prog. Photovoltaics Res. Appl.*, vol. 23, no. 2, pp. 160–169, Feb. 2015.

[44] H.-Y. Li, Y. Luo, C. Ballif, and L.-E. Perret-Aebi, "Effect of Cooling Press on the Optical Transmission Through Photovoltaic Encapsulants," *Polym. Plast. Technol. Eng.*, vol. 54, no. 4, pp. 416–424, Mar. 2015.

[45] D. C. Miller, M. D. Kempe, S. H. Glick, and S. R. Kurtz, "Creep in photovoltaic modules: Examining the stability of polymeric materials and components," in *Proc. 35th IEEE Photovoltaic Specialists Conference*, 2010, pp. 262–268.

[46] M. D. Kempe, D. C. Miller, J. H. Wohlgemuth, S. R. Kurtz, J. M. Moseley, Q. Shah, G. TamizhMani, K. Sakurai, M. Inoue, T. Doi, and A. Masuda, "Testing Protocol for Module Encapsulant Creep," in *Proc. NREL-PVMRW*, 2012.

[47] M. D. Kempe, D. C. Miller, J. H. Wohlgemuth, S. R. Kurtz, J. M. Moseley, D. L. Nobles, K. M. Stika, Y. Brun, S. L. Samuels, Q. A. Shah, G. Tamizhmani, K. Sakurai, M. Inoue, T. Doi, A. Masuda, and C. E. Vanderpan, "Multi angle laser light scattering evaluation of field exposed thermoplastic photovoltaic encapsulant materials," *Energy Sci. Eng.*, vol. 4, no. 1, pp. 40–51, Jan. 2016.

[48] C. Hirschl, L. Neumaier, W. Mühleisen, M. DeBiasio, G. Oreski, A. Rauschenbach, G. C. Eder, B. S. Chernev, and M. Kraft, "Post-Crosslinking in Photovoltaic Modules under Different Conditions," in *Proc. 29th European Photovoltaic Solar Energy Conference (2014)*, 2014, pp. 3133–3137.

[49] G. Oreski, A. Rauschenbach, C. Hirschl, M. Kraft, G. C. Eder, and G. Pinter, "Crosslinking and post-crosslinking of ethylene vinyl acetate in photovoltaic modules," *J. Appl. Polym. Sci.*, vol. 134, no. 23, Jun. 2017.

[50] A. Morlier, S. Klotz, S. Sczuka, I. Kunze, I. Schaumann, S. Blankemeyer, M. Siegert, T. Döring, T. Alshuth, U. Giese, M. Denz, and M. Köntges, "Influence of the Curing State of Ethylene-Vinyl Acetate on Photovoltaic Modules Aging," in *Proc. 28th EUPVSEC*, 2013, pp. 2832–2837.

[51] F. J. Pern and S. H. Glick, "Thermal processing of EVA encapsulants and effects of formulation additives [for solar cells]," in *Proc. 25th IEEE Photovoltaic Specialists Conference*, 1996, pp. 1251–1254.

[52] S. Jonai, K. Hara, Y. Tsutsui, H. Nakahama, and A. Masuda, "Relationship between cross-linking conditions of ethylene vinyl acetate and potential induced degradation for crystalline silicon photovoltaic modules," *Jpn. J. Appl. Phys.*, vol. 54, no. 8S1, p. 08KG01, Aug. 2015.

[53] K. Agroui, G. Collins, G. Oreski, M. Böhning, A. H. Arab, and D. Ouadjaout, "Effect of crosslinking on EVA-based encapsulant properties during photovoltaic module fabrication process," *Rev. Energies Renouv*, vol. 18, no. 2, pp. 303–314, 2015.

[54] G.-H. Kang, H.-B. Kim, T.-H. Jung, Y. Ju, S.-W. Ko, and H. Song, "Prediction of the Potential Induced Degradation of Photovoltaic Modules Based on the Leakage Current Flowing Through Glass Laminated With Ethylene-Vinly Acetate," *J. Sol. Energy Eng.*, vol. 137, no. 4, p. 41001, Aug. 2015.

[55] F. D. Novoa, D. C. Miller, and R. H. Dauskardt, "Adhesion and debonding kinetics of photovoltaic encapsulation in moist environments," *Prog. Photovoltaics Res. Appl.*, vol. 24, no. 2, pp. 183–194, Feb. 2016.

[56] J. M. Kuitche, G. Tamizh-Mani, and R. Pan, "Failure modes effects and criticality analysis

(FMECA) approach to the crystalline silicon photovoltaic module reliability assessment," in *Proc. SPIE 8112:19*, 2011, p. 81120L.

[57] K. Matsuda, T. Watanabe, K. Sakaguchi, M. Yoshikawa, T. Doi, and A. Masuda, "Microscopic Degradation Mechanisms in Silicon Photovoltaic Module under Long-Term Environmental Exposure," *Jpn. J. Appl. Phys.*, vol. 51, p. 10NF07, Oct. 2012.

[58] A. Jentsch, K.-J. Eichhorn, and B. Voit, "Influence of typical stabilizers on the aging behavior of EVA foils for photovoltaic applications during artificial UV-weathering," *Polym. Test.*, vol. 44, pp. 242–247, Jul. 2015.

[59] N. G. Dhere, N. S. Shiradkar, and E. Schneller, "Device for detailed analysis of leakage current paths in photovoltaic modules under high voltage bias," *Appl. Phys. Lett.*, vol. 104, no. 11, p. 112103, Mar. 2014.

[60] H. Li, "Open the Black Box: Understanding the Encapsulation Process of Photovoltaic Modules," École polytechnique fédérale de Lausanne, Switzerland, 2013.

[61] M. Knausz, G. Oreski, M. Schmidt, P. Guttmann, K. Berger, Y. Voronko, G. Eder, T. Koch, and G. Pinter, "Thermal expansion behavior of solar cell encapsulation materials," *Polym. Test.*, vol. 44, pp. 160–167, Jul. 2015.

[62] T. Kajisa, H. Miyauchi, K. Mizuhara, K. Hayashi, T. Tokimitsu, M. Inoue, K. Hara, and A. Masuda, "Novel lighter weight crystalline silicon photovoltaic module using acrylic-film as a cover sheet," *Jpn. J. Appl. Phys.*, vol. 53, no. 9, p. 92302, Sep. 2014.

[63] E. VANDYK, J. CHAMEL, and A. GXASHEKA, "Investigation of delamination in an edge-defined film-fed growth photovoltaic module," *Sol. Energy Mater. Sol. Cells*, vol. 88, no. 4, pp. 403–411, Sep. 2005.

[64] C. Liciotti, M. Cardinali, and J. D. L. Antolin, "Temperature dependence of encapsulant volumetris resistivity and influence on potential induced degradation of c-Si modules," in *Proc. 29th EUPVSEC*, 2014, pp. 3093–3099.

[65] M. C. López-Escalante, L. J. Caballero, F. Martín, M. Gabás, A. Cuevas, and J. R. Ramos-Barrado, "Polyolefin as PID-resistant encapsulant material in PV modules," *Sol. Energy Mater. Sol. Cells*, vol. 144, pp. 691–699, Jan. 2016.

[66] J. T. W. C. Reid, S.A. Ferrigan, J.I. Martinez, "Contribution of PV Encapsulant Composition to Reduction of Potential Induced Degradation (PID) of Crystalline Silicon PV Cells," in *Proc. 28th EUPVSEC*, 2013, pp. 3340–3346.

[67] J. Berghold, S. Koch, B. Frohmann, P. Hacke, and P. Grunow, "Properties of encapsulation materials and their relevance for recent field failures," in *Proc. IEEE 40th Photovoltaic Specialist Conference (PVSC)*, 2014, pp. 1987–1992.

[68] M. Kempe, "Overview of scientific issues involved in selection of polymers for PV applications," in *Proc. 37th IEEE Photovoltaic Specialists Conference*, 2011, pp. 000085–000090.

[69] S. Hoffmann and M. Koehl, "Effect of humidity and temperature on the potential-induced degradation," *Prog. Photovoltaics Res. Appl.*, vol. 22, no. 2, pp. 173–179, Feb. 2014.

[70] S. Pingel, O. Frank, M. Winkler, S. Daryan, T. Geipel, H. Hoehne, and J. Berghold, "Potential Induced Degradation of solar cells and panels," in *Proc. 35th IEEE Photovoltaic Specialists Conference*, 2010, pp. 2817–2822.

[71] C. Taubitz, M. Schütze, and M. B. Koentopp, "Towards a Kinetic moduel for Potential

induced shunting," in *Proc. 27th EUPVSEC*, 2012, pp. 3172–3176.

[72] S. Meyer, S. Timmel, M. Gläser, U. Braun, V. Wachtendorf, and C. Hagendorf, "Polymer foil additives trigger the formation of snail trails in photovoltaic modules," *Sol. Energy Mater. Sol. Cells*, vol. 130, pp. 64–70, Nov. 2014.

[73] S. Meyer, S. Timmel, S. Richter, M. Werner, M. Gläser, S. Swatek, U. Braun, and C. Hagendorf, "Silver nanoparticles cause snail trails in photovoltaic modules," *Sol. Energy Mater. Sol. Cells*, vol. 121, pp. 171–175, Feb. 2014.

[74] N. Kim, K.-J. Hwang, D. Kim, J. H. Lee, S. Jeong, and D. H. Jeong, "Analysis and reproduction of snail trails on silver grid lines in crystalline silicon photovoltaic modules," *Sol. Energy*, vol. 124, pp. 153–162, Feb. 2016.

[75] N. C. Park, J. S. Jeong, B. J. Kang, and D. H. Kim, "The effect of encapsulant discoloration and delamination on the electrical characteristics of photovoltaic module," *Microelectron. Reliab.*, vol. 53, no. 9–11, pp. 1818–1822, Sep. 2013.

[76] T. H. Kim, N. C. Park, and D. H. Kim, "The effect of moisture on the degradation mechanism of multi-crystalline silicon photovoltaic module," *Microelectron. Reliab.*, vol. 53, no. 9–11, pp. 1823–1827, 2013.

[77] K. Lin, Y.-H. Lee, W.-Y. Huang, G. Chen, Y.-W. Kuo, L.-K. Wang, and S.-Y. Yang, "Detection of soldering induced damages on crystalline silicon solar modules fabricated by hot-air soldering method," *Renew. Energy*, vol. 83, pp. 749–758, Nov. 2015.

[78] C. Dechthummarong, B. Wiengmoon, D. Chenvidhya, C. Jivacate, and K. Kirtikara, "Physical deterioration of encapsulation and electrical insulation properties of PV modules after long-term operation in Thailand," *Sol. Energy Mater. Sol. Cells*, vol. 94, no. 9, pp. 1437–1440, Sep. 2010.

[79] B. Ketola and A. Norris, "The Role of Encapsulant Moisture Permeability in the Durability of Solar Photovoltaic Modules," in *Proc. 25th Photovoltaic Solar Energy Conference/5th World Conference on Photovoltaic Energy Conversion*, 2010, pp. 4098–4102.

[80] T. Swonke and U. Hoyer, "Diffusion of Moisture and Impact of UV Irradiance in Photovoltaic Encapsulants," in *Proc. 24th EUPVSEC*, 2009, pp. 3373–3376.

[81] W. J. Gambogi, "Comparative Performance of Backsheets for Photovoltaic Modules," in *Proc. 25th European Photovoltaic Solar Energy Conference and Exhibition/5th World Conference on Photovoltaic Energy Conversion*, 2010, pp. 4079–4083.

[82] P. Hülsmann, D. Philipp, and M. Köhl, "Measuring temperature-dependent water vapor and gas permeation through high barrier films," *Rev. Sci. Instrum.*, vol. 80, no. 11, p. 113901, 2009.

[83] I. Duerr, J. Bierbaum, J. Metzger, J. Richter, and D. Philipp, "Silver Grid Finger Corrosion on Snail Track affected PV Modules – Investigation on Degradation Products and Mechanisms," *Energy Procedia*, vol. 98, pp. 74–85, 2016.

[84] C. Peike, S. Hoffmann, P. Hülsmann, B. Thaidigsmann, K. A. Weiβ, M. Koehl, and P. Bentz, "Origin of damp-heat induced cell degradation," *Sol. Energy Mater. Sol. Cells*, vol. 116, pp. 49–54, Sep. 2013.

[85] A. Richter, "Schadensbilder nach Wareneingang und im Reklamationsfall," in *Proc. 8. Workshop "Photovoltaik-Modultechnik" TÜV Rheinland*, 2011.

[86] G. Jorgensen, K. Terwilliger, J. Delcueto, S. Glick, M. Kempe, J. Pankow, F. Pern, and T.

McMahon, “Moisture transport, adhesion, and corrosion protection of PV module packaging materials,” *Sol. Energy Mater. Sol. Cells*, vol. 90, no. 16, pp. 2739–2775, Oct. 2006.

[87] M. D. Kempe, “Ultraviolet light test and evaluation methods for encapsulants of photovoltaic modules,” *Sol. Energy Mater. Sol. Cells*, vol. 94, no. 2, pp. 246–253, Feb. 2010.

[88] M. Paggi, S. Kajari-Schroder, and U. Eitner, “Thermomechanical deformations in photovoltaic laminates,” *J. Strain Anal. Eng. Des.*, vol. 46, no. 8, pp. 772–782, Nov. 2011.

[89] M. Paggi and A. Sapora, “An Accurate Thermoviscoelastic Rheological Model for Ethylene Vinyl Acetate Based on Fractional Calculus,” *Int. J. Photoenergy*, vol. 2015, pp. 1–7, 2015.

[90] G. Oreski and G. Pinter, “Comparative Study of the Temperature Dependent Delamination Behavior of Four Solar Cell Encapsulants to Glass and Backsheet-Laminate,” in *Proc. 28th EUPVSEC*, 2011, pp. 3305–3309.

[91] A. A. Dameron, M. O. Reese, T. J. Moricone, and M. D. Kempe, “Understanding moisture ingress and packaging requirements for photovoltaic modules,” *Photovoltaics Int.*, vol. 5, no. August 2010, pp. 121–130, 2010.

[92] M. Van Iseghem, A. Plotton, J.-F. Penneau, N. Chatagnon, D. Binesti, K. Radouane, and P.-G. Therond, “Failure modes after damp heat tests on PV modules,” in *Proc. 27th EUPVSEC*, 2012, pp. 3546–3548.

[93] F. D. Novoa, D. C. Miller, and R. H. Dauskardt, “Environmental mechanisms of debonding in photovoltaic backsheets,” *Sol. Energy Mater. Sol. Cells*, vol. 120, pp. 87–93, Jan. 2014.

[94] T. Friesen, “WP5 Deliverable 5.2 - Lifetime degradation mechanisms,” 2015. [Online]. Available: http://www.perfplus.eu/frontend/files/userfiles/files/308991_PerfPlus_Deliverable5_2_20150316_compressed.pdf. [Accessed: 24-Mar-2017].

[95] J. H. Wohlgemuth, M. D. Kempe, and D. C. Miller, “Discoloration of PV encapsulants,” in *Photovoltaic Specialists Conference (PVSC), 2013 IEEE 39th*, 2013, pp. 3260–3265.

[96] G. Oreski and K. Möller, “Qualification of polymeric components for use in PV modules,” in *Proc. SPIE - The International Society for Optical Engineering 8112:10*, 2011, p. 81120B–81120B14.

[97] A. Fell and K. R. McIntosh, “Determining the generation profile for silicon solar cells from lumped optical parameters,” in *Proc. IEEE 42nd Photovoltaic Specialist Conference (PVSC)*, 2015, pp. 1–5.

[98] M. Köntges, S. Altmann, T. Heimberg, U. Jahn, and K. A. Berger, “Mean Degradation Rates in PV Systems for Various Kinds of PV Module Failures,” in *Proc. 32nd EUPVSEC*, 2016, pp. 1435–1443.

[99] K. Morita, T. Inoue, H. Kato, I. Tsuda, and Y. Hishikawa, “Degradation factor analysis of crystalline-Si PV modules through long-term field exposure test,” in *Photovoltaic Energy Conversion, 2003. Proceedings of 3rd World Conference on*, 2003, vol. 2, pp. 1948–1951.

[100] D. Chianese, A. Realini, N. Cereghetti, S. Rezzonio, E. Burà, and A. Bernasconi, “Analysis of weathered c-Si PV modules,” in *Proc. 3rd World Conference On Photovoltaic Energy Conversion*, 2003, pp. 2922–2926.

[101] C. E. Chamberlin, M. A. Rocheleau, M. W. Marshall, A. M. Reis, N. T. Coleman, and P. A. Lehman, “Comparison of PV module performance before and after 11 and 20 years of field

exposure," in *Proc. 37th IEEE Photovoltaic Specialists Conference*, 2011, pp. 000101–000105.

[102] D. Berman, S. Biryukov, and D. Faiman, "EVA laminate browning after 5 years in a grid-connected, mirror-assisted, photovoltaic system in the Negev desert: effect on module efficiency," *Sol. Energy Mater. Sol. Cells*, vol. 36, no. 4, pp. 421–432, Apr. 1995.

[103] R. H. French and H. V. Tran, "Immersion Lithography: Photomask and Wafer-Level Materials," *Annu. Rev. Mater. Res.*, vol. 39, no. 1, pp. 93–126, Aug. 2009.

[104] P. Sánchez-Friera, M. Piliougine, J. Peláez, J. Carretero, and M. Sidrach de Cardona, "Analysis of degradation mechanisms of crystalline silicon PV modules after 12 years of operation in Southern Europe," *Prog. Photovoltaics Res. Appl.*, vol. 19, no. 6, pp. 658–666, Sep. 2011.

[105] S. V. Janakeeraman, J. Singh, J. Kuitche, J. K. Mallineni, and G. TamizhMani, "A statistical analysis on the cell parameters responsible for power degradation of fielded pv modules in a hot-dry climate," in *Proc. IEEE 40th Photovoltaic Specialist Conference (PVSC)*, 2014, pp. 3234–3238.

[106] A. Sinha, O. S. Sastry, and R. Gupta, "Detection and characterisation of delamination in PV modules by active infrared thermography," *Nondestruct. Test. Eval.*, vol. 31, no. 1, pp. 1–16, Jan. 2016.

[107] Y. Voronko, G. Eder, M. Weiss, M. Knausz, G. Oreski, T. Koch, K. Berger, and P. Leoben, "Long Term Performance of PV Modules: System Optimization through the Application of Innovative Non-Destructive Characterization Methods," in *Proc. 27th EUPVSEC*, 2012, pp. 3530–3535.

[108] J. H. Wohlgemuth, D. W. Cunningham, A. M. Nguyen, and J. Miller, "LONG TERM RELIABILITY OF PV MODULES," in *Proc. 20th European Photovoltaic Solar Energy Conference*, 2005, pp. 1942–1946.

[109] F. J. Pern and G. J. Jorgensen, "Enhanced adhesion of EVA laminates to primed glass substrates subjected to damp heat exposure," in *Proc. 31st IEEE Photovoltaic Specialists Conference, 2005.*, 2005, pp. 495–498.

[110] D. Wu, J. Zhu, T. R. Betts, and R. Gottschalg, "Degradation of interfacial adhesion strength within photovoltaic mini-modules during damp-heat exposure," *Prog. Photovoltaics Res. Appl.*, vol. 22, no. 7, pp. 796–809, Jul. 2014.

[111] R. Meitzner and S.-H. Schulze, "Method for determination of parameters for moisture simulations in photovoltaic modules and laminated glass," *Sol. Energy Mater. Sol. Cells*, vol. 144, pp. 23–28, Jan. 2016.

[112] N. Park, C. Han, and D. Kim, "Effect of moisture condensation on long-term reliability of crystalline silicon photovoltaic modules," *Microelectron. Reliab.*, vol. 53, no. 12, pp. 1922–1926, Dec. 2013.

[113] T. Carlsson, J. Halme, P. Lund, and P. Konttinen, "Moisture sensor at glass/polymer interface for monitoring of photovoltaic module encapsulants," *Sensors Actuators A Phys.*, vol. 125, no. 2, pp. 281–287, Jan. 2006.

[114] S. Rashtchi, P. D. Ruiz, R. Wildman, and I. Ashcroft, "Measurement of moisture content in photovoltaic panel encapsulants using spectroscopic optical coherence tomography: a feasibility study," in *Proc. SPIE 8472 Reliability of Photovoltaic Cells, Modules, Components, and Systems V*, 2012, p. 84720O.

[115] M. Köntges, I. Kunze, S. Kajari-Schröder, X. Breitenmoser, and B. Bjørneklett, “The risk of power loss in crystalline silicon based photovoltaic modules due to micro-cracks,” *Sol. Energy Mater. Sol. Cells*, vol. 95, no. 4, pp. 1131–1137, Apr. 2011.

[116] M. Paggi, I. Berardone, A. Infuso, and M. Corrado, “Fatigue degradation and electric recovery in Silicon solar cells embedded in photovoltaic modules,” *Sci. Rep.*, vol. 4, Mar. 2014.

[117] I. Berardone, M. Corrado, and M. Paggi, “A Generalized Electric Model for Mono and Polycrystalline Silicon in the Presence of Cracks and Random Defects,” *Energy Procedia*, vol. 55, pp. 22–29, 2014.

[118] J. Kasewieter, F. Haase, and M. Kontges, “Model of Cracked Solar Cell Metallization Leading to Permanent Module Power Loss,” *IEEE J. Photovoltaics*, vol. 6, no. 1, pp. 28–33, Jan. 2016.

[119] S. Dongaonkar and M. A. Alam, “Geometrical design of thin film photovoltaic modules for improved shade tolerance and performance,” *Prog. Photovoltaics Res. Appl.*, vol. 23, no. 2, pp. 170–181, Feb. 2015.

[120] J. I. van Mölken, U. A. Yusufoğlu, A. Safiei, H. Windgassen, R. Khandelwal, T. M. Pletzer, and H. Kurz, “Impact of Micro-Cracks on the Degradation of Solar Cell Performance Based On Two-Diode Model Parameters,” *Energy Procedia*, vol. 27, pp. 167–172, 2012.

[121] S. Spataru, P. Hacke, and D. Sera, “In-situ measurement of of power loss for crystalline silicon modules undergoing thermal cycling and mechanical load stress testing,” in *Proc. Workshop on Crystalline Silicon Solar Cells and Modules: Materials and Processes*, 2015.

[122] D. L. King, M. A. Quintana, J. A. Kratochvil, D. E. Ellibee, and B. R. Hansen, “Photovoltaic module performance and durability following long-term field exposure,” *Prog. Photovoltaics Res. Appl.*, vol. 8, no. 2, pp. 241–256, Mar. 2000.

[123] P. Hacke and D. L. Meier, “Analysis of fill factor losses using current-voltage curves obtained under dark and illuminated conditions,” in *Conference Record of the Twenty-Ninth IEEE Photovoltaic Specialists Conference, 2002.*, 2002, pp. 462–464.

[124] S. Bowden and A. Rohatgi, “Rapid accurate determination of series resistance and fill factor losses in industrial silicon solar cells,” in *Proc. 17th EUPVSEC*, 2001, pp. 1802–1806.

[125] V. Naumann, T. Geppert, S. Großer, D. Wichmann, H.-J. Krokoszinski, M. Werner, and C. Hagendorf, “Potential-induced Degradation at Interdigitated Back Contact Solar Cells,” *Energy Procedia*, vol. 55, pp. 498–503, 2014.

[126] A. Halm, A. Schneider, V. D. Mihailetchi, L. J. Koduvelikulathu, L. M. Popescu, G. Galbiati, H. Chu, and R. Kopecek, “Potential-induced Degradation for Encapsulated n-type IBC Solar Cells with Front Floating Emitter,” *Energy Procedia*, vol. 77, pp. 356–363, Aug. 2015.

[127] R. Swanson, M. Cudzinovic, D. DeCeuster, V. Desai, J. Jörn, N. Kaminar, W. Mulligan, L. Rodrigues-Barbarosa, D. Rose, D. Smith, A. Terao, and K. Wilson, “The Surface Polarization Effect in High-Efficiency Silicon Solar Cells,” in *Proc. 15th International Photovoltaic Science and Engineering Conference*, 2005, pp. 410–413.

[128] D. Lausch, V. Naumann, A. Graff, A. Hähnel, O. Breitenstein, C. Hagendorf, and J. Bagdahn, “Sodium Outdiffusion from Stacking Faults as Root Cause for the Recovery Process of Potential-induced Degradation (PID),” *Energy Procedia*, vol. 55, pp. 486–493, 2014.

[129] S. Pingel, S. Janke, and O. Frank, “Recovery methods for modules affected by potential

induced degradation (PID)," in *Proc. 27th EUPVSEC*, 2012, pp. 3379–3383.

[130] C. H. V. Naumann, K. Ilse, "On the Discrepancy between Leakage Current and Potential Induced Degradation of Crystalline Silicon Modules," in *Proc. 28th EUPVSEC*, 2013, pp. 3405–3410.

[131] J. Hattendorf, R. Loew, W.-M. Gnehr, L. Wulff, M. C. Koekten, D. Koshnicharov, A. Blauaermel, and J. A. Esquivel, "PID in monocrystalline silicon based modules: an acceleration model," in *Proc. 27th EUPVSEC*, 2012, pp. 3405–3410.

[132] M. Z. J. Hattendorf, W.-M. Gnehr, R. Loew, T. Roth, D. Koshnicharov, "PID and temperature-driven regeneration: a realistic simulation," in *Proc. 28th EUPVSEC*, 2013, pp. 3303–3308.

[133] C. Taubitz, M. Schütze, M. Kröber, and M. B. Koentopp, "PID: model calculations and correlation between laboratory tests and outdoor occurrence," in *Proc. 29th EUPVSEC*, 2014, pp. 2490–2494.

[134] P. Hacke, S. Spataru, K. Terwilliger, G. Perrin, S. Glick, S. Kurtz, and J. Wohlgemuth, "Accelerated Testing and Modeling of Potential-Induced Degradation as a Function of Temperature and Relative Humidity," *IEEE J. Photovoltaics*, vol. 5, no. 6, pp. 1549–1553, Nov. 2015.

[135] P. Hacke, S. Spataru, S. Johnston, K. Terwilliger, K. VanSant, M. Kempe, J. Wohlgemuth, S. Kurtz, A. Olsson, and M. Propst, "Elucidating PID Degradation Mechanisms and In Situ Dark I–V Monitoring for Modeling Degradation Rate in CdTe Thin-Film Modules," *IEEE J. Photovoltaics*, vol. 6, no. 6, pp. 1635–1640, Nov. 2016.

[136] E. Annigoni, M. Jankovec, F. Galliano, H. Y. Li, L.-E. Perret-Aebi, M. Topič, F. Sculati-Meillaud, A. Virtuani, and C. Ballif, "Modeling potential-induced degradation (PID) in crystalline silicon solar cells: from accelerated-aging laboratory testing to outdoor prediction," in *Proc. 32nd EUPVSEC*, 2016, pp. 1558–1563.

[137] N. A. Olsson, M. C. Richardson, and J. Hevelone, "Thin film PID field failures and root cause determination," in *Proc. IEEE 40th Photovoltaic Specialists Conference (PVSC) Volume 2*, 2014, pp. 1–4.

[138] V. Fjallstrom, P. M. P. Salome, A. Hultqvist, M. Edoff, T. Jarmar, B. G. Aitken, K. Zhang, K. Fuller, and C. K. Williams, "Potential-Induced Degradation of CuIn(1−x)Ga(x)Se(2) Thin Film Solar Cells," *IEEE J. Photovoltaics*, vol. 3, no. 3, pp. 1090–1094, Jul. 2013.

[139] S. Yamaguchi, S. Jonai, K. Hara, H. Komaki, Y. Shimizu-Kamikawa, H. Shibata, S. Niki, Y. Kawakami, and A. Masuda, "Potential-induced degradation of Cu(In,Ga)Se 2 photovoltaic modules," *Jpn. J. Appl. Phys.*, vol. 54, no. 8S1, p. 08KC13, Aug. 2015.

[140] G. Mathiak, N. Bogdanski, and F. Reil, "Potential-induced degradation (PID): Field monitoring data evaluation and climatic chamber tests with field modules," in *Proc. 32nd EUPVSEC*, 2016, pp. 1898–1900.

[141] G. R. Mon, J. Orehotsky, R. G. Ross, and G. Whitla, "Predicting Electrochemical Corrosion in Terrestrial Photovoltaic Modules," in *Proc. 17th IEEE Photovoltaic Spec. Conf.*, 1984, pp. 682–692.

[142] T. Shioda, "Acetic acid production rate in EVA encapsulant and its influence on performance of PV modules," in *Proc. 2nd Atlas/NIST PV Materials Durability Workshop*, 2013.

[143] A. Masuda, N. Uchiyama, and Y. Hara, “Degradation by acetic acid for crystalline Si photovoltaic modules,” *Jpn. J. Appl. Phys.*, vol. 54, no. 4S, p. 04DR04, Apr. 2015.

[144] A. Kraft, L. Labusch, T. Ensslen, I. Durr, J. Bartsch, M. Glatthaar, S. Glunz, and H. Reinecke, “Investigation of Acetic Acid Corrosion Impact on Printed Solar Cell Contacts,” *IEEE J. Photovoltaics*, vol. 5, no. 3, pp. 736–743, May 2015.

[145] D. Chenvidhya, K. Kirtikara, and C. Jivacate, “PV module dynamic impedance and its voltage and frequency dependencies,” *Sol. Energy Mater. Sol. Cells*, vol. 86, no. 2, pp. 243–251, Mar. 2005.

[146] C. Ballif, D. M. Huljić, G. Willeke, and A. Hessler-Wyser, “Silver thick-film contacts on highly doped n-type silicon emitters: Structural and electronic properties of the interface,” *Appl. Phys. Lett.*, vol. 82, no. 12, p. 1878, 2003.

[147] Z. G. Li, L. Liang, A. S. Ionkin, B. M. Fish, M. E. Lewittes, L. K. Cheng, and K. R. Mikeska, “Microstructural comparison of silicon solar cells’ front-side Ag contact and the evolution of current conduction mechanisms,” *J. Appl. Phys.*, vol. 110, no. 7, p. 74304, 2011.

[148] H. Morita, M. Miyashita, and A. Masuda, “Moisture ingress rate and route into c-Si PV modules,” in *Proc. Photovoltaic Module Reliability Workshop 2014*, 2014, p. 601.

[149] N. C. Park, W. W. Oh, and D. H. Kim, “Effect of Temperature and Humidity on the Degradation Rate of Multicrystalline Silicon Photovoltaic Module,” *Int. J. Photoenergy*, vol. 2013, pp. 1–9, 2013.

[150] J. Zhu, M. Koehl, S. Hoffmann, K. A. Berger, S. Zamini, I. Bennett, E. Gerritsen, P. Malbranche, P. Pugliatti, A. Di Stefano, F. Aleo, D. Bertani, F. Paletta, F. Roca, G. Graditi, M. Pellegrino, O. Zubillaga, F. J. C. Iranzo, A. Pozza, T. Sample, and R. Gottschalg, “Changes of solar cell parameters during damp-heat exposure,” *Prog. Photovoltaics Res. Appl.*, vol. 24, no. 10, pp. 1346–1358, Oct. 2016.

[151] M. Koehl, M. Heck, and S. Wiesmeier, “Modelling of conditions for accelerated lifetime testing of Humidity impact on PV-modules based on monitoring of climatic data,” *Sol. Energy Mater. Sol. Cells*, vol. 99, pp. 282–291, Apr. 2012.

[152] M. D. Kempe and J. H. Wohlgemuth, “Evaluation of temperature and humidity on PV module component degradation,” in *Proc. IEEE 39th Photovoltaic Specialists Conference (PVSC)*, 2013, pp. 0120–0125.

[153] P. Hülsmann and K.-A. Weiss, “Simulation of water ingress into PV-modules: IEC-testing versus outdoor exposure,” *Sol. Energy*, vol. 115, pp. 347–353, May 2015.

[154] S. Suzuki, T. Tanahashi, T. Doi, and A. Masuda, “Acceleration of degradation by highly accelerated stress test and air-included highly accelerated stress test in crystalline silicon photovoltaic modules,” *Jpn. J. Appl. Phys.*, vol. 55, no. 2, p. 22302, Feb. 2016.

[155] Y. Voronko, G. C. Eder, M. Knausz, G. Oreski, T. Koch, and K. A. Berger, “Correlation of the loss in photovoltaic module performance with the ageing behaviour of the backsheets used,” *Prog. Photovoltaics Res. Appl.*, vol. 23, no. 11, pp. 1501–1515, Nov. 2015.

[156] K. Whitfield, A. Salomon, S. Yang, and I. Suez, “Damp heat versus field reliability for crystalline silicon,” in *Proc. 38th IEEE Photovoltaic Specialists Conference*, 2012, pp. 001864–001870.

[157] M. A. Shirakawa, R. Zilles, A. Mocelin, C. C. Gaylarde, A. Gorbushina, G. Heidrich, M. C. Giudice, G. M. B. Del Negro, and V. M. John, “Microbial colonization affects the efficiency

of photovoltaic panels in a tropical environment," *J. Environ. Manage.*, vol. 157, pp. 160–167, Jul. 2015.

[158] J. Tanesab, D. Parlevliet, J. Whale, T. Urmee, and T. Pryor, "The contribution of dust to performance degradation of PV modules in a temperate climate zone," *Sol. Energy*, vol. 120, pp. 147–157, Oct. 2015.

[159] E. S. Kumar, D. B. Sarkar, and D. K. Behera, "Soiling and Dust Impact on the Efficiency and the Maximum Power Point in the Photovoltaic Modules," *Int. J. Eng. Res. Technol.*, vol. 2, no. 2, pp. 1–5, 2013.

[160] DEWA, "Soiling effect of PV modules," 2016. [Online]. Available: https://www.dewa.gov.ae/en/about-dewa/news-and-media/press-and-news/latest-news/2016/04/dewa-organises-soiling. [Accessed: 17-Mar-2017].

[161] "PV Quality Assurance Task Force (PVQAT), Task Group 12 'Soiling and Dust.'" [Online]. Available: http://www.pvqat.org/project-status/task-group-12.html. [Accessed: 16-Dec-2016].

[162] S. C. S. Costa, A. S. A. C. Diniz, and L. L. Kazmerski, "Dust and soiling issues and impacts relating to solar energy systems: Literature review update for 2012–2015," *Renew. Sustain. Energy Rev.*, vol. 63, pp. 33–61, Sep. 2016.

[163] W. Herrmann, "Time evolution of PV soiling loss at test locations in different climates," in *Workshop on "Soiling Effect on PV Modules,"* 2016.

[164] E. Klimm, L. Ost, B. Spiegelhalter, and K.-A. Weiss, "Tests of functional coatings on glass adapted to extreme - arid and maritime - climatic conditions for solar energy systems," in *Proc. IEEE 42nd Photovoltaic Specialist Conference (PVSC)*, 2015, pp. 1–5.

[165] E. Klimm, T. Lorenz, and K.-A. Weiss, "Can anti-soiling coating on solar glass influence the degree of performance loss over time of PV module drastically," in *Proc. 28th EUPVSEC*, 2013, pp. 3099–3102.

[166] "Photovoltaic (PV) module performance testing and energy rating – Spectral responsivity, incidence angle and module operating temperature measurements." IEC 61853-2:2016, 2016.

[167] "IEC 61215:2006, Crystalline silicon terrestrial photovoltaic (PV) modules – Design qualification and type approval." .

[168] Z. A. Darwish, H. A. Kazem, K. Sopian, M. A. Al-Goul, and H. Alawadhi, "Effect of dust pollutant type on photovoltaic performance," *Renew. Sustain. Energy Rev.*, vol. 41, pp. 735–744, Jan. 2015.

[169] R. Appels, B. Lefevre, B. Herteleer, H. Goverde, A. Beerten, R. Paesen, K. De Medts, J. Driesen, and J. Poortmans, "Effect of soiling on photovoltaic modules," *Sol. Energy*, vol. 96, pp. 283–291, Oct. 2013.

[170] S. Noack-Schönmann, O. Spagin, K.-P. Gründer, M. Breithaupt, A. Günter, B. Muschik, and A. A. Gorbushina, "Sub-aerial biofilms as blockers of solar radiation: spectral properties as tools to characterise material-relevant microbial growth," *Int. Biodeterior. Biodegradation*, vol. 86, pp. 286–293, Jan. 2014.

[171] H. Berberoglu, L. Pilon, and A. Melis, "Radiation characteristics of Chlamydomonas reinhardtii CC125 and its truncated chlorophyll antenna transformants tla1, tlaX and tla1-CW+," *Int. J. Hydrogen Energy*, vol. 33, no. 22, pp. 6467–6483, Nov. 2008.

[172] E. Lee, R.-L. Heng, and L. Pilon, “Spectral optical properties of selected photosynthetic microalgae producing biofuels,” *J. Quant. Spectrosc. Radiat. Transf.*, vol. 114, pp. 122–135, Jan. 2013.

[173] N. R. Moheimani, “Long-term outdoor growth and lipid productivity of Tetraselmis suecica, Dunaliella tertiolecta and Chlorella sp (Chlorophyta) in bag photobioreactors,” *J. Appl. Phycol.*, vol. 25, no. 1, pp. 167–176, Feb. 2013.

[174] A. Sayyah, M. N. Horenstein, and M. K. Mazumder, “Energy yield loss caused by dust deposition on photovoltaic panels,” *Sol. Energy*, vol. 107, pp. 576–604, Sep. 2014.

[175] D. K. Prasad and M. Snow, “Examples of successful architectural integration of PV: Australia,” *Prog. Photovoltaics Res. Appl.*, vol. 12, no. 6, pp. 477–483, Sep. 2004.

[176] R. Hammond, D. Srinivasan, A. Harris, K. Whitfield, and J. Wohlgemuth, “Effects of soiling on PV module and radiometer performance,” in *Proc. Twenty Sixth IEEE Photovoltaic Specialists Conference*, 1997, pp. 1121–1124.

[177] J. Solórzano and M. A. Egido, “Automatic fault diagnosis in PV systems with distributed MPPT,” *Energy Convers. Manag.*, vol. 76, pp. 925–934, Dec. 2013.

[178] R. R. Hernandez, S. B. Easter, M. L. Murphy-Mariscal, F. T. Maestre, M. Tavassoli, E. B. Allen, C. W. Barrows, J. Belnap, R. Ochoa-Hueso, S. Ravi, and M. F. Allen, “Environmental impacts of utility-scale solar energy,” *Renew. Sustain. Energy Rev.*, vol. 29, pp. 766–779, Jan. 2014.

[179] L. A. Lamont and L. El Chaar, “Enhancement of a stand-alone photovoltaic system’s performance: Reduction of soft and hard shading,” *Renew. Energy*, vol. 36, no. 4, pp. 1306–1310, Apr. 2011.

[180] M. C. Peel, B. L. Finlayson, and T. A. McMahon, “Updated world map of the Köppen-Geiger climate classification,” *Hydrol. Earth Syst. Sci.*, vol. 11, no. 5, pp. 1633–1644, Oct. 2007.

[181] I. Kaizuka, R. Kurihara, H. Matsukawa, G. Masson, S. Nowak, S. Orlandi, and M. Brunisholz, “Trends 2014 in photovoltaic applications,” IEA PVPS, 2014.

[182] R. Dubey, S. Chattopadhyay, V. Kuthanazhi, J. John, C. Solanki, A. Kottantharayil, B. Arora, K. Narasimhan, V. Kuber, and J. Vasi, “All-India India Survey of Photovoltaic Module Degradation : 2013,” Mumbai, India, 2013.

[183] S. Djordjevic, D. Parlevliet, and P. Jennings, “Detectable faults on recently installed solar modules in Western Australia,” *Renew. Energy*, vol. 67, pp. 215–221, Jul. 2014.

[184] C. E. Packard, J. H. Wohlgemuth, and S. R. Kurtz, “Development of a visual inspection data collection tool for evaluation of fielded PV module condition,” 2012.

[185] A. Jacobson, D. Kammen, R. Duke, and M. Hankins, “Field performance measurements of amorphous silicon photovoltaic modules in Kenya,” *Sol. Conf.*, pp. 95–100, 2000.

[186] A. B. Maish, C. Atcitty, S. Hester, D. Greenberg, D. Osborn, D. Collier, and M. Brine, “Photovoltaic system reliability,” in *Conference Record of the Twenty Sixth IEEE Photovoltaic Specialists Conference -*, 1997, pp. 1049–1054.

[187] K. Stokes and J. Bigger, “Reliability, cost, and performance of PV-powered water pumping systems: a survey for electric utilities,” *IEEE Trans. Energy Convers.*, vol. 8, no. 3, pp. 506–512, 1993.

[188] K. Kato, “PVRessQ!: a research activity on reliability of PV systems from an user’s viewpoint

in Japan," in *Proc. SPIE 8112, Reliability of Photovoltaic Cells, Modules, Components, and Systems IV*, 2011, p. 81120K–81120K–9.

[189] A. Skoczek, T. Sample, and E. D. Dunlop, "The results of performance measurements of field-aged crystalline silicon photovoltaic modules," *Prog. Photovoltaics Res. Appl.*, vol. 17, no. 4, pp. 227–240, Jun. 2009.

[190] R. J. van der Plas and M. Hankins, "Solar electricity in Africa: a reality," *Energy Policy*, vol. 26, no. 4, pp. 295–305, Mar. 1998.

[191] S. Kumar, S. C. Bhattacharya, and M. Augustus Leon, "A Survey on PV Systems and Accessories in Asia," in *World Renewable Energy Congress VI*, Brighton, UK: Elsevier, 2000, pp. 860–863.

[192] E. D. Dunlop, D. Halton, and H. A. Ossenbrink, "20 years of life and more: where is the end of life of a PV module?," in *Proc. Thirty-first IEEE Photovoltaic Specialists Conference, 2005.*, pp. 1593–1596.

[193] L. M. Fraas and L. D. Partain, *Solar cells and their applications*, 2nd ed. Wiley, 2010.

[194] A. Zaman, D. Parlevliet, M. Calais, S. Djordjevic, S. Pulsford, and R. Passey, "PV System Reliability – Preliminary Findings from the PV Module and System Fault Reporting Website," in *Proc. Asia Pacific Solar Research Conference*, 2014.

[195] H. Laukamp, K. Kiefer, R. Kaiser, H. Schmidt, and H. Becker, "Reliability Issues in PV Systems - Experience and Improvements," in *Proc. 2nd World Solar Electric Buildings Conference*, pp. 88–94.

[196] H. Laukamp, T. Schoen, and D. Ruoss, "Reliability Study of Grid Connected PV Systems, Field Experience and Recommended Design Practice," Paris, France, 2002.

[197] Z. Scheftalovich, "Solar power survey results," 2015. [Online]. Available: http://www.choice.com.au/reviews-and-tests/household/energy-and-water/solar/solar-power-pv-system-survey-results.aspx. [Accessed: 20-Feb-2017].

[198] A. Realini, E. Burà, N. Cereghetti, D. Chianese, and S. Rezzonico, "Mean time before failure of photovoltaic modules (MTBF-PVm)," Annual Report 2002-Swiss Federal Office of Energy, Canobbio, Switzerland, 2002.

[199] "160815__PV-failure_survey_blank.xlsm," *160815 PV-failure survey blank*, 2016. [Online]. Available: http://www.iea-pvps.org/index.php?id=344. [Accessed: 23-Feb-2017].

[200] "160815 Explanation PV-failure survey.pdf," *Explanation of the PV-system-survey-sheet*, 2016. [Online]. Available: http://www.iea-pvps.org/index.php?id=344. [Accessed: 23-Feb-2017].

[201] B. Burger, K. Kiefer, C. Kost, S. Nold, S. Philipps, R. Preu, J. Rentsch, T. Schlegl, G. Stryi-Hipp, G. Willeke, H. Wirth, I. Brucker, A. Häberle, and W. Warmuth, "Photovoltaics Report," Freiburg, Germany, 2016.

[202] D. C. Jordan, S. R. Kurtz, K. VanSant, and J. Newmiller, "Compendium of photovoltaic degradation rates," *Prog. Photovoltaics Res. Appl.*, vol. 24, no. 7, pp. 978–989, Jul. 2016.

[203] J. Berghold, S. Koch, S. Pingel, S. Janke, A. Ukar, P. Grunow, and T. Shioda, "PID: from material properties to outdoor performance and quality control counter measures," in *Proc. SOPHIA Workshop 2016*, 2015, p. 95630A.

[204] BP, "BP Statistical Review of World Energy June 2016," *Excel workbook*, 2016. [Online].

Available: http://www.bp.com/content/dam/bp/excel/energy-economics/statistical-review-2016/bp-statistical-review-of-world-energy-2016-workbook.xlsx.

[205] J. Herrmann, K. Slamova, R. Glaser, and M. Köhl, "Modeling the Soiling of Glazing Materials in Arid Regions with Geographic Information Systems (GIS)," *Energy Procedia*, vol. 48, pp. 715–720, 2014.

[206] "150121 Documentation of module condition." [Online]. Available: http://www.iea-pvps.org/index.php?id=344. [Accessed: 07-Nov-2016].

[207] M. Kottek, J. Grieser, C. Beck, B. Rudolf, and F. Rubel, "World Map of the Köppen-Geiger climate classification updated," *Meteorol. Zeitschrift*, vol. 15, no. 3, pp. 259–263, Jul. 2006.

[208] M. Streib, "Bilder aus meiner Arbeit als Sachverständiger." [Online]. Available: http://www.gutachten.streib.de/bilder/index.html. [Accessed: 16-Dec-2016].

[209] R. Mayfield, "Common Residential PV System Code Violations," *Solar Professional, , Issue 3.1*, 2010. [Online]. Available: http://images.google.de/imgres?imgurl=http%3A%2F%2Fsolarprofessional.com%2Fsites%2Fdefault%2Ffiles%2Farticles%2Fimages%2F8_AluminumLug.jpg&imgrefurl=http%3A%2F%2Fsolarprofessional.com%2Farticles%2Fdesign-installation%2Fcommon-residential-pv-system-code-vi. [Accessed: 20-Apr-2017].

[210] S. Chattopadhyay, R. Dubey, V. Kuthanazhi, J. J. John, C. S. Solanki, A. Kottantharayil, B. M. Arora, K. L. Narasimhan, V. Kuber, J. Vasi, A. Kumar, and O. S. Sastry, "Visual Degradation in Field-Aged Crystalline Silicon PV Modules in India and Correlation With Electrical Degradation," *IEEE J. Photovoltaics*, vol. 4, no. 6, pp. 1470–1476, Nov. 2014.

[211] Y. Hu, V. Y. Gunapati, P. Zhao, D. Gordon, N. R. Wheeler, M. A. Hossain, T. J. Peshek, L. S. Bruckman, G.-Q. Zhang, and R. H. French, "A Nonrelational Data Warehouse for the Analysis of Field and Laboratory Data From Multiple Heterogeneous Photovoltaic Test Sites," *IEEE J. Photovoltaics*, vol. 7, no. 1, pp. 230–236, Jan. 2017.

[212] Y. Hu, "Temporal Change in the Power Production of Real-world Photovoltaic Systems Under Diverse Climatic Conditions," Western Reserve University, 2017.

[213] "World Map of the Köppen-Geiger climate classification updated," *Meteorol. Zeitschrift*, vol. 15, no. 3, pp. 259–263, Jul. 2006.

[214] F. Rubel and M. Kottek, "Observed and projected climate shifts 1901-2100 depicted by world maps of the Köppen-Geiger climate classification," *Meteorol. Zeitschrift*, vol. 19, no. 2, pp. 135–141, Apr. 2010.

[215] W. Köppen, "The thermal zones of the Earth according to the duration of hot, moderate and cold periods and to the impact of heat on the organic world," *Meteorol. Zeitschrift*, vol. 20, no. 3, pp. 351–360, Jun. 2011.

[216] Meteonorm, "Meteonorm Features." [Online]. Available: http://www.meteonorm.com/en/features%0A. [Accessed: 01-Feb-2016].

[217] K. Slamova, "Mapping atmospheric corrosion in coastal regions: methods and results," *J. Photonics Energy*, vol. 2, no. 1, p. 22003, Jun. 2012.

[218] K. Slamova, J. Wirth, C. Schill, and M. Koehl, "Ultraviolet radiation as a stress factor for the PV-modules - Global approach," in *Proc. IEEE 39th Photovoltaic Specialists Conference (PVSC)*, 2013, pp. 1594–1599.

[219] A. Ndiaye, C. M. F. Kébé, P. A. Ndiaye, A. Charki, A. Kobi, and V. Sambou, "Impact of dust

on the photovoltaic (PV) modules characteristics after an exposition year in Sahelian environment: The case of Senegal," *Int. J. Phys. Sci.*, vol. 8, no. 21, pp. 1166–1173, 2013.

[220] C. Schill, S. Brachmann, and M. Koehl, "Impact of soiling on IV-curves and efficiency of PV-modules," *Sol. Energy*, vol. 112, pp. 259–262, Feb. 2015.

[221] K. Slamova, C. Schill, J. Herrmann, P. Datta, and C. Wang Chih, "Global Stress Classification System for Materials Used in Solar Energy Applications," in *Living Planet Symposium, ESA-SP Volume 740*, 2016, p. 178.

[222] C. Peike, S. Hoffmann, I. Dürr, M. Köhl, and K.-A. Weiß, "PV Module Degradation in the Field and in the Lab - How Does It Fit Together?," in *Proc. 29th EUPVSEC*, 2014, pp. 3110–3114.

[223] S. C. Saunders, *Reliability, Life Testing and the Prediction of Service Lives*. New York, NY: Springer New York, 2007.

[224] M. Köhl, B. Carlson, G. J. Jorgensen, and A. . Czaderna, *Performance and Durability Assessment Optical Material for Solar Thermal Systems*. Elsevier, 2004.

[225] P. Lechner, "PID Failure of c-Si and Thin-Film Modules and Possible Correlation with Leakage Currents," in *Proc. NREL PV Module Reliability Workshop*, 2013.

[226] P. Hacke, K. Terwilliger, S. H. Glick, G. Perrin, J. Wohlgemuth, S. Kurtz, K. Showalter, J. Sherwin, E. Schneller, S. Barkaszi, and R. Smith, "Survey of potential-induced degradation in thin-film modules," *J. Photonics Energy*, vol. 5, no. 1, p. 53083, Dec. 2015.

[227] T. Berghold and J. Weber, "Potential-induced degradation of thin- film modules: Prediction of outdoor behavior," *Photovoltaics Int.*, vol. 27, 20151.

[228] N. Shiradkar, E. Schneller, and N. G. Dhere, "Finite element analysis based model to study the electric field distribution and leakage current in PV modules under high voltage bias," in *Proc. SPIE 8825*, 2013, p. 88250G.

[229] P. Borowski and F. Karg, "PID-Free CIGS Thin Film Modules," in *Proc. 29th EUPVSEC*, 2014, pp. 2356–2362.

[230] P. Manz, V. Wesselak, S. Voswinckel, B. Trautmann, E. Fokuhl, and C. Schmidt, "Leakage current pathways and magnitudes in correlation to PID of CIGS thin film modules," in *29th European Photovoltaic Solar Energy Conference*, 2014, pp. 3194–2199.

[231] P. Hacke, R. Smith, K. Terwilliger, G. Perrin, B. Sekulic, and S. Kurtz, "Development of an IEC test for crystalline silicon modules to qualify their resistance to system voltage stress," *Prog. Photovoltaics Res. Appl.*, vol. 22, no. 7, pp. 775–783, Jul. 2014.

[232] K. W. Jansen and A. E. Delahoy, "A laboratory technique for the evaluation of electrochemical transparent conductive oxide delamination from glass substrates," *Thin Solid Films*, vol. 423, no. 2, pp. 153–160, Jan. 2003.

[233] T. Weber, J. Berghold, F. Heilmann, M. Roericht, S. Krauter, and P. Grunow, "Test Sequence Development for Evaluation of Potential Induced Degradation on Thin-Film Modules," in *28th European Photovoltaic Solar Energy Conference*, 2013, pp. 3324–3331.

[234] P. Hacke, R. Smith, S. Kurtz, D. Jordan, and J. Wohlgemuth, "Modeling current transfer from PV modules based on meteorological data," in *Proc. IEEE 43rd Photovoltaic Specialists Conference (PVSC)*, 2016, pp. 1083–1089.

[235] P. Hacke, M. Kempe, K. Terwilliger, S. Glick, N. Call, S. Johnston, S. Kurtz, I. Bennett, and M.

Kloos, “Characterization of multicrystalline silicon modules with system bias voltage applied in damp heat,” in *Proc. 25th EUPVSEC/ 5th World Conference on Photovoltaic Energy Conversion*, 2010, pp. 3760–3765.

[236] J. A. del Cueto and T. J. McMahon, “Analysis of leakage currents in photovoltaic modules under high-voltage bias in the field,” *Prog. Photovoltaics Res. Appl.*, vol. 10, no. 1, pp. 15–28, Jan. 2002.

[237] P. Hacke, P. Burton, A. Hendrickson, S. Spataru, S. Glick, and K. Terwilliger, “Effects of photovoltaic module soiling on glass surface resistance and potential-induced degradation,” in *Proc. IEEE 42nd Photovoltaic Specialist Conference (PVSC)*, 2015, pp. 1–4.

For further information about the IEA Photovoltaic Power Systems Programme and Task 13 publications, please visit www.iea-pvps.org.

ISBN 978-3-906042-54-1